Bandgap Engineering of 1300 nm Quantum Dots/Quantum Well Nanostructures Based Devices

Dissertation by
Hala Hashim Alhashim

In Partial Fulfillment of the Requirements
For the Degree of Doctor of Philosophy

King Abdullah University of Science and Technology

Thuwal, Kingdom of Saudi Arabia, 2016

The dissertation of Hala Alhashim is approved by the examination committee.

Committee Chairperson: Boon S. Ooi
Committee Member: Pierre Beaujuge
Committee Member: Alexander Rothenberger
Committee Member: Vincent Aimez

ABSTRACT

Bandgap Engineering of 1300 nm Quantum Dots/Quantum Well Nanostructures Based Devices

Hala Hashim Alhashim

The main objectives of this thesis are to develop viable process and/or device technologies for bandgap tuning of 1300-nm InGaAs/GaAs quantum-dot (QD) laser structures, and broad linewidth 1300-nm InGaAsP/InP quantum well (QW) superluminescent diode structures. The high performance bandgap-engineered QD laser structures were achieved by employing quantum-dot intermixing (QDI) based on impurity free vacancy diffusion (IFVD) technique for eventual seamless active-passive integration, and bandgap-tuned lasers. QDI using various dielectric-capping materials, such as HfO_2, $SrTiO_3$, TiO_2, Al_2O_3 and ZnO, etc, were experimented in which the resultant emission wavelength can be blueshifted to ∼ 1100 nm – 1200 nm range depending on process conditions. The significant results extracted from the PL characterization were used to perform an extensive laser characterization. The InAs/GaAs quantum-dot lasers with QDs transition energies were blueshifted by ~185 nm, and lasing around ~1070 – 1190 nm was achieved. Furthermore, from the spectral analysis, a simultaneous five-state lasing in the InAs/InGaAs intermixed QD laser was experimentally demonstrated for the first time in the very important wavelength range from 1030 to 1125 nm. The QDI methodology enabled the facile formation of a plethora of devices with various emission wavelengths suitable for a wide range of applications in the infrared. In addition, the wavelength range achieved is also applicable for coherent light generation in the green – yellow – orange visible wavelength band via frequency doubling, which is a cost-effective way of producing compact devices for pico-projectors, semiconductor laser based solid state lighting, *etc*. [1, 2]

In QW-based superluminescent diode, the problem statement lies on achieving a flat-top and ultra-wide emission bandwidth. The approach was to design an inhomogeneous active region with a comparable simultaneous emission from different transition states in the QW stacks, in conjunction with anti-reflection coating and tilted ridge-waveguide device configuration. In this regard, we achieved 125 nm linewidth from InGaAsP/InP multiple quantum well (MQW) superluminescent diode with a total output power in excess of 70 mW with an average power spectral density of 0.56 mW/nm, and a spectral ripple of ≤1.2 ± 0.5 dB. The high power and broadband SLD with flat-top emission spectrum is a desirable as optical source for noninvasive biomedical imaging techniques employing low coherence interferometry, for instance, optical coherence tomography (OCT).

DEDICATION

THIS DISSERTATION IS DEDICATED TO THE FOUNDER OF KAUST, KING ABDULLAH AL SAUD. HE FOUNDED THIS HOUSE OF WISDOM WITH THE INTENTION TO CREATE AN ENDURING MODEL FOR ADVANCED EDUCATION AND SCIENTIFIC RESEARCH AND TO BECOME A BEACON OF HOPE AND PEACE TO THE WHOLE WORLD. I HOPE MY DISSERTATION IS A STEPPING STONE TO MAKE HIS AND OUR DREAM COME TRUE.

ACKNOWLEDGEMENT

I am grateful to the God for giving me faith, power, love, the good health and well-being that were necessary to complete this dissertation.

I would like to express my gratitude to my supervisor, Prof. Boon Ooi, whose *expertise, understanding, and patience considerably enriched my academic experience. I appreciate his vast knowledge and skills in many areas. By his supervision, he consistently allowed this dissertation to be my own work, but steered me to the right direction whenever he thought I needed it. He has supported me academically and emotionally through the rough road to finish this dissertation. Thanks to him I have learned that being kind with people is the best accomplishment ever. Also, I would like to thank the other members of my committee for taking time out from their busy schedule to serve as my PhD committee.*

Special thanks for my lab-mates Zahed, Majed and Tien Khee for their support, motivation and care. My very special thanks goes to my wonderful lab team, who allowed me to feel lucky that I'm part of them, thank you all.

To my wonderful parents, Mum and Dad, you were the first to hold my hand to write, were extremely pleased to record my first words in life, were seeing my future in my eyes, and dreaming of that day. Thank you for giving me the strength to pursue my dreams. Endless thanks for your unconditional love and support.

To my kids, the storm of happiness in my life, thank you for being the icing sugar to my cake.

A special thank goes out to my friends, who wish me the best, and pray for me in secret.

To the *people who were the rainfall in my life, and the E to my* mc^2.

TABLE OF CONTENTS

LIST OF ABBREVIATIONS

APSD	Average power spectral density
AR	Anti-reflection
ASE	Amplified spontaneous emission
BA	Broad Area
DOS	Density of States
EL	Electroluminescence
ES	Excited state
FPL	Fabry-Perot laser
GS	Ground State
HH	Heavy Hole
IFVD	Impurity free vacancy diffusion
Ith	Threshold Current
Ith	Threshold Current Density
LH	Light hole
MQW	Multiple Quantum Well
OCT	Optical Coherence Tomography
PICs	Photonic integrated circuits
PL	Photoluminescence
PBP	Power-bandwidth product
QDI	Quantum dot intermixing
QDs	Quantum Dots
QW	Quantum Well
QWI	Quantum well intermixing
SAQDs	Self-Assembled quantum dots
S-K	Stranski-Krastanow
SLD	Superluminescent Diode
SLD	Super luminescent diode
To	Characteristic Temperature
V.B	Valence Band
WPE	Wall-plug efficiency

LIST OF FIGURES

LIST OF TABLES

1-INTRODUCTION

1.1 Optical Communications

New technology allows the world to keep shrinking in the form of communications and transportation; the data traffic carried by core transport networks is growing at a steady and remarkable rate of 30-40% year-over-year, and the accessible network capacity demands double almost every two years [3]. such a rapid growth is primarily due to the dramatic paradigm shift that was observed in internet usage over recent years with the emergence of multimedia traffic, especially video, which consumes the largest share of the available capacity [4] In the near future, all introduced innovations in the network architecture and technologies are expected not to be able to support the new network capacity targets and service requirements. If no considerable changes occur in the infrastructure characteristics, technologies, and architecture Towards that direction, the situation of optical transmission and networking technologies is fundamental to support the future requirements [5]. No other transmission medium has the present capabilities of optical fibers, and no technology other than photonic can operate at an ultra-high bit-rates and ultra-low powered consumption rate. Advancements in photonic devices and optical communications systems and networks are absolutely required to continue to satisfy the traffic requirements by delivering content over the network infrastructure in a cost- and energy-efficient manner.

1.2 Photonic Integration in Optical Communications.

Optical systems contain footprint-consuming packaging that includes electrical, optical and optoelectronic components, all of which must work together. This situation calls for an important technology for shrinking optical components to enable integration of multiple functionalities onto a single chip, thus reducing the time-delay associated with interconnections, and therefor increasing speed. Such integrated systems are known as Photonic Integrated Circuits (PICs). PICs offer the promise of cost reduction, dramatically reduced size and increased packaging robustness. A PIC is a device that integrates multiple photonic functions, which provides functionality for information signals imposed on optical wavelengths, typically in the visible spectrum or the near-infrared spectrum over the wavelength range of 850 nm - 1650 nm. To enhance the performance and reliability and increase the functionality while lowering the manufacturing cost, increasing numbers of optoelectronic devices have been integrated on a single chip, i.e., the integration of waveguides, detectors, lasers and modulators, each of which may require different optical properties to achieve optimized performance. For example, for a device to interact properly with incoming photons, the waveguides require the photon energy of the light to be less than the electronic transition in the waveguide material, so that the material is transparent to the incoming photons. Contrarily, lasers require the photon energy to be equal to or greater than that of the transition energy of the semiconductor laser gain medium, so that the photons can interact with the carriers of the semiconductor.

To realize PICs, spatially selective control over the optical and electrical characteristics of the active region, for example, multiple quantum wells, is required. Approaches including regrowth of the quantum well active layers, selective area epitaxy (growth on a patterned substrate), and quantum well intermixing (QWI) [6], etc., have been reported. Due to the considerable interest promoted by its simplicity, QWI (discovered in 1981 by Laidig et al. [7, 8]) has been comprehensively studied in the aspects of physics, material science and device engineering. QWI is one of the most effective techniques to shift the transition energy because it is a post-growth technique and it is able to obtain a wide range of bandgap in a straightforward manner on the same wafer. In this technique, the bandgap of the QW structures is modified in selected regions after growth by interdiffusing the barrier and well species to form an alloy semiconductor. The band gap of the intermixed QW is then usually larger than that of the original QW. This provides a method of producing low loss optical waveguides and modulators as well as variably intermixed lasers and detectors possessing different operating wavelengths. Recently, this technique has also been applied to the zero-dimensional SAQD device structures because of the demonstrated high performance characteristics of QDs based devices compared to their QW counterpart. For example, QDs -based lasers exhibited low-threshold current densities (J_{th}), higher gain, temperature insensitivity, and low chirp under direct modulation. Several SAQD intermixing techniques, such as laser-radiation induced intermixing [9, 10], neutral ion implantation induced intermixing [11], and impurity free vacancy disordering Impurity free vacancy diffusion IFVD [12, 13], have been developed and studied. Among these techniques, the IFVD process has been the most widely used because of its simplicity and ability to tune the bandgap of long wavelength InAs SAQD for achieving PICs.

1.3 Quantum Confined Light Emitters

1.3.1 Quantum Confined Nanostructures

In the field of nanotechnology, quantum confined is used to describe the effect of size shrinkage of the nanomaterial or the carrier wavefunction.

The length scale corresponding to the regime of quantum confinement ranges from 1 to 25 nm, in which the confinement scale is comparable with the carrier wave function; hence, electrons feel the presence of the particle boundaries and respond to the particle size changes by adjusting their energy. Controlling the properties by controlling the size is known as quantization effects. This effect becomes important when the dimension of a semiconductor become comparable the bulk semiconductor Bohr exciton radius; as a result, the materials properties are size dependent in this regime. Increase in quantum confinement causes an increase of the excitonic binding energy and a blue shift in the absorption and luminescence bandgap energies. Quantum confinement leads to a collapse of the continuous energy bands of a bulk material into discrete, atomic-like energy levels. Figure 1-1 shows the density of state (DOS) for particles with three spatial degree of freedom.

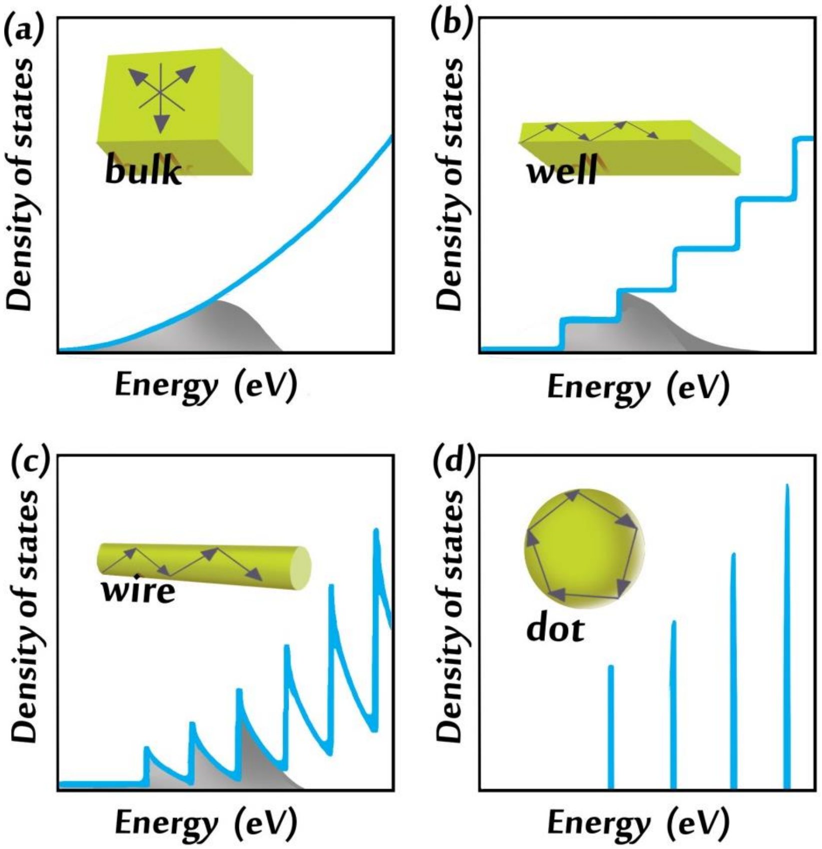

Figure 1-1: Density of state for particles with three (bulk), two (quantum well), one (quantum wire), and zero (quantum dot) spatial degrees of freedom.

A quantum confined structure is one in which the motion of the carriers (electron and hole) are confined in one or more directions by potential barriers. Such a structure is classified into three categories: quantum well, quantum wire, and quantum dots (QDs). This confinement leads to a certain allowed quantized energies in quantum well/dot.

In quantum well with a width of d, Energy state is given by:

$$E_n = \frac{n^2 h^2}{8md^2}$$

Where n=1, 2, 3, 4, …………….

But in (QDs)., the carrier motion is quantized in all three directions. If the dot has spatial sizes of L_x, L_y, L_z, then the total quantization energy can be written as a sum of three separate terms:

$$E_n = \frac{n^2h^2}{8mL_X^2} + \frac{m^2h^2}{8mL_y^2} + \frac{l^2h^2}{8mL_z^2}$$

where (n, m, l) = 1, 2, 3, 4, …

As the active layer material is scaled down from bulk (3D) to (QDs). (0D), the population inversion* -necessary for laser action occurs- exhibit more efficient. This can be explained through DOS for different material scale. In bulk semiconductor, DOS is dependent on the square root of energy. This requires large current to be injected to real population inversion. Moving to a quantum well, quantum wire (QWR) and quantum dot, the DOS changes from stepwise to delta like state with energy leading in part to reduce the operating current. Additional benefit of delta function DOS of QDs is the narrow emission linewidth as compared to QW and QWR. This is because only fixed photon energy released during electron-hole recombination.

Discrete atomic like structure of QW,QDs open a wider possibility to engineer emission wavelength.

1.3.2 Quantum Confined Nanostructure Based Lasers

The use of the quantum potential effect in photonic devices has a great impact in enhancing the performance of photonic devices. The source of the interesting quantum effects is that the electronic and vibrational properties of a low-dimensional material are modified as a result of their lower dimensions and symmetries. In the previous paragraph, both the form of the electronic energy levels and how they are distributed energetically in a QD have been explained. Henry and Weigmann, in 1974, were the first to report the confined state in a quantum well; they indicated that “the active layers are thin enough to separate the quantum levels of electrons confined therein. These laser exhibit wavelength tunability by changing the thickness of the active layer. This is due to the interface between the active region and the wide bandgap layers from a pair of heterojunction which provide both optical and carrier confinement.” [14]

In addition to lasing tunability, the lasing threshold of conventional double-heterostructure lasers is a function of the active region thickness. In these lasers, the threshold decreases with the reduction of active region thickness until at approximately half of the emission wavelength, the waveguide formed by the heterojunction fails to provide adequate optical confinement. thus, the lasing threshold begins to increase, and the discrete energy levels associated with confined electrons are so closely spaced that quantum effects are negligible [14].

In particular, the increase in the exciton binding energy due to the quantized confinement effect has opened up the possibility of many optical device applications. Nevertheless, the double heterostructure continues to pave the way for further developments of great significance for the diode laser. This fact stems from the effect of the different bandgap energies in the different parts of the heterostructures that allow them to function as a waveguide for electrons confined in the well. The energies of the confined states in a thin quantum well depend upon the dimensions of the waveguide.

Intermixing proved to be an effective means to vary the effective confining potential; further details will be discussed in chapter 3.

1.3.2.1 Quantum Dots laser

(QDs) form the basis of the novel generation of optoelectronic devices, e.g., edge and surface emitting lasers, amplifiers, etc. In these devices, (SAQDs) which are nano-scale strained island structures usually grown through an MBE, which enables one to control the growth process with an accuracy of single monolayers. When two different crystals with different lattice constants (more than 1.8% difference) are grown, the growth kinetics is controlled by three competing energies to forms: the strain energy, the surface free energy of the materials, and the interfacial surface energy between the crystals. During epitaxial growth, different growth conditions, such as growth temperature, lattice mismatch and active region thickness, can be engineered to make the formation of 3D QDs islands more energetically favorable to minimize the sum of these energies. This method of forming SAQDs in III-V semiconductors is known as the Stranski-Krastanov (S-K) growth method. These (QDs) are often only a few nanometers high and approximately 20 nm wide for InGaAs dots grown on GaAs. However, if the strain energy is too high, dislocations & defects will form in the SAQD structure to lower the strain energy, which will form non-radiative centers, and resulting in PL intensity quenching [15]. Other parameters should be taken into consideration when choosing the substrate materials, e.g., the QD should have large band offset to ensure high confinement of the electrons. The confinement of carriers within a quantum dot leads to an atom-like density of states; which improves device performance. If the energy levels separation in a QD is greater than kT, then emission and absorption at single wavelength is possible [8]. Moreover The size of the QD determines the energy levels and hence the emission wavelengths. Because the QD size can be controlled during the growth process, lasers of virtually any wavelength (including 1300 nm) can be created [16, 17]. The 1300 nm lasers are of special interest for their usage in short-range optical communications systems [2].

To obtain 1300 nm emission, the QDs must be either grown in the middle of a InGaAs QW or directly onto GaAs and then barried by an InGaAs layer. In this case, the surface density of QDs is approximately 3 $\times 10^{10}$ to 5 $\times 10^{10}$ cm^{-2}. The presence of In in the covering material can reduce In out-diffusion from QDs, resulting in a sharper heterointerface and, in turn, deeper energy levels in the QDs [18]. The growth conditions, including growth temperature, growth rate, V–III ratio, thickness of deposited layers, and In content of the InGaAs layer, are the subject of careful optimization to improve the characteristics of the QDs. We found that the reduction of the total amount of InAs (in the QDs plus QW) is one of the key routes to achieving high brightness photoluminescence (PL) at the desired wavelength [19].

This growth technique can be followed by a post growth technique to tune the lasing wavelength to the desired wavelength. Modifying the lasing wavelength after growth is highly desirable in such long wavelengths of 1300–1700 nm and have been the subject of intense research for long-haul optical fiber communications and atmospheric pollution control [20]. Tuning of the lasing wavelength after growth can be performed via many methods; comparing these methods, the intermixing technique has been proven to be one of the effective, easy approaches to tune wavelength into the desired wavelength [21]. , the details of which will be described in the next paragraph. Although intermixing has proved to be one of the efficient methods for tuning the lasing wavelength, this method can cause a decrease in the band offset due to the parabolic shape produced in the well, which results in reduction of the electron confinement and an increase in the leakage current. Therefore Designing a high confinement laser structure is therefore extremely important.

In this work, a laser structure is designed in such a way to achieve high electron and photon confinements.

1.4 Post Growth Bandgap Engineering via Intermixing

Different quantum intermixing techniques were developed over the last 25 years. We can classify these techniques in four different categories:

- impurity induced intermixing (IID) (Laidig, W. D et al. *1981)* [7].
- ion implantation (S. Charbonneau *et al.* 1998) [22].
- laser induced QWI (B.S. Ooi *et al.* 1997)[23].
- impurity-free vacancy diffusion (IFVD) (ES Koteles et al. *1991*) [24].

In general, QWI techniques are based on the diffusion of point defects. This diffusion is accomplished either by introducing an extra concentration of defects in the material or by applying an external force on the defects. The details of each technique are presented below.

1.4.1 Impurity Induced Disordering

Impurity induced disordering (IID) in (Al)GaAs structures is certainly the most studied of all of the intermixing techniques, starting in the early 1980s, when Laidig *et al.* [7]

unexpectedly found that transition from order to disorder in superlattice occurred when diffusion when atoms diffusion. This technique is based on injecting energetic ions a material to form, interstitial dislocation which blue shifts of the PL emission energy due to changes in the Fermi level [24]. In this method, the depth can be controlled by varying the implantation energy, with high spatial resolution [25]. However, the impurity induced disordering will always result in increased optical losses due to free-carrier trapping by the introduced impurities with the active region. Which limits, its application for photonic integration is limited. As a result, due to the increased optical losses, this technique can only be used for an application that does not directly involve passive light propagation in the intermixed areas [26]

1.4.2 Ion Implantation Induced Intermixing

As a well-established technique, ion implantation can initiate intermixing [22, 27] by creating defects within or in the vicinity of the active region, followed by thermal annealing. Ion implantation has several advantages, such as compatibility with planar processing, high uniformity, good selectivity and reproducibility. However, the low crystallinity induced by this technique is undesirable because most optoelectronic devices require pristine crystallinity.

To reduce this drawn back, Ion implantation is usually followed by thermal annealing at a temperature high enough to allow these defects to diffuse from the damaged region through the QWs and also repair the implantation damage. However, thermal annealing is usually not sufficient to fully recover the crystallinity. It is therefore crucial to optimize the implantation species and conditions to achieve large intermixing with minimal residual damage to the material devices [28].

1.4.3 Laser Induced Intermixing

This technique is based on the thermal effects produced by absorption of high power laser beam. The beam is focused across the semiconductor surface, causing melting; the surface is then re-crystallized to produce an alloy semiconductor. Photons with energy higher than the absorption edge of the semiconductor are absorbed easily and increase the lattice temperature, while photons with smaller energy can only be absorbed at defect sites or through multi-photon processes [29].

Although this approach is in general not very different from IFVD, there are some benefits in terms of obtaining high special resolution between intermixed and non-intermixed material. However, CW radiation process requires a high power density to melt the material, thus introducing thermal shock damage, which in turn causes undesired redistribution of dopants in the structure [29]. Furthermore, melting of the semiconductor results in complete intermixing; hence, partial bandgap control is difficult to achieve using this technique. An alternative laser-induced disordering process, photo-absorption induced disordering (PAID), was developed by McLean et al. PAID does not involve a melting phase in the semiconductor process. The interdiffusion that occurs in this PAID process is due to the effect of heat generation and involves the band-to-band absorption of the incident CW laser radiation in the active region. One of the most important additional advantages is that this technique is layer composition selective, i.e., it is not restricted to a near surface layer. However, the major drawback of the technique is that the low spatial selectivity which is limited by lateral heat flow. For monolithic integration of optical devices, this lateral heat flow leads to poor performance, as the interface abruptness is - 1 0 0 pm [29] .

Another LID technique is pulsed-PAID (P-PAID).This technique provides better resolution, as involves irradiating the InP-based materials with a high energy Q-switched Nd:YAG laser pulses, with a pulse length of a few nanoseconds and a repetition rate of 10 Hz. Absorption of the high-energy pulses results in transient heating in the crystal. Rapid thermal expansion will then cause bond breaking and disruption of the lattice, leading to localized increase in the density of point defects [30].

1.4.4 Impurity-free Vacancy Disordering (IFVD).

Among the previous listed intermixing techniques, the IFVD process has been used to selectively enhance the amount of intermixing in III-V semiconductor materials for optoelectronic devices. As the process is essentially impurity free, the optical loss and degradation of the electrical properties resulted from extended defects and free carriers are illuminated. This simple and effective technique to tune the bandgap of long wavelength InAs SAQDs is attractive for achieving PICs [31] .

IFVD of (QDs) is a simple and effective technique to tune the bandgap of long wavelength InAs SAQDs, and GaAs/AlGaAs for achieving PICs. This technique has been used to fabricate PIC's, such as extended cavity lasers and integrated waveguide modulators [32]. IFVD involves depositing a dielectric cap, usually SiO_2 (silicon dioxide) on the GaAs surface. During annealing, Ga atoms out diffused into SiO_2 cap generating group-III vacancies (V_{III}) in the underlying semiconductor. Diffusion of V_{III} towards the active region at elevated temperature promotes atomic interdiffusion of group-III elements between the barrier and QW/QD, thus shifting the QW/QD transition energy to a higher level. In addition, the different thermal expansion coefficient between the dielectric capping layer and the semiconductor result in stress accumulation at the interface during annealing. This factor was found to either promote stress (when GaAs surface is compressively strained) or inhibit stress (when GaAs surface is tensile strained) [33-36]. IFVD has increased in importance mainly because it offers the possibility of intermixing without doping, thereby preventing strong free-carrier absorption, without implantation induced crystal damage that would otherwise be responsible for scattering loss [37].

The first experiments using this technique were in 1987; the authors reported that the interdiffusion depend upon the crystal encapsulation conditions and that strain effects were a major source of anisotropic Al-Ga interdiffusion [37]. In 1988, J.D. Ralston et al. were the first to report the increase in energy of room temperature exciton transitions in a GaAs/AlGaAs super lattice using SiO_2 encapsulation [38]. In the same year, E.

Koteles et al. report the modification in QW shape using vacancy generation by SiO_2 encapsulation; this modification was investigated by monitoring exciton energy using low temperature (PL) [24]. Soon afterwards, other dielectrics, such as SiON or Si_3N_4, were used for the purpose of creating vacancies, thereby enhancing intermixing. In 1993, a researcher reported the inhibition of intermixing by using a fluoride material, such as SrF_2, or AlF_3 [39]. The one-step "selective intermixing in selected area" technique was used for the first time in 1997 by B. Ooi et al; they utilized the effect of using different encapsulations to induced different degrees of intermixing in a single annealing step. Based on that effect, they fabricated multiple-wavelength lasers and a multichannel wavelength division multiplexer [40]. In 1999, it was reported that the reduction of the energy spacing between Ground state (GS) and excited state (ES) due to interdiffusion that gives a wide range in tunability for applications such as QD infrared photodetectors and QD lasers [41]. Interdiffusion is not only affected by the type of encapsulation, annealing temperature, but is also affected by the deposition technique. In 2000, D. Bhattacharyya et al. used sputtering and plasma deposition to achieve a bandgap shift of up to 100 meV [42]. In 2012, K. J. Zhou et al. utilized the spectral broad band results and energy shifts to achieve high broadband spectra for Optical Coherence Tomography (OCT) application[43].

Our contribution in this field is that we qualitatively compared the degree of intermixing induced by seven different capping types by extracting the rate of intermixing and the temperature for ground-state and excited-state convergences. Based on our systematic characterization, we established reference intermixing processes based on seven different dielectric encapsulation materials [44].

1.5 Thesis Motivation

Post-growth thermal annealing can be used as an important alternative approach to tune the lasing wavelength in an efficient and cost-effective manner. By using novel methods to engineer the bandgap, multiple wavelength emission can be achieved on one chip, using one structure without the need for regrowth. Many research groups have already made significant contributions to the development of band gap engineering. Nevertheless, there is still room for improvement. Specifically, further improvements in the emission properties of intermixed quantum dot lasers can still be achieved. The following research gaps can be readily identified.

- Although many groups were using intermixing in the development of quantum dot lasers, to the best of our knowledge, a comparative study of different capping layers has not been performed, in addition to an exploration of new capping materials.
- Moreover, it is necessary to build an understanding for choosing the intermixing conditions for proper wavelength selection. This task has not been properly addressed.
- The utilization of different capping material properties in achieving broadband emission has not been studied.

It is the objective of this thesis to study and fill these research gaps.

1.6 Thesis Preview

This dissertation aims to highlight the important results achieved during my research on engineering devices with an emission wavelength of 1300 nm. It starts with chapter 1 that highlighting the fundamental development steps to set the stage for strong analysis foundation. It also explains the essential terminology for better understanding of the field phenomena. It shows the effort to create a practical technology platform for the devices used and how it helped to achieve desired results. As part of the effort, a survey was conducted to check out the market for available technologies used in the post growth engineering supported with literature review. This is to help understanding the advantages and disadvantages for each technology to insure the highest possible accuracy.

Furthermore I described the electrons movements in semiconductors nanostructure quantitatively, this information helps to visualize, design and engineer electronic devices. The details of the high quality Nano structure used in this work -quantum dot/quantum well laser structure- was describe in the second chapter, followed by explaining the homemade setups used for materials/device characterization.

The usage of this nanostructure in light emitting devices can be extended through a simple technology named impurity free vacancy diffusion. This technology allows modifying bandgap of the structure after growth; the importance of this technique and an extensively conditions applied was explained in the third chapter. The approach was taken in addition to the comparison between all results were presented. From this comparison, two intermixed laser has been chosen. Both selected intermixed lasers in addition to the "As Grown" laser were fabricated with the standard broad area laser (BAL) design. The standard fabrication process is documented in Appendix C.

In chapter 4, the three fabricated lasers have been tested through series of performance experiments to measure how well the lasers perform. This is to quantitatively assess the quality performance and characteristic of laser diodes before and after intermixing. The analysis divided into two sections, the DC characteristics and the spectral analysis.

Principle parameters calculated from DC Characteristics helps to compare laser performance after intermixing, the parameters are; transparency current density (J_0), external & internal quantum efficiency (η_i), internal loss (α_i), characteristic temperature (T_0), and saturation modal gain (G_{sat}). From spectra analysis I extracted the following: the maximum tuned wavelength that can be achieved using intermixed lasers, the multi-state lasing observed in these intermixed lasers, and the sub-1100nm lasing from post-growth intermixed quantum dot lasers. Finally, summary of all important results was provided at the end of this chapter

Fifth chapter covers, the 1300 nm superluminescent diode (SLD) that uses the engineering growth condition unlike the intermixed laser using postgrowth engineering. Both materials and device were characterized from PL and EL spectra. This followed by illustration of the behavior and most important observations.

Finally, this thesis' conclusion and the outlook of future work were summarized in chapter six.

2 PROCESS AND EXPERIMENTAL SETUPS

2.1 Semiconductor Laser Structure

2.1.1 Quantum Dots Structure and Emission Wavelength.

The laser structure was grown on Si-doped GaAs substrate using molecular beam epitaxy (MBE) technique. The schematic diagram of SAQD full structure utilized in the intermixing experiments is shown in Figure 2-1(a). Each QD layer was covered with a thin InGaAs strain-reducing layer (SRL), followed by partially p-doped GaAs barrier. The thickness of each QD stack (QD layer, SRL and barrier) is 40 nm. The active region was sandwiched between n-type $Al_{0.4}Ga_{0.6}As$ lower-cladding layer and the p-type $Al_{0.4}Ga_{0.6}As$ upper-cladding layer, with a 400 nm p-type GaAs:Be contact layer. Figure 2-1(b) correspond to the (004) bright field cross-sectional transmission electron microscopy (TEM) image of our SAQD samples, where the active region consists of eight-stack QD layers. The QD energy states represented in (PL) spectra in Figure 2-1 (c) shows the excitation power dependent low temperature (77K) PL from the as-grown (AG) laser structure sample using 980 nm diode laser as the excitation source. At low excitation power, a single PL peak emission at 1200 nm is visible which is attributed to the QD GS emission. A progressive increase in the PL emission from a high-energy shoulder at 1110 nm is observed at high excitation power, which is related to the emission from the QD ES emission besides the GS emission. An energy separation of ~90meV at 77K is observed between the two peaks, consistent with the value reported in the literature for InAs/GaAs QDs material system [45]. Henceforth, for the ease of discussion, we refer the main peak of annealed sample 77K PL spectrum as emission from GS, and the higher energy shoulder or peak as the emission from QD ES transition.

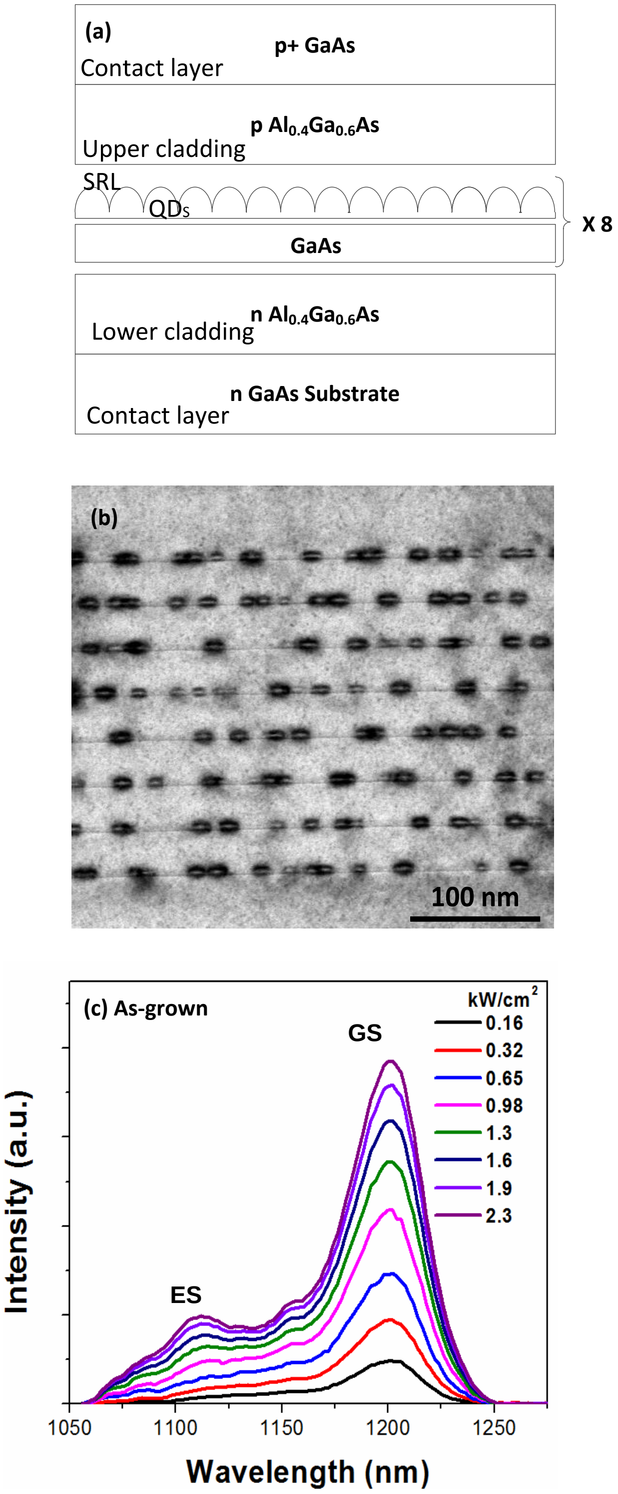

Figure 2-1: (a) Schematic diagram of SAQD full structure utilized in the intermixing experiments, (b) cross-sectional (004) bright field TEM micrographs of the as-grown active region showing eight-stack QD layers, and (c) the corresponding excitation power dependent 77K PL showing the GS and ES peaks.

2.1.2 Quantum Well Structure

In addition to QDs, QW will be studied. The device active region consists of four 6.7 nm thick compressively strained $InGa_{0.84}As_{0.59}P$ QWs separated by 10 nm thick tensile strained $InGa_{0.863}As_{0.255}P$ barrier layers. The un-doped active region is sandwiched between 100 nm thick lattice-matched $InGa_{0.882}As_{0.249}P$ separate confinement heterostructure layers. The waveguide core is later covered with ~0.8 µm and ~1.7 µm thick n- and p-type In cladding layers with Si and Zn dopant, with doping concentration varying from 1×1018 – 2×1018 cm^{-3} and 5×1017 –5×1018 cm^{-3}, respectively. The cladding layers are lattice-matched to the n-doped In substrate and the metal-oxide chemical vapor deposition (MOCVD) grown device structure is completed by a 100 nm thick highly doped (>1.5×1019 cm^{-3}) $In_{0.467}Ga_{0.533}$ As contact layer.

2.2 Experimental Setups

2.2.1 Photoluminescence (PL) Setup

(PL) spectroscopy is a common and standard method for the optical characterizations of a semiconductor. The PL schematic setup is shown in Figure 2-2 . The PL system uses a 980-nm diode laser as the excitation source, a 1 × 2 -3 dB optical fiber splitter/coupler with a 62.5-µm core diameter multi-mode fiber as the signal probe, and a 0.26 m monochromator with an InGaAs photodetector to measure the PL.

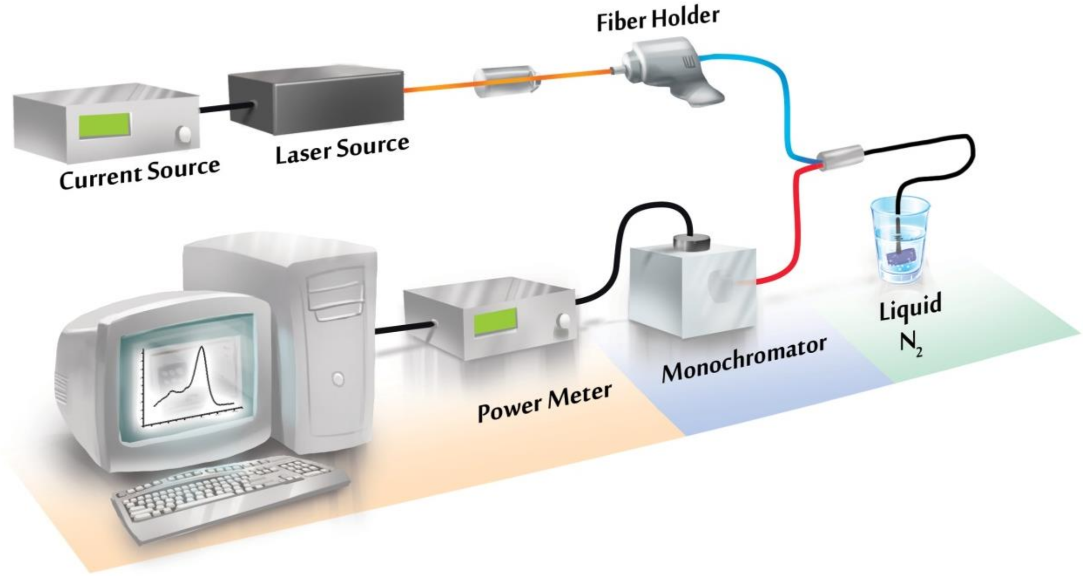

Figure 2-2: Schematic of PL setup.

The principle of PL is presented in Figure 2-3. A light source of wavelength $\hbar\omega_{exc,}$ larger than the structure bandgap, excites electrons from the valence band (VB) to the conduction band (CB). The excited carriers exist as electron-hole pairs (excitons) due to the columbic interaction between them. These pairs can be excited directly into discrete levels in quantum confined nanostructures, such as QWs or QDs Figure 2-3 (b). When the electron-hole pair subsequently relaxes to the lowest energy (GS of the quantum confined state) and recombines, photons of energy ħω are emitted which then can be detected/measured. The recombination of excitons will give rise to sharp luminescence spectra due to strong overlap of electron, and hole wavefunctions. Exciton has a binding energy which if take into consideration will minimize the detected energy transition And can be calculated by subtracting the binding energy (E_B) of the exciton from the bandgap ($E_{exciton}$=$E_{bandgap}$-E_B). In bulk semiconductor this effect is neglected since the exciton binding energy is ~4meV which is lower than K_BT. Compare to quantum confined structure where the exciton relatively stronger and need to be consider. The blue shift observed which Increase with the degree of confinement.

As we go to low temperature the exciton recombination is commonly observed due to negligible interaction with phonon. At room temperature, band-to-band recombination dominates due to electron-phonon interaction, so the exciton effect can be negligible. Due to the properties of discrete energy levels in Qdots, emission from GS and ES can be detected if the luminescence peak are sharp and sufficient excitation power is supplied [46].

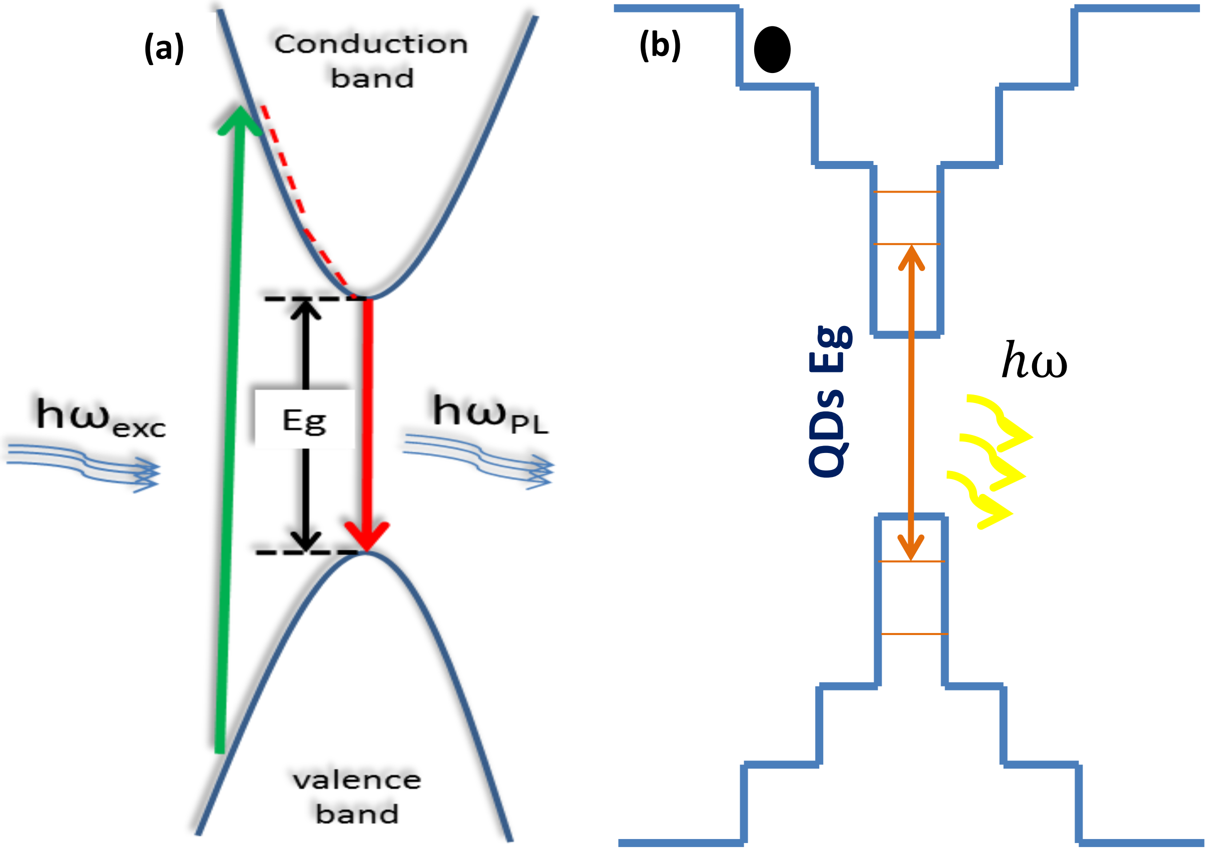

Figure 2-3: Schematic of PL principle for: (a) bulk semiconductor, and (b) QDs semiconductor.

2.2.2 Laser Diode Characterization Setup

The power-current-voltage (L-I-V) measurement is the basic setup used to measure the device performance. Figure 2-4 illustrated the schematic of (L-I-V) measurement. The laser is mounted on a thermoelectric cooler (TEC), which keeps the heat sink temperature constant during the testing. The TEC is mounted such that it allows for easy access to the top of the device for electrical contacts and a temperature controlled brass base (ILX-LDC-3900) to hold the bare laser bars In addition, the lasers are mounted on a tile for ensuring heat dissipation. A clamp is used to introduce uniform pumping during current injection. The laser is tested (L-I) using current in pulsed mode, (2 µs current pulse width, and 1.961% duty cycle), however SLD devices were tested using both, pulsed mode (0.5 µs current pulse width, and 0.01% duty cycle), and continues wave (CW) operation. The current was swept from 1mA to 2000 mA. The Labview software was used for spectra measurement communication, Electroluminescence (EL) and data recording, fixing the current injected into a laser diode just above J_{th}. Keithley 2520 system was used in the operation of the probe-positioners in InGaAs detector in the form of integrating sphere from Labsphere. For the spectral measurements, we couple the laser light from the bare laser device facet into a lens-shaped multi-mode fiber connected to an optical spectrum analyzer (Yokogawa 6370B).

Unless stated otherwise, this setup is the standard setup used for all succeeding measurements. The data are used to analyze the properties measured from broad area lasers fabricated before and after intermixing for many different cavity lengths and wavelength tuning.

The primary data collected from this setup is used by a specific equation to analyze the laser performance (see appendix A).

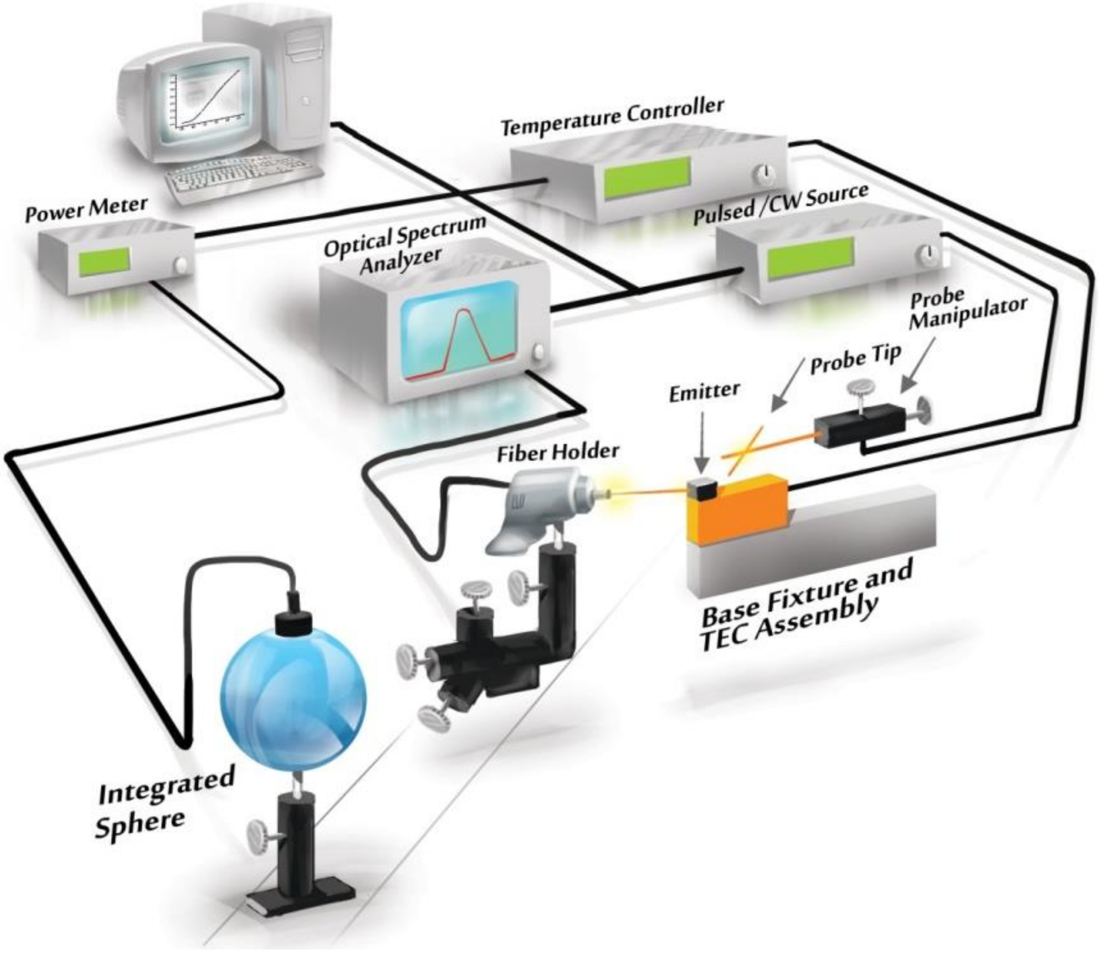

Figure 2-4: Schematic of laser diode characterization setup

3 INTERMIXING QUANTUM WELL & QUANTUM DOT STRUCTURES BY VARIOUS DIELECTRIC ENCAPSULANTS

3.1 Introduction

Integrating SAQD laser diodes with other functional devices on the same chip to achieve a high density photonic integrated circuit (PIC) is highly desirable for broadband and telecom systems. Instead of the hybrid integration based on discrete components, a seamless integration of active and passive components based on a monolithic integration is crucial to the success of PIC. Notably, the use of selective area post-growth intermixing technique [40, 47-49] to achieve two or more optical elements with various transition energies on the same quantum dot (QD) wafer [42, 50] is attractive. Therefore, capping materials for a selective area intermixing need to be carefully selected for proper bandgap engineering of different regions to avoid an absorption [51]. In addition, the overlapping transition energies of intermixed region broadens the emission bandwidth for various broadband applications, such as biomedical imaging [52], optical communications, etc [53]. Furthermore, the wavelength window of ~1060 – 1200 nm is garnering attention because of it has a multitude of applications, for example, as a source for pumping solid state lasers [54] and in visible light generation [55, 56] laser-based gas sensing [57], and metrology. Therefore, an intermixed InAs/GaAs QD laser in this wavelength range would be a promising candidate to challenge the currently dominant InGaAs(N)/GaAs multiple quantum well (QW) lasers and Nd-YAG based solid-state lasers [58].

QWI using the IFVD technique is one of the simplest and most versatile ways of controlling the bandgap of the QW after growth. This technique is essentially impurity free. Therefore, QWI using IFVD can avoid degrading the electrical properties or increasing the optical loss by introducing free-carrier absorption.

Particularly in InGaAs/GaAs structures, this technique uses a dielectric cap to induce outdiffusion of Ga atoms during annealing, As a result, group III vacancies are generated in the underlying GaAs–InGaAs material. Due to the concentration gradient between Ga in the QW and Al in the barriers, the group III vacancies promote the diffusion of In into a buried GaAs QW and Ga into the barriers, and hence shift the QW bandgap to a higher energy by partially intermixing the QW.

Quantum dot intermixing (QDI) is found to be more complicated than quantum well intermixing (QWI) due to the difference in thermal expansion coefficient between the SAQDs and the surrounding materials and the strong influence of the shape, size, composition and strain distribution in and around the SAQDs [35, 50, 59]. Furthermore, the high sensitivity of the SAQDs to annealing parameters (temperature and duration) is very difficult to trace. In the existing literature, several capping materials have been reported using the IFVD annealing process. For inhibiting interdiffusion, TiO_2 (titanium oxide) [60, 61], Al (aluminum) [61], and Si_3N_4 (silicon nitride) materials [33] were utilized. enhancing interdiffusion, SiO_2 capping was used [13, 34]. TiO_2 film has been demonstrated to reduce intermixing due to the larger thermal expansion coefficient compared to the GaAs substrate [60]. Following the same argument, the smaller thermal expansion coefficient of the SiO_2 film showed a larger degree of intermixing. Furthermore, the degree of intermixing was found to enhance with increasing thickness of SiO_2 film [33]. Because there is always a limit to the solubility of Ga in the SiO_2 film, once saturation is reached, no more Ga vacancies can be generated. Therefore, higher solubility in a thicker film enhanced intermixing compared to the thin film. In addition, higher stress at the capping layer/GaAs interface due to its increased thickness also favors Ga atoms out-diffusion into the SiO_2 capping material. In general, these capping materials (SiO_2, TiO_2, Al, and Si_3N_4) are deposited by plasma enhanced chemical vapor deposition (PECVD), electron-beam evaporation, or sputtering methods.

In this work, a comparative study of IFVD InAs/GaAs SAQDs with PECVD grown SiO_2 and Si_3N_4 dielectric films is demonstrated in conjunction with other novel capping materials such as HfO_2 (hafnium dioxide) and $SrTiO_3$ (strontium titanate). These are grown using pulsed laser deposition (PLD), beside Al_2O_3 (aluminum oxide), TiO_2 and ZnO (Zinc oxide), which are deposited using atomic layer deposition (ALD). Low temperature (PL) spectroscopy on these samples revealed that HfO_2 cap induced significant blue shift in the SAQD's (GS) emission. This indicated a comparatively higher degree of intermixing compared to the SiO_2 cap. Whereas $SrTiO_3$ and ZnO caps behaved as control caps with reduced rate of intermixing. Furthermore, merging of GS and ES transitions was observed at high annealing temperatures from the SiO_2, TiO_2 and HfO_2 samples. Also, we discuss the PL observations of different capping materials versus annealing temperature, and qualitatively characterize them by extracting two degrees of intermixing parameters: (i) critical temperature (TC), at which SAQDs GS and ES merged; and (ii) rate of GS peak energy shift with annealing temperature (δE). These parameters are yardsticks for assessing the amount of inter-diffusion. Generally, our systematic IFVD study provides choices from seven different dielectric caps. These choices are promising towards post-growth bandgap engineering for fabricating selective-area bandgap tuned PICs based on SAQDs. This likewise provides an excellent control over the required design parameters. Moreover, realization of single state lasing (with large and differential gain) in SAQD lasers by a simple post growth bandgap engineering method (i.e. annealing using selected capping material at corresponding TC) might be addressed which otherwise employ complicated gratings [37]or dichroic mirror [38] assisting techniques.

Alternatively, the IFVD effect of these capping layers in InGaAsP/InP Quantum-Well Structure is also studied towards the end of this chapter highlighting the degree of intermixing in terms of the GS peak energy shift. A similar behavior is observed in this case as well with ZnO and $SrTiO_3$ caps behaving as intermixing inhibitors, particularly in the intermediate annealing range of 750 to 800 ^{o}C. While TiO_2 and Al_2O_3 behaved as the intermixing promoting caps along with the classical SiO_2 cap.

3.2 Quantum Dots Intermixing (QDI)

In our QDI study, seven SAQD samples are prepared using different capping material and with various deposition techniques. They are summarized as follows: (i) 300°C PECVD of 200nm thick SiO_2 and 100nm thick Si3N4 caps; (ii) 160°C ALD of 100nm ZnO, TiO2 and Al_2O_3 caps; and (iii) 300°C PLD of 100nm $SrTiO_3$ and HfO_2 caps. Since the effect of SiO_2 capping layer thickness beyond 100nm does not appreciably change the In – Ga intermixing process in InGaAs/GaAs SAQDs and multiple quantum well system (with GS PL emission shift within an error margin of ± 15 meV). Our comparison of SiO2 with other 100nm thick capping layers is reasonable [35, 39] these samples are then subjected to rapid thermal processing (RTP) in nitrogen ambient at temperature values of 650 to 725°C in step of 25°C for 120s, and under. As over-pressure, provided by GaAs proximity cap, to minimize arsenic desorption during annealing. A fixed excitation power density of 2.3kW/cm2 is used for the rest of PL measurements to evaluate the degree of bandgap shift, and with a short wavelength detection limit of 1000 nm.

3.2.1 Plasma-enhanced Chemical Vapor Deposition grown SiO_2 and Si_3N_4

Figure 3-1 (a) and (b) show the normalized 77K PL spectra obtained from the PECVD SiO_2 and Si_3N_4 capped SAQD samples at different annealing temperatures. Also, PL spectrum of the AG sample is included for reference as well. Notice in Figure 3-1 (a) that by increasing the annealing temperature of SiO_2 capped samples from 650 to 725°C caused a gradual blue shift in the QD (PL) as compared to the AG SAQD sample. This implies IFVD facilitated Ga vacancies started to promote intermixing right from low annealing temperatures [34]. In addition PL intensity improvement (*Table 3-1*) and decrease in the SAQD PL linewidth (Figure 3-1(c)) is noted which is ascribed to the improved dot size homogeneity and reduction in the grown-in-defects due to low-temperature growth of QDs . From Figure 3-1 (c), a GS differential shift of ~145nm (red arrow) was observed between the AG and 725°C annealed SiO_2 sample, with associated linewidth reduction to ~25 nm (~40% of the AG sample, obtained via Gaussian fit). The PL peak intensity improvement was also found to improve by > 2 times of the AG sample, as shown in Table 3-1. In general, the successive QD bandgap shift with increasing annealing temperature is significantly attributed to the effective sinking of Ga by SiO_2 film and enhanced vacancy diffusion deeper into the sample due to high compressive strain developed at SiO_2/GaAs interface and weakly to the thermal annealing effect. It is also worth mentioning that higher annealing temperatures reduced the inter-sublevel energy spacing of QD GS and ES emissions with observation of single emission peak at 725°C, possibly due to masking of the ES emission by the dominant GS peak or by the detection limit of our PL system. However, in the case of Si_3N_4 capped sample at 725°C, as illustrated in Figure 3-1 (b), a clear two-peak QD (PL) is visible. This implies a comparatively slow inter-diffusion rate offered by Si_3N_4 film, and is further substantiated by overlapping PL spectrum of 650°C annealing temperature sample with the AG sample. In other words, Si_3N_4 layer work as a control cap to partially inhibit diffusion of vacancies in the SAQD structure at this particular temperature (650°C). We postulate that small group-V out-diffusion from the Si_3N_4 capped sample might be responsible for suppression of inherent thermal shift [11], and negligible IFVD effect due possibly to inefficient Ga vacancies generation (insolubility of Ga or As atoms in Si_3N_4) and diffusion into the SAQD sample (smaller compressive stress at Si_3N_4/GaAs interface) at this low temperature [33]. Nevertheless, at 675°C and beyond, the PL spectra blue shifts in conjunction with narrow GS and ES PL linewidths, and reduction in their energy spacing, at high annealing temperatures, as depicted in Figure 3-1(c). This is indicative of enhanced interdiffusion mediated through competing thermal annealing and IFVD process. Note that our observations are in agreement with most reported results [11, 60, 62] on similar In(Ga)As/GaAs QD material system ,however, are These observations are in contrast to Wang et al [63]. Work which that reported a high degree of intermixing from Si_3N_4 cap compared to SiO_2 on InAs/InGaAlAs/InP QD-in-well material system, and attributed to dominant In out diffusion with respect to Ga .However, We believe Ga out diffusion to be dominant in our InAs/GaAs SAQD sample. Referring to

Figure 3-1(a) and (b), it is worth mentioning that selectively intermixing SAQD sample with Si_3N_4 and SiO_2 film at 650°C may result in ultra-broad simultaneous and comparable PL emission from QD GS and ES, with -3dB bandwidth spanning ~250nm. Devices exhibiting such broad emissions are highly attractive for applications in optical communications, such as broadband lasers, detectors, modulators, etc [9, 61] which is discussed later in this chapter. In addition, a blue shifted and broad emission with peak PL intensity at ES rather than GS with linewidth of ~78 nm is observed with Si_3N_4 capped SAQD sample at an intermediate temperature of 675°C (GS emission shoulder is still visible at ~1200 nm). In fact, analogous behavior is noticed in the PL results of other capping materials (HfO_2, Al_2O_3, ZnO, and TiO_2 caps) at low and intermediate annealing temperatures. We attribute this observation to an increased interface fluctuation between SAQDs and the surrounding matrix at low and intermediate temperatures, and possible defect annealing near the interface [11, 64]. This improved with increasing temperature as a result of higher In – Ga intermixing. The normalized integrated PL intensity and the GS peak PL intensity of Si_3N_4 and SiO_2 capping layers at different annealing temperatures are summarized in Table 3-1. The results suggest that the optical quality of the SAQDs is maintained at low and intermediate temperatures via possible reduction of the defect density and the non-radiative recombination centers. At a relatively high annealing temperature, the enhanced In – Ga intermixing resulted in improvement in the QD size distribution and the structural quality [63, 65].

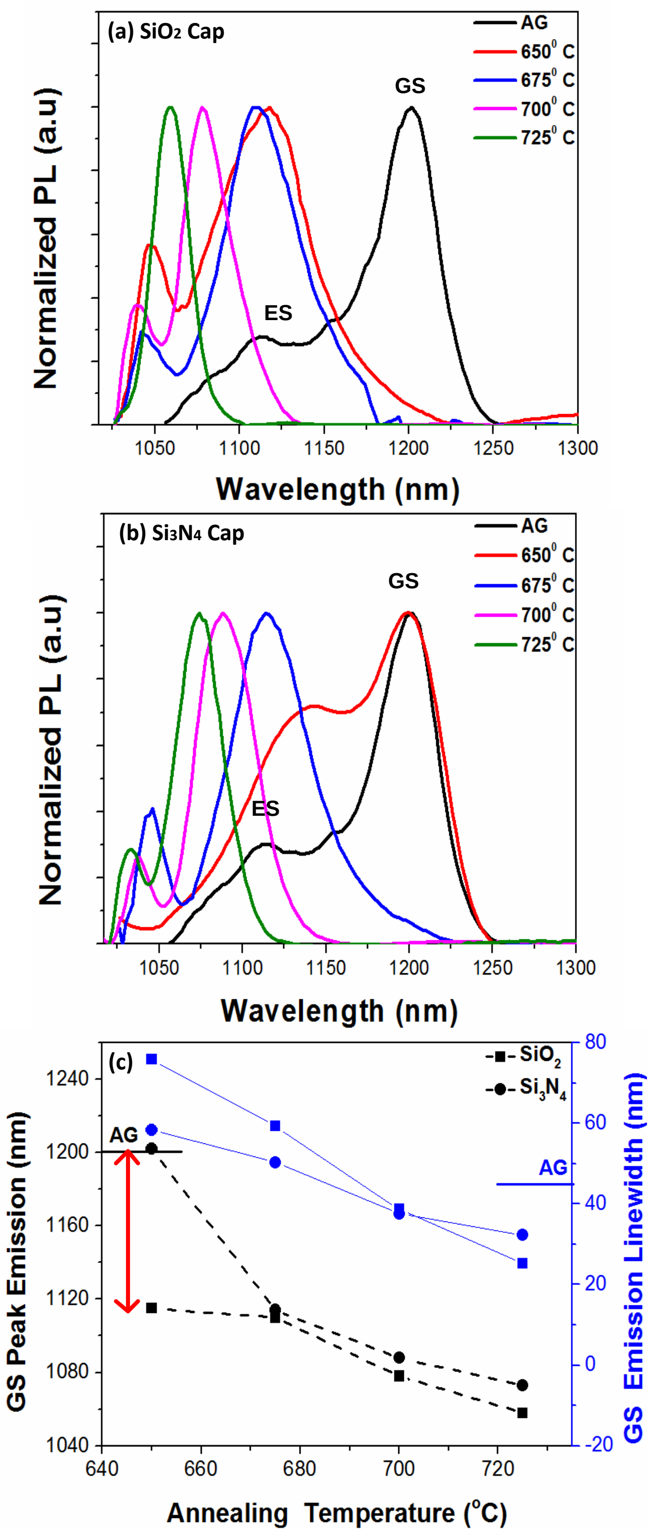

Figure 3-1: Normalized 77 K PL spectra obtained from the AG and annealed samples of InAs/GaAs SAQDs at different annealing temperatures for PECVD deposited (a) SiO_2 and (b) Si_3N_4 dielectric capping layers. (c) Summary of the corresponding change in GS peak emission and linewidth as a function of annealing temperatures. The solid horizontal lines near both the vertical axes of (c) correspond to the as-grown values.

Table 3-1:Summary of the GS peak PL intensity and the total integrated PL intensity (shown in the parenthesis), normalized to the as-grown sample's GS peak PL intensity and the total integrated PL intensity, respectively, at different annealing temperatures, and for different capping materials.

Annealing Temperature	SiO_2	Si_3N_4	HfO_2	$SrTiO_3$	Al_2O_3	TiO_2	ZnO
650°C	0.96 (2.39)	1.11 (1.07)	1.08 (0.75)	0.81 (0.84)	0.83 (1.76)	1.17 (1.71)	0.92 (1.38)
675°C	1.89 (0.98)	1.15 (1.57)	2.91 (3.01)	0.97 (0.97)	---- (----)	2.72 (2.36)	1.10 (1.40)
700°C	2.94 (2.26)	2.83 (2.33)	3.97 (1.05)	0.71 (1.02)	2.60 (2.53)	3.00 (2.13)	1.18 (1.43)
725°C	3.25 (1.46)	2.22 (1.55)	6.09 (1.69)	1.13 (1.57)	2.80 (2.10)	3.22 (1.83)	2.46 (1.86)

3.2.2 Pulsed Laser Deposition Grown HfO_2 and $SrTiO_3$ Caps

Figure 3-2 (a) and (b) shows the PL spectra of the samples capped with 100nm PLD HfO_2 and $SrTiO_3$ caps at different annealing temperatures. The corresponding changes in the peak GS emission wavelength and PL linewidth are summarized in Figure 3-2 (c). The HfO_2 capped sample shows inhibition to intermixing at 650^oC with no differential shift in the GS peak emission. The ES PL intensity is found to increase in this case, similar to the Si_3N_4 capped samples at intermediate temperature. Apart from possible defect annealing near the QD/barrier interface [11], we attribute this observation to the minor outdiffusion of Ga from smaller size QDs in particular due to comparatively larger surface to volume ratio, than larger size QDs, at low annealing temperatures [63]. As the temperature is increased to 675^oC and to 700^oC, a high degree of intermixing with a differential GS PL peak shift (compared to AG sample) of ~175nm was noted. Moreover, observation of ~4.0 (2.5) times increase (decrease) in the GS peak PL intensity (linewidth) compared to the AG sample further substantiate this material being a highly efficient intermixing cap, as summarized in Table 3-1. Note that IFVD effect saturated at 700^oC with no further blue shifting of the GS (PL) peak beyond this annealing temperature. Moreover, a single peak emission at 725^oC possibly indicates merging of GS and ES emissions. The PL linewidth at this annealing temperature was found to be similar in value (~18nm) compared to the 700^oC annealed sample except with an increase in the peak PL intensity (~50%) and comparable integrated PL intensity. This might be due to complete inhabitation of intrinsic defects, possible oxygen vacancies, in the 100nm thick HfO_2 film by Ga outdiffusion [66]. In addition, the alteration of strain at the HfO_2/GaAs interface (possibly from thermal matching to tensile strained GaAs surface region) at elevated annealing temperatures could also play a role in suppressing interdiffusion process [60, 62]. A selection of a thick HfO_2 capping layer would probably enable observation of intermixing effect beyond 700°C. In general, annealing SAQD samples with SiO_2 and HfO_2 caps enhanced the QD luminescence with spectral narrowing and has been attributed to the improvement in the QD inhomogeneity. On the contrary, dissolving of QDs into QD-QW metamorphic structure (two dimensional-like system) at high temperatures is also possibly due to strong lateral In-Ga interdiffusion in the three dimensional QD structures, and might lead to improved material quality, as has been indicated in refs [61, 67]. In either case, an emission window of 1030 – 1060nm at 77K translates to ~1100 – 1160 nm at room temperature (RT). Hence, employing high temperature (>700°C) annealed SiO_2 or HfO_2 capped SAQD lasers with superior characteristics would enable realization of frequency–doubled green–orange–yellow band lasers [55]. Alternatively, SAQDs deposited with the $SrTiO_3$ film is found to be a highly effective cap for intermixing suppression, as depicted in Figure 3-2 (b). A remarkable inhibition to the thermal shift and Ga vacancy diffusion up to 700°C is demonstrated with a mere ~16nm GS differential shift compared to the AG sample. Moreover, the PL intensity and the PL linewidth are found to be analogous to the AG sample, thus representative of preserving the optical quality of the annealed samples, as depicted in Table 3-1. We postulate that a high degree of tensile stress created at the $SrTiO_3$/GaAs interface impede the down diffusion of Ga vacancies and thus inhibit group-III intermixing between QDs and surrounding barrier layers. A large thermal expansion coefficient of the $SrTiO_3$ cap, which is ~ 22% larger than the typical TiO_2 cap, further upholds our postulation [60]. On the other hand, $SrTiO_3$ may also cause reduction of Ga vacancies generation due possibly to various factors during annealing such as layer quality, diffusion of inherent defects and the metallurgical reaction between GaAs and $SrTiO_3$ films [62]. Note that, at 725°C, a PL blue shift accompanied by a broad emission with peak at ES rather than GS (shoulder at longer wavelength region) is observed, indicating that the limit for intermixing inhibition is up to 700^{o}C. We postulate that the emission peaks observed at 1125 nm and 1050 nm is from the GS and ES of highly interdiffused QDs with small sizes and the long wavelength shoulder to the GS emission of least interdiffused QDs with larger size where the interdiffusion is minimal. We also believe that the shift in the GS peak emission wavelength at 725^{o}C is also controlled by the intrinsic thermal annealing induced disordering effect [11].

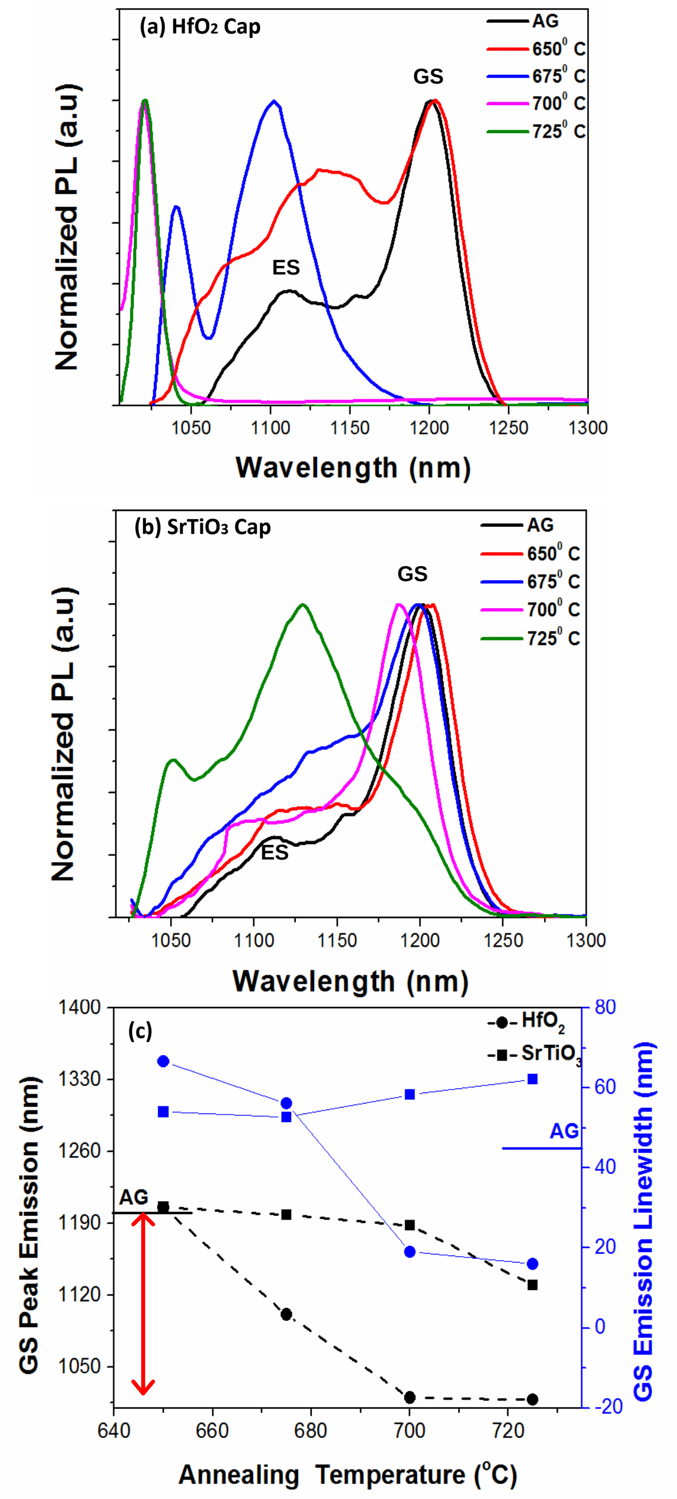

Figure 3-2: Normalized 77K PL spectra obtained from the as-grown and annealed samples of InAs/GaAs SAQDs at different annealing temperatures for PLD deposited (a) HfO_2 and (b) $SrTiO_3$ dielectric capping layers. (c) Summary of the corresponding change in GS peak emission and linewidth as a function of annealing temperatures. The solid horizontal lines near both the vertical axes of (c) correspond to the AG values

3.2.3 Atomic Layer Deposition Grown Al_2O_3, ZnO, and TiO_2 Caps

Low temperature PL spectra of ALD deposited Al_2O_3, ZnO and TiO_2 capped SAQD samples at annealing temperatures from 650°C to 725°C, are plotted in Figure 3-3 (a), (b), and (c), respectively. For all capping materials we observed inhibition of intermixing at low annealing temperature of 650°C, similar to the Si_3N_4, HfO_2, and $SrTiO_3$ caps, and the same reason holds for these ALD grown dielectric films. As the annealing temperature is increased beyond 650°C, a progressive blue shift in the GS peak PL emission is observed in all three (Al_2O_3, ZnO and TiO_2) samples, as shown in Figure 4(d). In all the cases, an improvement in the material quality is noted and the results are summarized in Table 3-1. However, GS and ES peaks did not merge in all the three capped samples even at the highest annealing temperature of 725°C. Distinct peak emissions from both the transition states are clearly observed in Al_2O_3, ZnO capped samples whereas the TiO_2 capped sample showed bimodal peak behavior, a result of reduction in the inter-sublevel energy spacing of QD GS and ES emissions. Nonetheless, the TiO_2 film showed the highest degree of intermixing when compared to the other two ALD films with a GS peak blue shift of ~165 nm and similar PL linewidth value compared to the AG data, as elaborated in Figure 3-3(d). This observation is most likely due to our ALD technique which might alter the film porosity and thus promote intermixing [33], as compared to the literature [60, 61] where e-beam evaporated TiO_2 film was shown to inhibit intermixing. On the other hand, 675°C and 700°C annealed ZnO capped samples showed a small GS wavelength blue shift of ~32nm compared to the AG sample indicative of partial inhibition of IFVD process. However, the GS PL linewidth broaden at this temperature by ~40% (compared to the AG sample) and accompanied by increased luminescence from the ES of QDs. This suggests increased QD size and composition dispersion as observed in other PECVD and ALD samples. In general, at low annealing temperatures (650°C and 675°C) most of the capping layers showed increased GS PL linewidth which has been attributed to the interface fluctuation between SAQDs and the surrounding matrix, thus affecting the QD transition states. In addition, an inhomogeneous rate of In-Ga diffusion in different QD sizes given three dimensional and complex intermixing process, could also be ascribed for this observation [11]. In the case of the Al_2O_3 capped sample, typical blue shifting of the GS peak wavelength is observed with progressive narrowing and enhancement of the PL linewidth and intensity, respectively, with a maximum peak shift of ~ 125nm at 725^{o}C compared to the reference AG data. In general, this layer behaves similar to the other IFVD promoting caps (SiO_2, HfO_2, and Al_2O_3) and retains (improves) the optical quality of the material after low (high) temperature annealing, as illustrated in Table 3-1. A remarkable observation that is worth mentioning about this film is the broadened emission with equal intensities from both GS and ES transitions of QDs annealed at low temperature (650^{o}C), indicating increased compositional fluctuation at the interface between the QD and the surrounding matrix as compared to TiO_2 and ZnO capping, leading to a dispersive QD potential profiles, affecting in particular, the smaller dots with higher intermixing rate, as discussed earlier [68]. An ultra-broad PL linewidth of ~165 nm from this single capped low temperature intermixed SAQD structure, centered at ~1140nm is again highly attractive for bio-medical imaging, in the low-coherence interferometry systems such as (OCT) [9, 53].

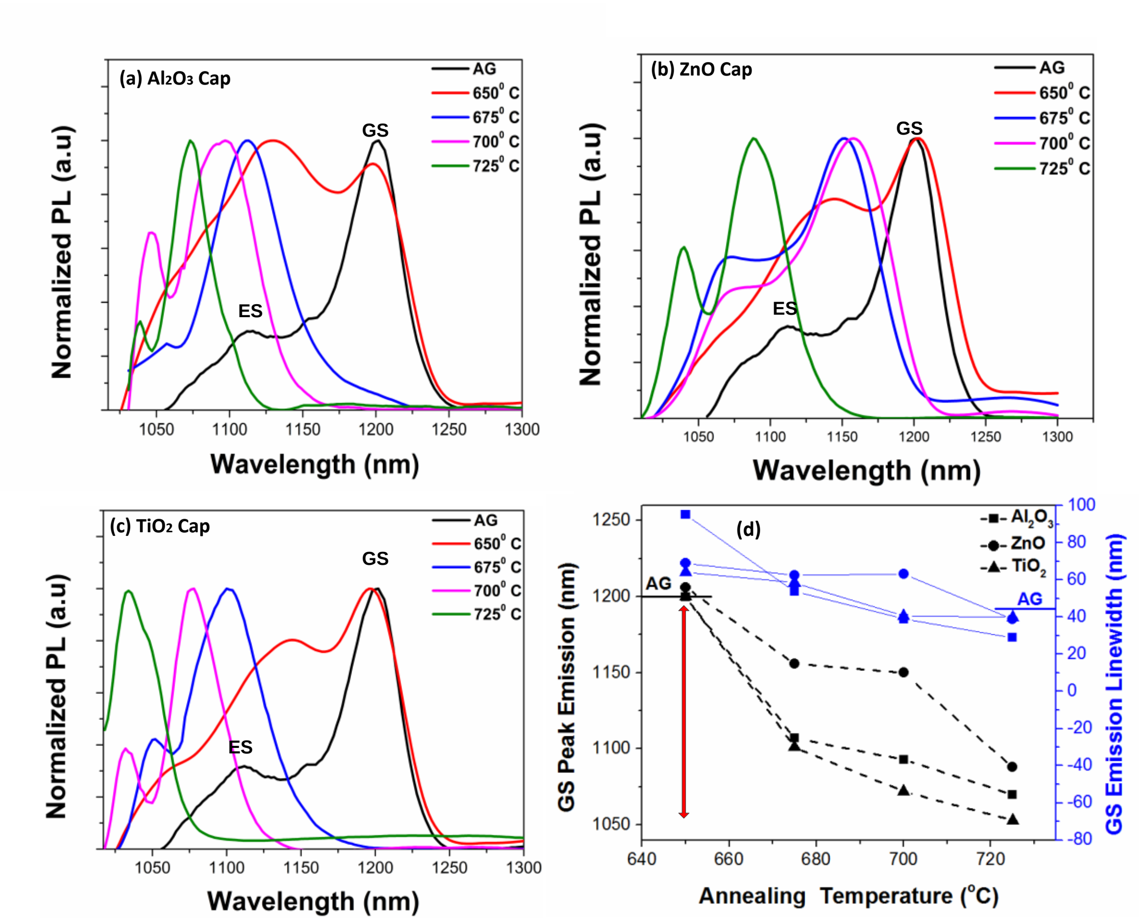

Figure 3-3 Normalized 77K PL spectra obtained from the as-grown and annealed samples of the InAs/GaAs QDs at different annealing temperatures for ALD deposited (a) Al_2O_3, (b) ZnO, and (c) TiO_2. (c) Summary of the corresponding change in GS peak emission and linewidth as a function of annealing temperatures. The solid horizontal lines near both the vertical axes of (d) correspond to the AG values

3.2.1 Comparative Study

To compare the performance of different capping layers, we extracted two parameters that characterize their degree of intermixing, namely, the intermixing rate (δE) and the critical temperature (T_C). Figure 3-4 (a)-(c) and Figure 3-5 (a)-(c) show the GS peak energy shift, and the energy separation between GS and ES (ΔE), extracted from the 77K PL spectra, as a function of annealing temperature, and corresponding to PECVD, PLD, and ALD deposited capping materials, respectively. The results are summarized in

Table 3-2. For simplicity in analysis, we selected the region that showed linear interdiffusion (promotion by all the samples except $SrTiO_3$ and ZnO which showed inhibition of interdiffusion) and ΔE behavior, for estimating δE and T_C [13, 34], respectively, with ± 20°C margin of error in the latter case (ΔE values are extracted from GS and ES Gaussian fittings). A reasonably good linear fitting is obtained in both the parameter extraction cases, as depicted in Figure 3-4 and Figure 3-5 with close agreement of T_C value obtained from linear interpolation and the experiments. For instance, possible merging of QD GS and ES emissions is observed in HfO_2 and with some uncertainty in SiO_2 and Al_2O_3 capped samples, at 725°C; meanwhile the corresponding extracted T_C values are 725°C, 770°C, and 788°C, respectively. The rate of intermixing is found to be highest for the HfO_2 film with δE = 3.7meV/°C and T_C = 725°C. Compared to SiO_2 film, an increase in δE by a factor of more than 3 (1.05 meV/°C for SiO_2) with similar T_C values is noted. This suggests that PLD HfO_2 cap has better capability to promote In-Ga interdiffusion between barrier layers and QDs compared to PECVD SiO_2 cap. A similar increase in δE value (by a factor of 2.5 – 4.5) is also observed on comparing HfO_2 capped sample with other IFVD promoting caps *i.e.* ALD deposited TiO_2 (1.46 meV/°C) and Al_2O_3 (0.77 meV/°C) films; the former latter also showing relatively higher degree of intermixing with larger (smaller) δE (T_C) values. This observation might most likely be attributed to the quality of the capping layer with possible increase in porosity for the PLD film compared to ALD caps, which changes the interdiffusion rate [33]. In contrast, the extracted slope of the linear fit for PLD $SrTiO_3$ capped sample data (within the linear region) with value δE = 0.31 meV/°C and covering higher annealing temperatures signifies strong IFVD inhibition compared to ZnO (0.22 meV/°C but obtained with smaller annealing temperature range) and Si_3N_4 (1.00 meV/°C) caps with similar predicted T_C value of 856°C (compared to 842°C and 822°C, respectively). Thus, $SrTiO_3$ is more attractive due to its ability to inhibit intermixing within larger and higher range of annealing temperatures. Note that Si_3N_4 dielectric layer, in our case, behaved more as an enhancing intermixing induced film rather than an inhibiting cap at high annealing temperatures, and is found to be in good agreement with other reports [11, 50, 63]. Another The possible reason for this efficient control of QD emission during IFVD process by using $SrTiO_3$ is the large tensile stress created at the surface, more than a factor of 2, compared to the ZnO and Si_3N_4 caps. This Following, this possibly resulted in more effective defect agglomeration and cluster formation [11]. The δE value of $SrTiO_3$ induced QDI is found to be one order of magnitude smaller than that of HfO_2 cap, providing a differential bandgap shift of ~175 nm between them. We also observed that in spite of δE value being similar for Al_2O_3, TiO_2, Si_3N_4 and SiO_2 (~1.0 ± 0.3 meV/^oC) capped samples, the extracted T_C value of TiO_2 and Si_3N_4 films are found be larger than the other capping layers. We postulate that the increased outdiffusion of Ga from small dots (dominating the ES emission) as compared to the larger dots (dominating the GS emission) might be responsible for this observation.

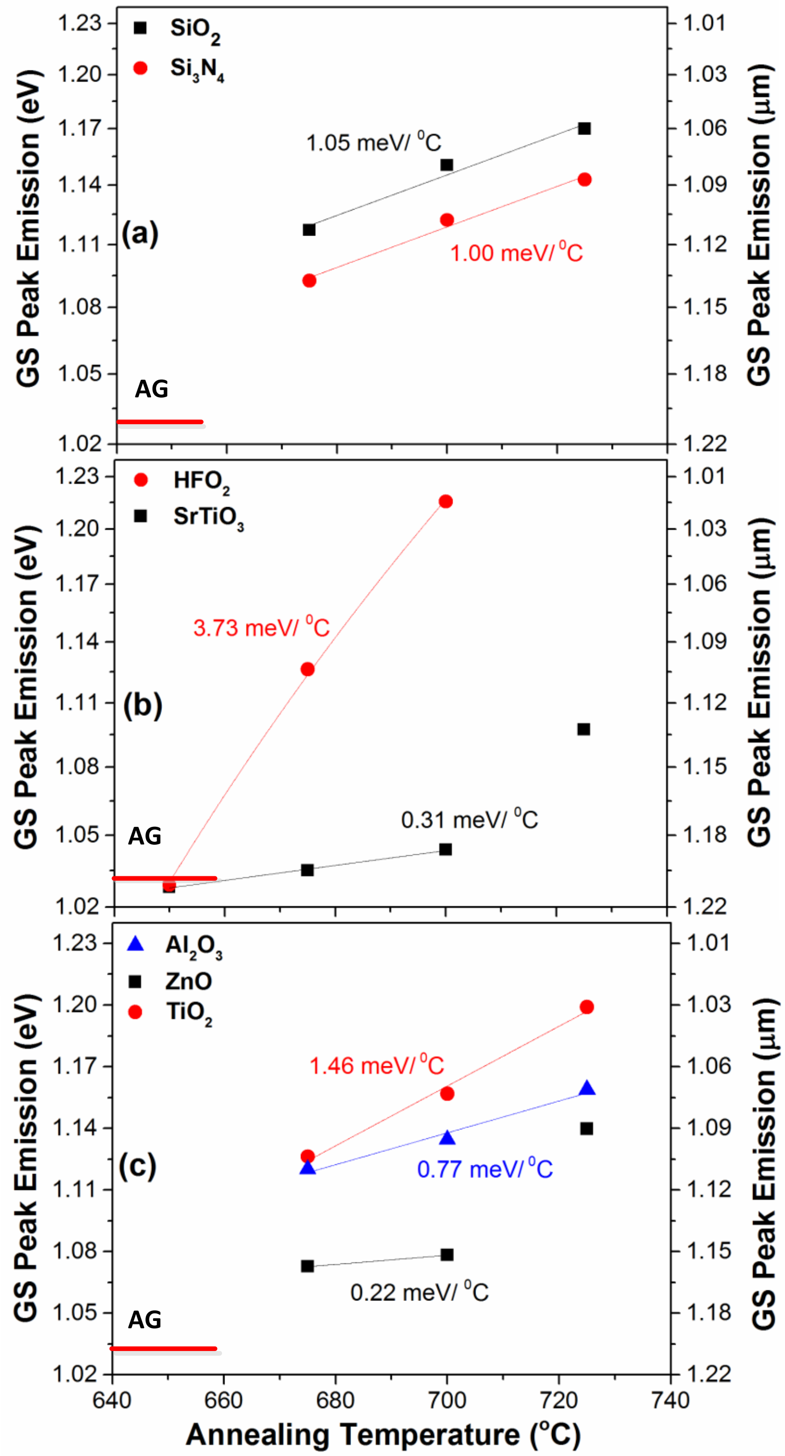

Figure 3-4: Linear fitting of the GS peak energy shift as a function of annealing temperatures for (a) PECVD grown SiO_2 and Si_3N_4, (b) PLD grown HfO_2 and $SrTiO_3$, and (c) ALD grown Al_2O_3, TiO_2 and ZnO capped InAs/GaAs SAQD structure, respectively. The slope of the linear fit provides the rate of interdiffusion δE. The solid horizontal line near the vertical axis corresponds to the AG GS peak energy.

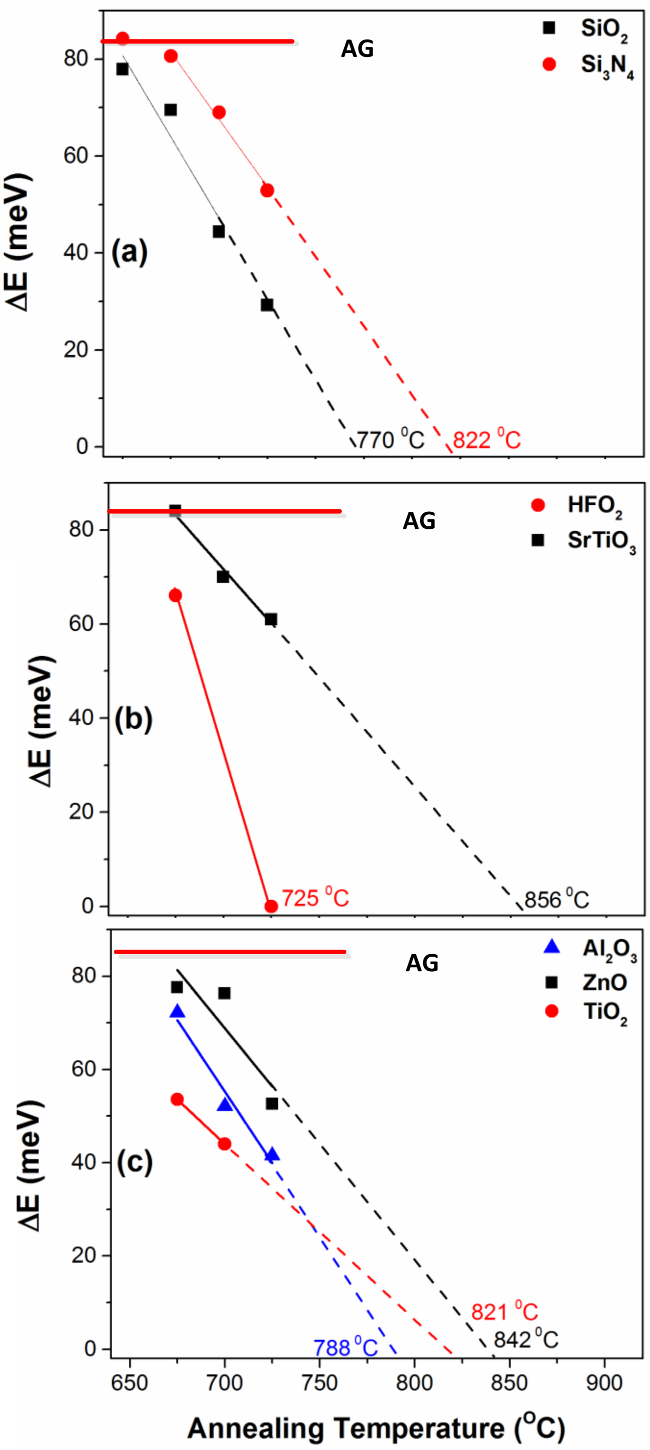

Figure 3-5: Linear fitting of the GS and ES peak energy separation as a function of annealing temperatures for (a) PECVD grown SiO_2 and Si_3N_4, (b) PLD grown HfO_2 and $SrTiO_3$, and (c) ALD grown Al_2O_3, TiO_2 and ZnO capped InAs/GaAs SAQD structure, respectively. The critical temperature T_C is calculated by subsequent linear extrapolation. The solid horizontal line near the vertical axis corresponds to the AG ΔE value

Table 3-2: Summary of the extracted δE and T_C values of different capping materials for InAs/GaAs SAQD degree of intermixing (DOI) assessment

Capping Material	Growth Technique	DOI parameters	
		δE (meV/°C)	Tc (°C)
SiO_2	PECVD	1.05	770
Si_3N_4	PECVD	1.00	822
HfO_2	PECVD	3.73	725
$SrTiO_3$	PLD	0.31	856
Al_2O_3	PLD	0.77	788
TiO_2	ALD	1.46	821
ZnO	ALD	0.22	842

3.2.2 Potential Applications

Our analysis of characterizing the degree of intermixing via δE and T_C qualitatively provides a series of data to exploit seven different capping layers as interdiffusion suppressors or promoters for various applications. In the following, we highlight three potential applications employing either one or combination of different caps:

(i) Bandgap engineered GS peak differential shift of ~35 meV between 675^0C annealed HfO_2 (or SiO2), ZnO, and $SrTiO_3$ capping layers could possibly be utilized in photonic integration for lasers (detectors), electro-absorption modulators, and waveguide (combiners), respectively, thus enabling various benefits such as excellent alignment, negligible reflection losses, and intrinsic mode matching [40, 47, 51]. Besides, a larger GS differential bandgap shift of ~50meV and ~80meV could also be achieved using HfO_2 - Al_2O_3 - $SrTiO_3$ combination at 700^oC and 725^oC annealing temperatures, respectively.

(ii) Ultra-broadband devices superluminescent diodes (SLD), laser diodes, SOA, photodetectors, modulators, etc.) might be realized employing multiple caps combination in addition to a single Al_2O_3 (650^oC); for instance, combination of $SrTiO_3$ - ZnO - Al_2O_3 - HfO_2 at 700^oC would provide a possible emission bandwidth of ~200nm centered at ~1100 nm. These ultra-broadband components are highly attractive for applications in optical communications, short pulse generation, tunable lasers, etc [45, 61, 69], besides serving as attractive compact broadband light sources for bio-medical imaging [53, 64].

(iii) Post-growth wavelength tuned SAQD lasers with 725°C annealed SiO_2 or HfO_2 or TiO_2 caps, with lasing wavelengths in ~1060 – 1200nm range, could potentially provide high power wide green – yellow – orange band coherent light by intracavity frequency doubling [55, 56] and use in pico-projectors. Moreover, the distinct advantages of reduced (J_{th}), temperature sensitivity, filamentation, and mirror degradation, in QD lasers, will enable realization of high –performance devices in this wavelength range compared to their InGaAs/GaAs and InGaNAs/GaAs multiple-QW laser counterparts [58]. Moreover, a bandgap tuned ~1064 nm QD laser could be used for injection seeding of typical Nd-Yag 1064nm solid-state laser [70]. Or It's as a substitute because of its small footprint, high power, and comparatively superior performance. The field of metrology and gas sensing would also benefit from the bandgap tuned ~ 1060 – 1200nm QD laser diodes in detection of water, HBr, HI, HCl molecules, ethanol and water in gasoline, etc. for process and environmental control [57, 71]. The low atmospheric absorption window of ~ 1000 – 1100nm will also enable deployment of post growth bandgap tuned QD lasers in LiDAR (light detection and ranging) systems where currently 1064nm Nd-YAG lasers dominate [72], besides free space optical communications.

3.3 Quantum Well Intermixing (QWI)

In QWI study also, the dielectric capping material growth techniques, conditions, and thickness, are similar to that of the QDI study, as discussed in the previous subsection. Figure 3-6 (a) shows the normalized 77K PL spectra obtained from the AG and annealed InGaAsP/InP QW samples at 800°C, and at an excitation density of 2.3 kW/cm^2. Notice that different dielectric caps resulted in various degrees of intermixing; for instance, 70 nm GS PL peak shift is achieved using TiO_2 material while ZnO cap showed only a 20 nm PL peak shift, compared to the AG sample. This suggests the former dielectric material working as intermixing promoter while the latter is suppressing the IFVD effect, at 800 ^{o}C. In general, this diverse behavior of IFVD process for different capping materials is attributed to the rate of In – Ga intermixing between the QW and the barrier layers, which in turn is a function of the various parameters such the compressive stress at dielectric/InGaAs(P) interface, deposition techniques, etc., as discussed in the previous section on QDI.

As a summary, Figure 3-6 (b) and (c) summarized the result of the GS PL peak emission and the PL linewidth, as a function of annealing temperature, for various encapsulates, respectively. It can be observed that at a low annealing temperatures (700 ^{o}C and 725^{o}C), the GS PL peak wavelength of different capped samples showed slight red shifted by 10 - 20 nm, compared to the AG sample. This is most probably due to the strain effect at the interface between the cap and InGaAs(P) layer. However, with increasing annealing temperature, a gradual blue shift of in QW GS PL peak wavelength is observed, for a majority of the capping materials. As discussed earlier, the largest PL peak wavelength shift of ~ 70 nm is achieved using aTiO$_2$ cap, while the Al$_2$O$_3$ and the traditional SiO$_2$ caps showed a blue shift of ~60 nm. This behavior is followed by a gradual reduction in the associated PL linewidths, as depicted in Figure 3-6(c). In general, increasing annealing temperature significantly improves the sinking of Ga by TiO$_2$/SiO$_2$/Al$_2$O$_3$ films besides enhanced vacancy diffusion deeper into the sample due to high compressive strain developed at dielectric/InGaAs(P) interface, as elaborated in the QDI section.

In the case of On the other hand, ZnO and SrTiO$_3$ capped sample, showed slowed inter-diffusion rate which is further substantiated by significantly overlapped respective PL spectra at 750^{o}C, 775^{o}C, and 800^{o}C annealing temperatures. A mere ± 15 (± 5) nm shift in the QW GS PL peak wavelength with associated PL linewidth variation of ± 5 (± 6) nm, corresponding to the ZnO (SrTiO$_3$) capped QW sample, is observed among the PL spectra at 750^{o}C, 775^{o}C, and 800^{o}C annealed temperatures. In other words, ZnO and SrTiO$_3$ material layers work as a control cap to partially inhibit the diffusion of vacancies in the QW structure at this particular annealing temperature range.

Another factor that can show the effect of intermixing clearly is the full-width at half maximum (FWHM). The behavior of the PL linewidth as a function of the annealing temperature, as illustrated in Figure 3-6(c), show a substantial reduction in value at an initial annealing temperature of 725^{o}C. In fact, an average reduction by 35% is observed compared to the AG PL linewidth. This implies that the quality of the material improved and remains high after the initial annealing temperature. However, the PL linewidth degrades at the intermediate temperatures, similar to the observation in QDI case, which has been attributed to the compositional fluctuation at the interface between the QW and the surrounding layers. Moreover, it can be observed that the IFVD promoting caps (TiO_2/SiO_2/Al_2O_3) showed a continuous improvement (i.e. reduction) in PL linewidth with increasing annealing temperature up to 800 ^{o}C, thus corroborating that the material quality is being maintained or improved. In contrast, the PL linewidths of samples capped with $SrTiO_3$ and ZnO showed 5% (20%) variation compared with the AG sample, up to 800 ^{o}C, an indication of a superior intermixing inhibitor that maintains the QW GS PL peak wavelength similar to the AG sample, and without degrading the material quality This makes these capping layers highly attractive for PIC applications. For instance, utilizing ZnO and SiO_2 (or TiO_2) a differential PL peak energy shift of ~50 nm could be achieved employing an annealing temperature of either 775 ^{o}C or 800 ^{o}C. A differential PL peak energy shift of ~ 25 nm could be achieved with ZnO - $SrTiO_3$, and $SrTiO_3$ - TiO_2/Al_2O_3, at 800 ^{o}C. The latter possibility is highly attractive in achieving three different QW GS PL peak wavelengths on a single wafer, seamlessly, if annealed at 800^{o}C.

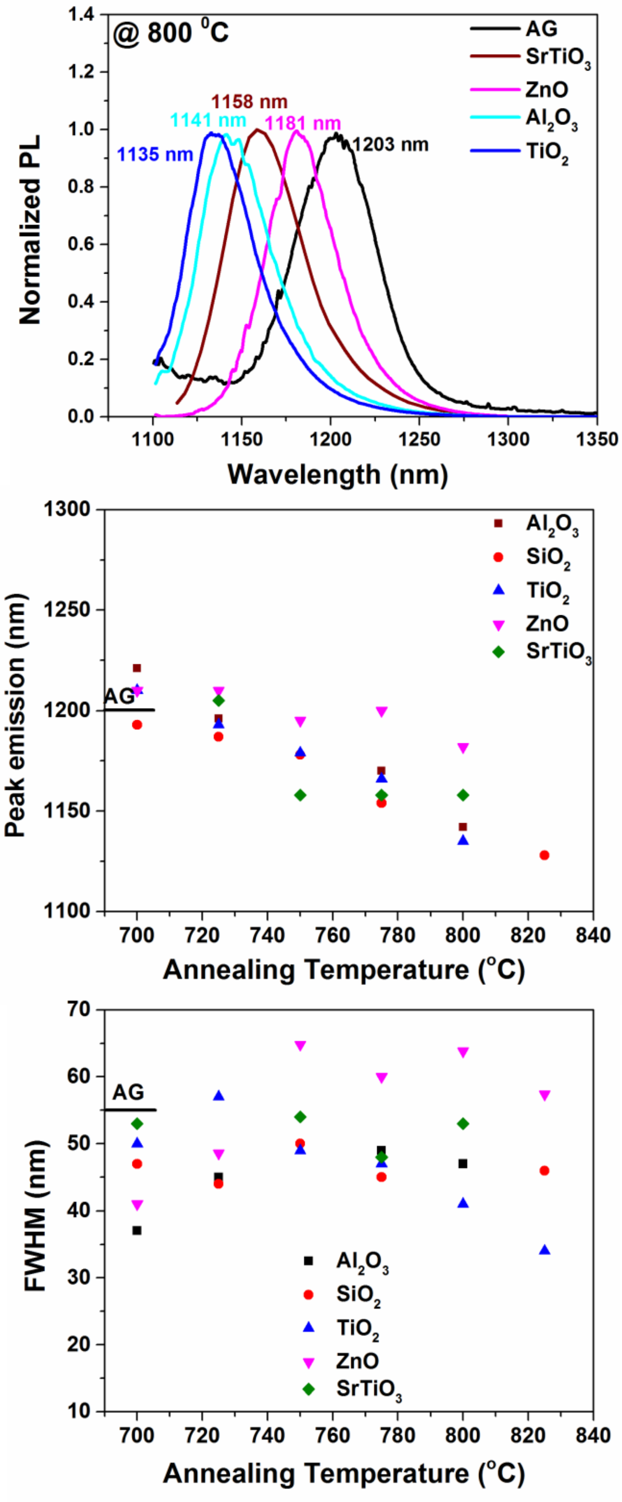

Figure 3-6: Normalized 77K PL spectra obtained from the AG and annealed samples of InGaAsP/InPs QW structure at 800 ^{o}C annealing temperature. Summary of the corresponding change in: (a) GS peak emission, and (b) PL linewidth, as a function of annealing temperature. The solid horizontal lines near the vertical axes of (b) and (c) correspond to the AG values.

3.4 Summary

We have demonstrated the viability of the IFVD process on InAs/GaAs SAQDs SAQD and InGaAsP/InP QW structures by various dielectric capping materials. With emission wavelength trimming to ~ 1100–1200 nm, in the former case, for potential realization in photonics integrated circuits and post-growth wavelength tuned optoelectronic devices. Compared with the traditional dielectric capping layers, we presented HfO_2 and $SrTiO_3$ as potential candidates for tailoring the bandgap properties of QDs with superior optical properties. The corresponding extracted interdiffusion rates in these materials of HfO_2 and $SrTiO_3$ were found to be 3.73 and 0.31 meV/°C, respectively. These rates are significantly higher than those for common SiO_2 and Si_3N_4 dielectric films. Moreover, the assessment of other uncommon dielectric capping layers, such as TiO_2, Al_2O_3, and ZnO, were also performed, revealing attractive features and thus increasing the flexibility in capping layer selection for selective bandgap engineering for a plethora of multidisciplinary applications. In general, all of the films exhibited linewidth narrowing and peak/integrated PL intensity improvement after annealing, thus suggesting enhanced material quality.

4 INTERMIXED QUANTUM DOTS LASER CHARACTERIZATION

4.1 Introduction

The study of Self- assembled quantum dots (SAQDs) has attracted considerable interest in the field of high-performance optoelectronic devices fabrication. SAQDs were selected due to the superior properties such as temperature stability, low (J_{th}), high-speed operation, and low frequency chirping [11, 34] .

For certain optoelectronic devices applications, such as mode locking, fiber-optic sensing, and optical coherence imaging [50]. The three-dimensional carrier confinement is essential for gaining higher performance. This can be provided by using QDs as an active media in these devices. Optoelectronic devices require compact size, high speed, and low optical losses in the integrating circuit. This integration can be achieved among integrated several QDs devices on a single chip producing several wavelengths [73]. In the previous chapter, we highlight the simple method used to achieve that.

Most of the studies and best practices emphasize that, maintaining the high quality of the intermixed materials is challenging and essential to avoid any modification in the laser characteristics after intermixing [9, 10]. In this work, I was able to maintain high quality of intermixed materials which led to improved laser characteristics. This achievement was due to careful engineering of the atomic composition, atomic ordering, and the degree of strain between the (QDs) and quantum barriers. Based on Material characterization results in chapter 3 two intermixed samples (Si_3N_4, SiO_2 caps /annealed @725^oC) was chosen, followed by fabricated them as Broad area laser using standard recipe written in Appendix C. In this chapter, intermixed laser diodes are tested and characterized, followed by a detailed comparison highlighting the significant results. In particular we demonstrated lasing at ~1070-1190 nm from intermixed sample while preserving the device characteristics.

4.2 DC Characteristics

To determine the effect of intermixing, lasing from single facet output power – current (P-I) curves were measured and plotted. Figure 4-1 (a,b,c) shows the AG, those annealed (SiO_2 and Si_3N_4 capped), at 725˚C for 120 s. In Figure 4-1 (a), the P-I was measured for L=3 mm, and the obtained I_{th}, of the AG laser for a GS lasing is 900 mA. The device annealed exhibit an I_{th} of 1170, and 2100 mA, for SiO_2, Si_3N_4 respectively. The I_{th} was found to be increased if the degree of intermixing increased. In chapter 3, we conclude that the SiO_2 capped annealed laser sample shows a higher degree of intermixing than the Si_3N_4 capped annealed laser sample. Therefore, the I_{th} shows a higher value in the SiO_2 capped annealed laser. This variation of the I_{th} value was attributed to the effect of intermixing in decreasing the confinement energy which causes the spillover of the injected carriers. As a result of spill-over the modification of bandgap energy takes place due to atoms inter-diffusion in the active region. The bandgap shift at room temperature is obtained from the AG, and annealed (SiO_2 and Si_3N_4 capped) samples. the spectra shows room-temperature lasing at ~1300 nm, ~1123nm, and ~1190 nm for AG,SiO_2 and Si_3N_4 samples. Further details are discussed in subsection 4.3.1.

Figure 4-1 (b) shows a decrease in the I_{th} at L=1000 µm compared with L=3000 µm, and the corresponding I_{th} values are 340, 610, and 860mA, with a tuned lasing wavelength up to 180 nm. At smaller cavity length of 500µm, the Si_3N_4 shows higher threshold (I_{th}) as compare to SiO_2. This observation does not match with the trend in the degree of intermixing effect explained previously. That trend is attributed to the switch of the lasing wavelength from GS to ES in the SiO_2 capped sample in this particular length, while the Si_3N_4 capped sample maintaining lasing from the GS.

From the DC characteristics, important laser parameters are extracted and discussed in the next sections. The definition of the laser parameters are given in Appendix B.

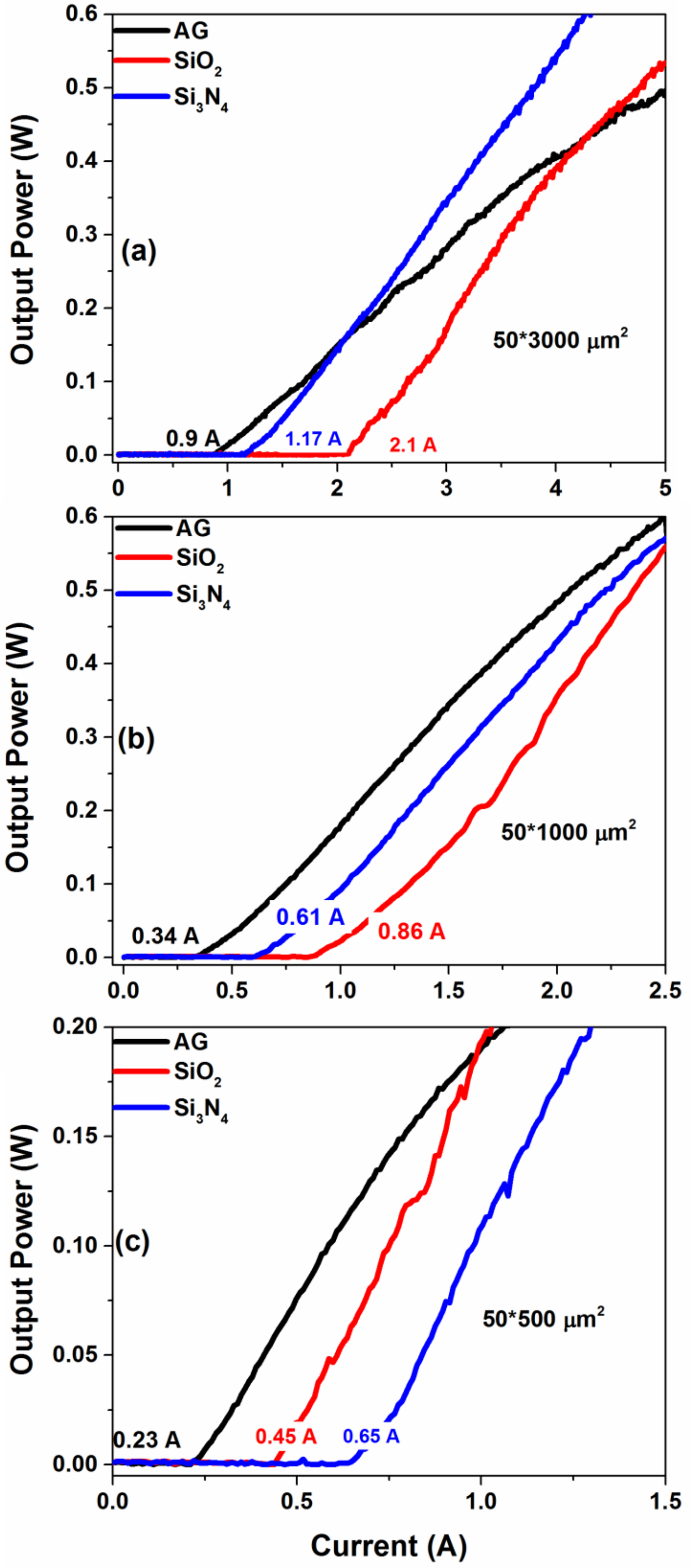

Figure 4-1: Room temperature L-I characteristics of (a)50×3000 μm^2 (b) 50×1000 (c) 50×500 μm^2 broad area AG and annealed laser diodes under a pulsed current operation.

4.2.1 Transparency Current Density (J_0)

The extracted transparency current density (J_0) from the inverse cavity length versus J_{th} for AG and those annealed (SiO_2 and Si_3N_4 capped) is shown in Figure 4-2 . As shown in this figure, J_0 gives a value of ~330 A/cm^2 for the AG devices (black line) and ~600 A/cm^2 for the annealed devices of SiO_2 (red line) and Si_3N_4 (blue line). At a short cavity length of ≤250 µm, J_{th} shows a significant increase with values up to three times higher than that at a long cavity length. This high value is due to an emission from ES lasing. The increase in the J_0 value could be attributed to many reasons, including the reduction in the optical confinement factor and being a consequence of the QD size reduction. In addition, J_0 increase due to the weakly localized QD layers as a result of shallow conduction band offsets [6-8]. The reduction in gain and the increase in optical loss may be the other factors affecting the increasing J_0. Further details will be discussed in the gain calculation section.

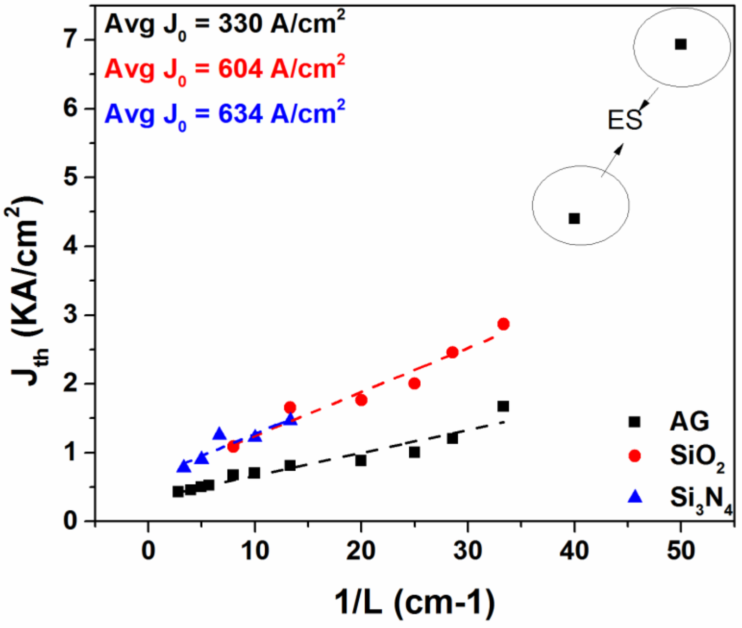

Figure 4-2 Threshold current density, J_{th}, versus the inverse cavity length, 1/L, for lasers of different cavity lengths for AG, SiO_2, and Si_3N_4 Caps Annealed laser.

4.2.2 External and Internal Quantum Efficiency (η_{ext}, η_i) and Internal Loss (α_i).

In Figure 4-3, η_{ext} vs. L values have been plotted for three devices, and α_i and η_i have been calculated. An improvement in η_i from 87% (AG) to 93% (SiO_2) noted, and for (Si_3N_4) 86.6% is deduced. A small increase in α_i from 4.4 cm^{-1} (AG) to 5.2 cm^{-1} (SiO_2) and 6.3 cm-^{1} (Si_3N_4) is noted. We attribute the improvement in η_i to the annealing of the defect at high temperatures near the QD–barrier interface. Due to a low-temperature growth and a high-stress field around QDs, the non-radiative recombination is reduced [9]. Several researchers used this technique to improve the quality of this device [74]. The unique contribution of our results is that we could preserve the device performance while tuning the lasing wavelength.

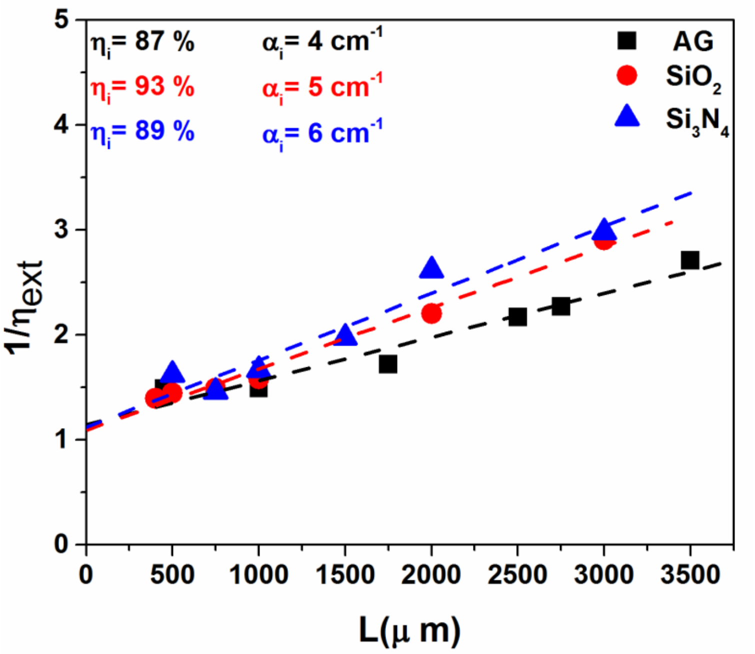

Figure 4-3: Room temperature inverse external efficiency as a function of devices length for AG, SiO_2, and Si_3N_4 annealed lasers.

4.2.3 Characteristic Temperature (T_0)

A single facet output power – current (P-I) curve has been plotted for AG, annealed lasers in a temperature range between 14˚C and 75˚C, *Figure.4-4* (a,b,c)., By comparing three lasers behavior, it is clearly observed that the increase in J_{th} in annealed lasers is comparable with AG. To clarify the effects, ln(J_{th}) vs. T was plotted in *Figure.4-4* (d). The AG laser diode exhibited a (T_0) of ~300 K from 15˚C to 60˚C. This value is found to be decreased considerably at ~65 K in the SiO_2 annealed laser and further down to ~55 K in the Si_3N_4 annealed laser diode within the same temperature range. A substantial blue shift in the lasing wavelength dictates a significant increase in the GS transition energy of the QDs. Effectively reducing the conduction band offsets and hence promoting thermal injection in the QDs [8].

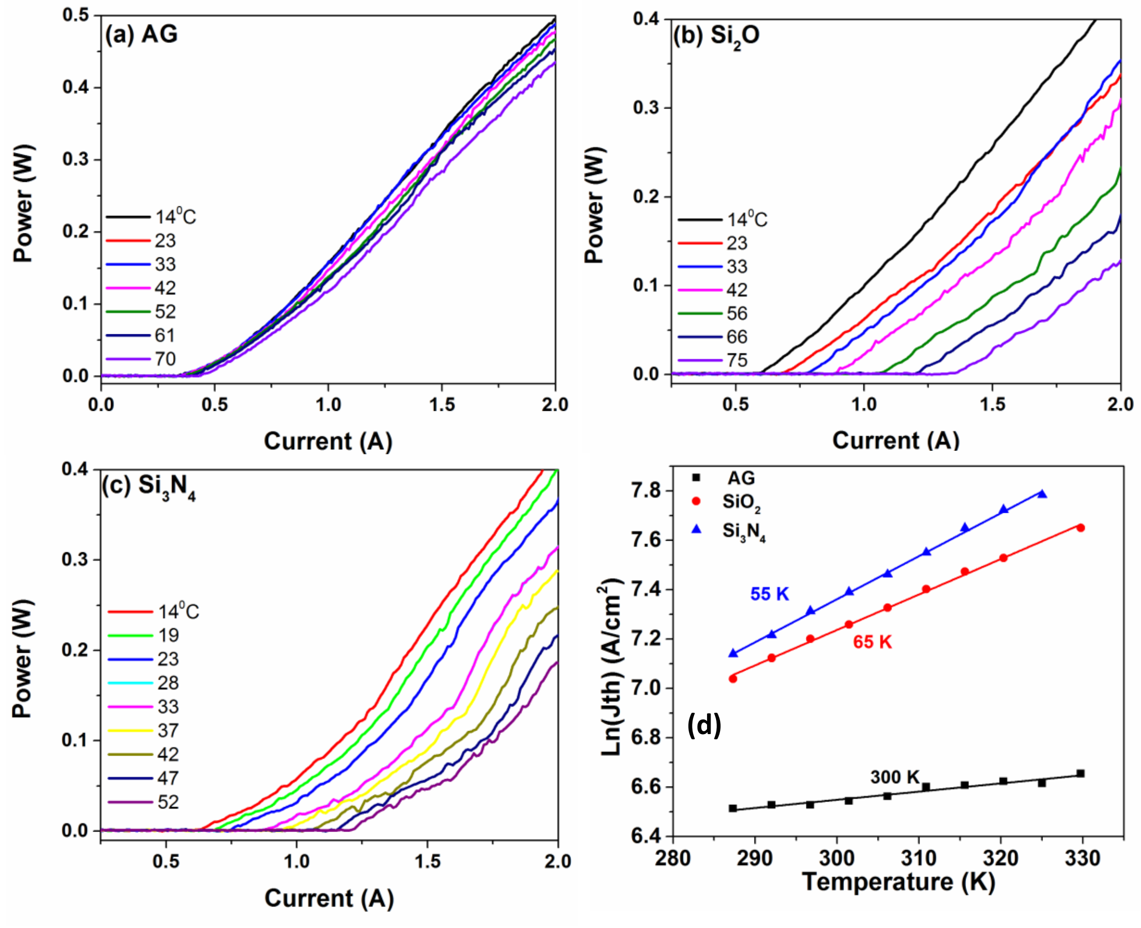

Figure.4-4: (L-I) Curve, and temperature dependent for (a) AG, (b) SiO_2 cap annealed, and (c) Si_3N_4 cap/annealed. (d) A summary graph of logarithm of (J_{th}) *as a function of temperature for three devices.*

4.2.4 Modal Gain

By plotting the cavity lengths depending on lasing wavelength for AG and those annealed (SiO_2 and Si_3N_4 capped) QD lasers at room temperature, we can predict the changes in QDs gain as shown in Figure 4-5.

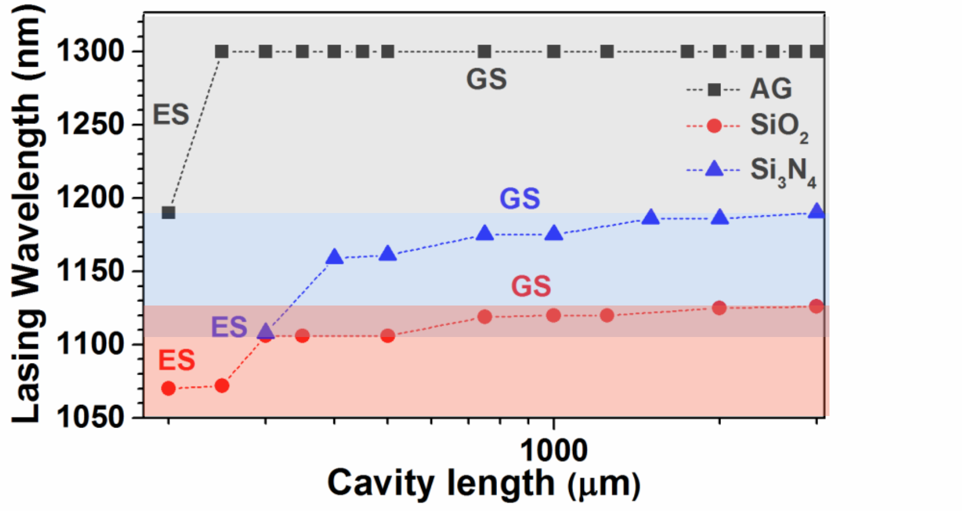

Figure 4-5: Cavity length vs. lasing wavelength for the AG and 725°C annealed SiO_2 and Si_3N_4 capped QD lasers at room temperature.

By comparing the three curves in *Figure 4-5* it is observed that lasing from ES at larger cavity lengths than the one in AG laser, which means in annealed sample GS saturated in cavity lengths larger than the one in AG. Laser with Si_3N_4 capping, showing the lasing from ES, where with the same cavity lengths AG and SiO_2 capped leased from GS. The net modal gain-current density curve is shown in Figure 4-6. The dependence of the gain on current density is one of the main characteristics of the active medium in an injection laser, closely related to the electronic structure of the active region. From the figure we observe two regions of different gain behavior. And Both can be fitted by an empirical equation. The ground state saturated net gain in this case is 50, 45, 35 cm^{-1}. For AG, and SiO_2, Si_3N_4 respectively. And the excited state net gain shows higher value is 64, 65,46 cm^{-1} respectively. Adding the internal loss to the gains values will easily help to extract the saturated modal gain for the respective states. A zero gain can be estimated at J=J_0. The J_o values are comparable with the value calculated previously in this chapter.

In summary the parameters of AG, and intermixed laser samples (Si_3N_4,SiO_2Caps /Annealed @725°C) is considered in Table 4-1.

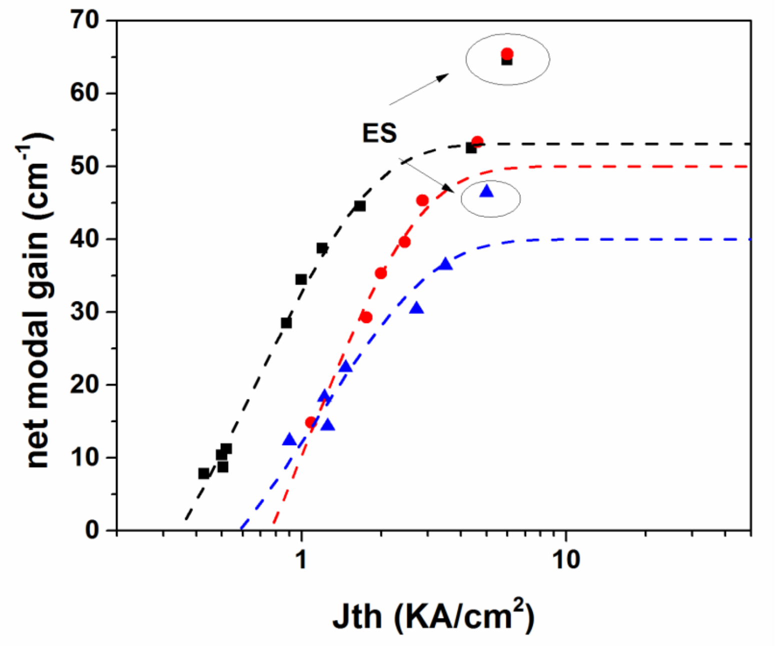

Figure 4-6 Net modal gain versus threshold current density spectra of AG, SiO_2, Si_3N_4 capped samples, all annealed at 725°C.

4.3 Analysis of Lasing Spectra

4.3.1 Tuned Lasing Emission

Intermixing was proved and considered to be as a promising technique for shifting the lasing wavelength. By carefully choosing the intermixing condition, the degree of intermixing can be controlled as discussed in subsection 3.2.1. Figure 4-7 (a,b,c) shows the lasing spectra for AG and tuned lasers using SiO_2, Si_3N_4 for three different cavity lengths, 3000, 1000, and 500 µm, respectively. In general for the three cavity lengths, wavelength shift is as large as 188 nm obtained by using for SiO_2 capped laser sample at 1mm length. with a L = 3000 µm In Figure 4-7 (a), the shift was measured to be 117 nm between the AG and Si_3N_4 laser, whereas this shift value increases up to 130 nm for

L=1000 µm, as shown in Figure 4-7 (b), and reached up to 140 nm for L=500 µm. In summary, Si_3N_4 shows increased variation in its shifting with different cavity lengths than the one using SiO_2, which indicates that the enhancement in shifting is attributed to the rise in the gain for a small cavity length, leading to lasing from the ES instead of GS, as small as larger shift is observed as compare to AG.

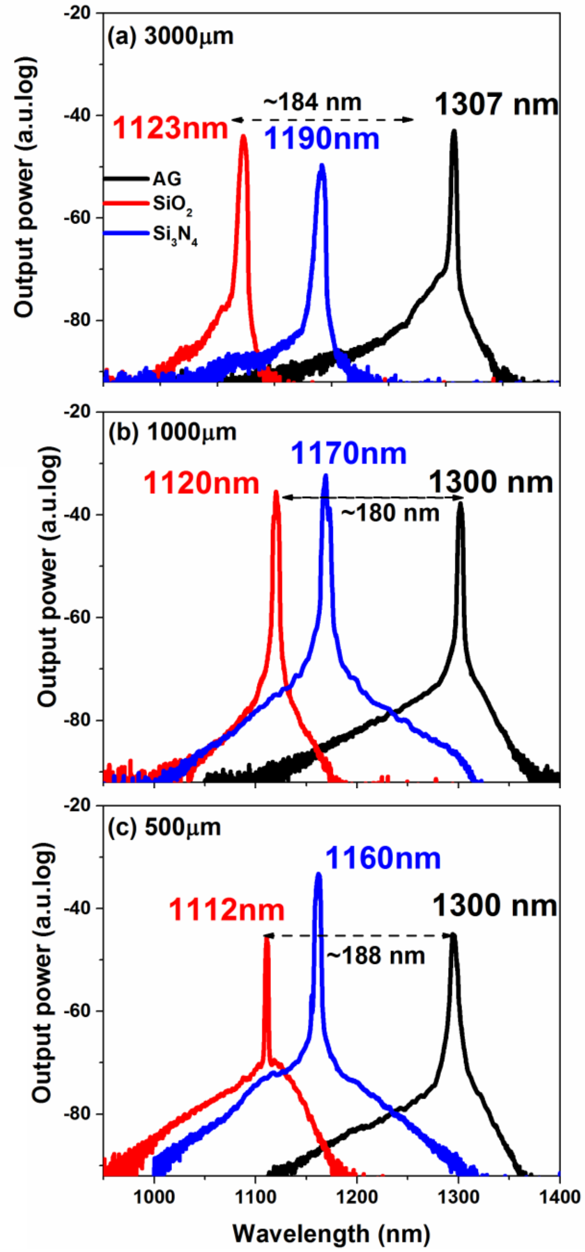

Figure 4-7: lasing wavelength for AG samples annealed at 1.5 I_{th}, with cavity length (L) of: (a) 3000 µm, (b) 1000 µm, and (c) 500 µm.

To further study the lasing from ES in small cavity length, we plot the spectra for AG, Si_3N_4, and SiO_2 (L=500 µm) at an injection current where the ES1 starts to show up as shown in Figure 4-8. With increasing injection current ES emission is noticed, which can be explained by the state filling effect, and the δ-like density of states. The limited gain of the GS increased the probability of recombination from higher energy state ES [75] . QD intermixing have a significant effect on ES. As lasing from ES occur at current smaller than that in the AG.

Figure 4-8 shows the EL spectra for AG and annealed devices as a function of injected current. Due to the decrease in the gain and the confinement for the annealed devices, the ES starts to show up since doubling the (I_{th}) compared with AG that appears at the seventh time of the (I_{th}). In addition, a significant blue shift of the emission energy associated with the reduction of the intersublevel spacing energy is observed.

Figure 4-8 shows the separation between states that formed to be 123 nm, 50 nm, 42 nm for AG, annealed Si_3N_4 and SiO_2 devices respectively, and also we notice that this separation decreased as the degree of intermixing increased. This observation is attributed to a lateral out diffusion, which causes the state to become closer [76]. This behavior is due to the reduction of the intersublevel spacing energy with increasing annealing temperature to a modification in the QDs composition without a significant change in the dot's size [76]. In the present work, the observation of a reduction in the intersublevel spacing energy, together with the appearance of an additional ES emission line for the high temperature annealed sample's PL spectra, could be explained by the variation of the volume/diameter ratio, which tends to enlarge the annealed QDs. This interpretation is in agreement with theoretical [77] and structural investigations [78-80].

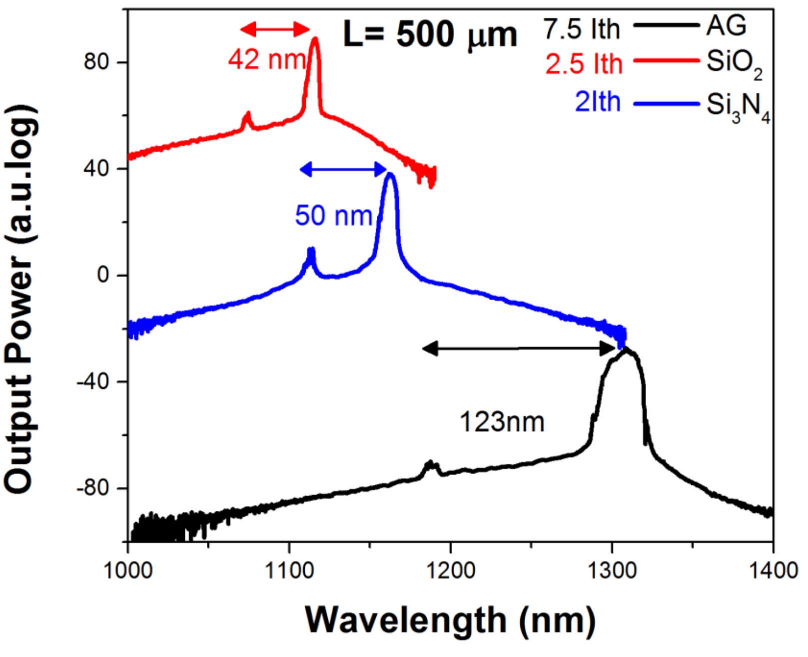

Figure 4-8: simultaneous lasing from GS and ES as a function of injected current at L=500 µm for AG, and SiO_2, Si_3N_4 (Capped/annealed@725°C) laser devices.

4.3.2 Multi-state Lasing

In this work, by utilizing a high current density and an appropriate choice of cavity lengths, a simultaneous five-state lasing in the InAs/InGaAs intermixed quantum dot laser is experimentally demonstrated for the first time in a very important wavelength range of 1030 to 1125 nm (doubled frequency for green light generation). Figure 4-9 shows the multi-state lasing using the SiO_2 cap at 4.45 I_{th}. We attribute the multistate lasing to a significant reduction in the energy separation of electronic states, a high carrier population in the QDs Energy levels, and a long relaxation time from a high energy level to lower energy levels. Also increasing the degeneracy of ES and 2D InGaAs or metamorphic QDs/QW levels is a reason of observing this behavior. several groups have observed this simultaneous lasing from different energy levels in QDs or QW [74, 81], especially for short cavity lengths, and they have explained this phenomenon in terms of high cavity losses, which lead to an increase in threshold and thus to increasing band filling [82], S. Mokkapati et. al. reported multi-color QDs lasers using an ion implantation induced intermixing [27]. Increasing the operation temperature would also require a higher injection and lead to the same effect [81].

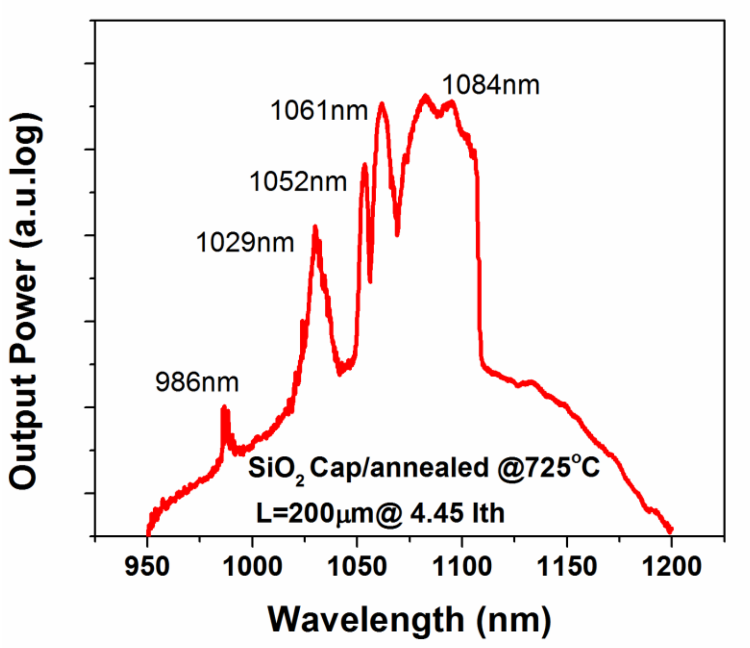

Figure 4-9: multi states lasing in intermixed samples using SiO_2 cap/annealed @725°C, measure @4.45I_{th}.

4.3.3 Sub – 1100 nm Lasing

The summary of the lasing wavelengths as a function of cavity length is plotted in Figure 4-10, Figure 4-11 shows room temperature L-I characteristics of 50 µm stripe width annealed SiO_2 and Si_3N_4 for different cavity lengths -in addition to the laser spectra results-. Figure 4-10 (a) shows A single lasing wavelength of ~1070 nm at ES this is from 300 µm long SiO_2 capped QD laser. A power up to 0.8 W can be obtained from this device at 1.4 A which is approximately 3I_{th}. By measuring the spectra from longer cavity Lasing 1250 µm, 1118 nm lasing from GS is obtained as shown in Figure 4-10 (b) with a power reached up to 1.5W at 2A.

Figure 4-11 represent device capped with Si_3N_4, at short (long) cavity length 300 µm, (3000 µm) lasing from GS, ES respectively ~1108 nm, 1190 nm with power 0.5 W, 1.4 W.

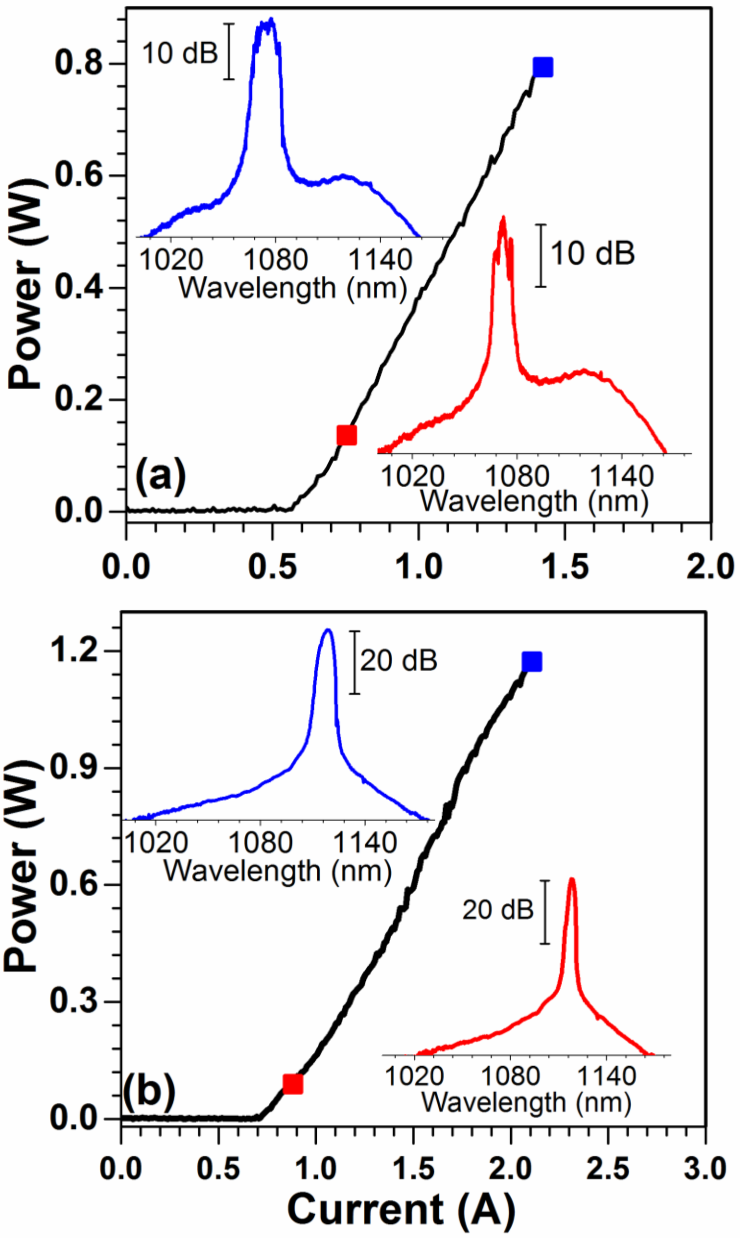

Figure 4-10 Room temperature L-I characteristics of 50 µm stripe width annealed SiO_2 laser diodes with different cavity lengths. a) L-I characteristics of 300 µm long SiO_2 capped Qdot laser. b) L-I characteristics of 1250 µm long SiO_2 capped QDs laser. Insets: Lasing spectra at respective indicated injection currents.

A slope efficiency of ~0.95 (~0.82) W/A from SiO_2 and ~0.71 (~0.40) W/A from Si_3N_4 annealed short (long) cavity lasers was extracted from the L-I curve, which corresponds to a differential quantum efficiency (η_d) of ~81% (~74%) and ~64% (~39%). Compared with the AG laser results, annealed lasers exhibited a lasing wavelength blue shift of

>180 nm with a better slope efficiency (SiO_2 capped lasers was found to be superior to Si_3N_4 capped lasers). A noted decrease in their lasing bandwidths (not shown).

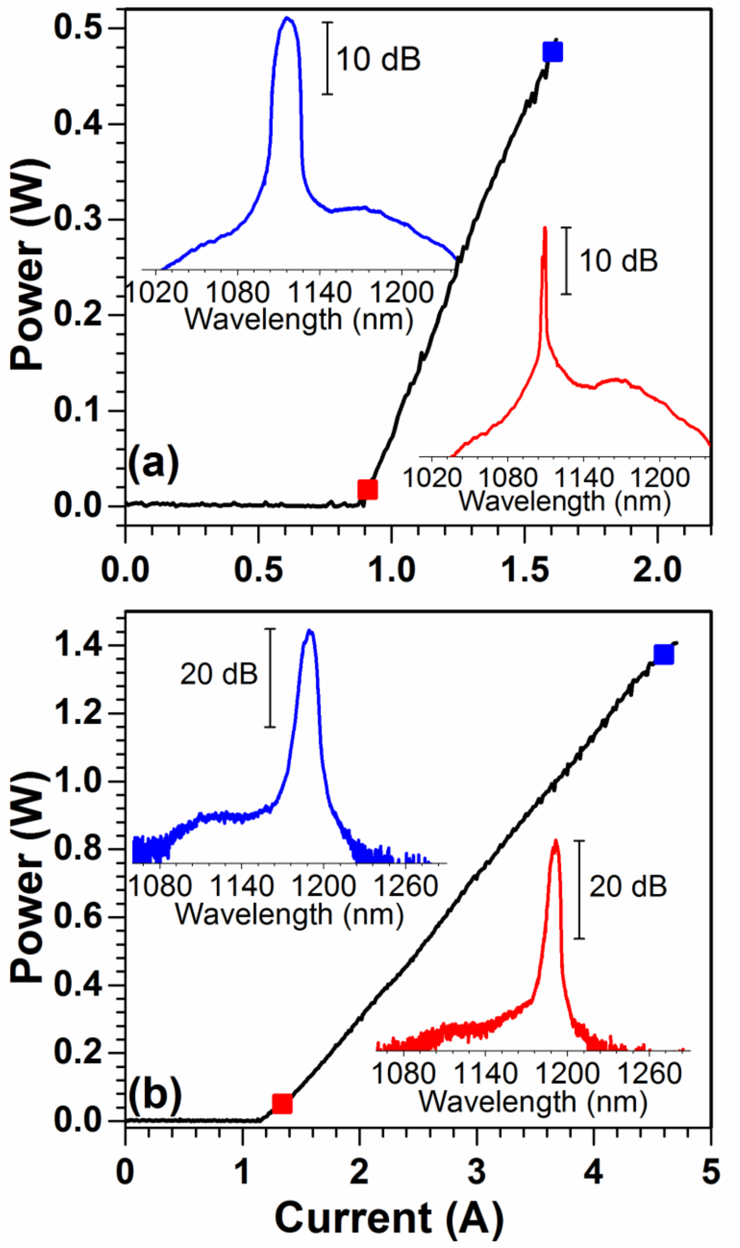

Figure 4-11 Room temperature L-I characteristics of 50 µm stripe width annealed Si_3N_4 laser diodes with different cavity lengths: a) L-I characteristics of 250 µm long Si_3N_4 capped Qdot laser, and b) L-I characteristics of 3000 µm long Si_3N_4 capped QDs laser. Insets: Lasing spectra at respective indicated injection currents.

We further compared the lasers performance by extracting internal quantum efficiency (η_i), internal loss (α_i), transparency current density (J_0), characteristics temperature (T_0), and GS saturated modal gain (Γg_{sat}). The summary of laser performance for AG, SiO2, and Si_3N_4 annealed laser is listed in Figure 4-11. An increase in J_0 is observed in the annealed devices compared to the AG device, which is attributed to the reduction in the optical confinement factor as a result of the QDs size reduction and to the weakly localized QDs layers due to a reduced conduction band offsets as a result of annealing (blue shift of lasing wavelength) [57]. In fact, T_0 is also reduced possibly due to the latter effect, promoting a thermal injection of carriers out of the QDs. On the other hand, an improvement in η_i from 87% (AG) to 93% (SiO_2) and 89% (Si_3N_4) that is derived from a small increase in the α_i value is observed.

This improvement is ascribed to the possible annealing of the defect at high temperatures, which might be present near the QDs–barrier interface owing to the low temperature growth process, in addition to the high stress field around QDs [72]. The small increase in α_i might be a result of minor alteration in the scattering loss of photons due to a localized variation of refractive index at the QDs–barrier interface during the doping. The cumulative effect of these parameters resulted in a minor decrease (0.5 cm^{-1}/layer) in the GS saturated modal gain of SiO_2 annealed laser, whereas Si_3N_4 capped laser showed a decrease of 1.75 cm^{-1}/layer. In general, all of these parameters indicate a comparable performance from IFVD tuned QDs lasers, being able to emit in ~1060–1190 nm range under a stimulated emission with a similar active region optical quality and an inhomogeneity. We believe that an optimized design of the laser active region with enough conduction band offset might further improve these parameters [83].

Table 4-1: Summary of the extracted as-grown and annealed laser performance parameters with an error margin of ± 5%.

Sample	J_0 (A/cm^2)	η_i (%)	α_i (cm^{-1})	T_0 (K)	Γg_{sat} (cm^{-1})
As-grown	330	87	4.4	~295	53
SiO_2 cap	604	93	5.2	~65	50
Si_3N_4 cap	634	89	6.3	~55	39

4.4 Summary

An extensive laser characterization was performed, and the feedback emphasizes significant results extracted from the PL characterization in chapter 3. Both DC characterization and spectral analysis show that this simple cost-effective, post-growth, bandgap engineering method can provide superior changes in the devices. InAs/GaAs quantum-dot lasers with Qdot transition states blue shifted by ~185 nm and lasing at ~1070 – 1190 nm were achieved. The devices are demonstrated to maintain their performance characteristics. Such high-power devices pave the way for a potential achievement of visible light via the frequency doubling technique for use in various cross-disciplinary field applications. The current demonstration also paves the way for a possible realization of a multiple wavelength application from a single dedicated wavelength (1300 nm) InAs/GaAs QDs epitaxial wafer. From spectral analysis, a simultaneous five-state lasing in the InAs/InGaAs intermixed quantum dot laser was experimentally demonstrated for the first time in a very important wavelength range of 1030 to 1125 nm. In addition, the blue shifting proved the ability of this method to tune lasing wavelength for those materials.

5 QUANTUM WELL SUPERLUMINESCENT DIODE (SLD) CHARACTERIZATION

5.1 Introduction

High power and broadband (SLD) with flat-top emission spectrum is a desirable optical source in noninvasive biomedical imaging techniques employing low coherence interferometry, for instance, OCT [84]. Several broadband SLDs have been reported for OCT applications, encompassing emission wavelength ~1000 nm [85, 86], ~1300 nm [43, 53, 87-92] and ~1500 nm [93-95], and using different quantum confined nanostructure based active regions, ranging from quantum-wells (QW) [89-93, 96] to (QDs) [43, 53, 86, 87], and very recently quasi-zero dimensional quantum dashes [94, 95]. For the ~1300 nm wavelength window, active region designs based on both multi-stack QDs and MQW nanostructures have been investigated. In the design of QDs based SLDs, both identical and chirped multi-stack InAs/GaAs active region have been demonstrated. Moreover, intermixing and p-doping techniques were also employed to extend the QDs SLD emission bandwidth and device performance [61]. In general, output power in tens-of-milliwatts up to ~180 mW, and emission bandwidth (-3dB) in tens of nm to ~310 nm have been achieved, and very recently, reaching ~350 nm via simultaneous emission from hybrid QW-QDs active region [53, 97]. As for the conventional ~1300 nm QW based SLDs, high power of >100 mW have been reported with optical bandwidth reaching few tens of nm to about 100 nm [88-92]. The improvement in the SLD figures of merits, such as optical power, large spectral bandwidth, and flat-top spectral shape are required for achieving higher axial resolution, improved signal-to-noise ratio, and penetration depth in an OCT system. However, simultaneous optimization of power and bandwidth [i.e. power-bandwidth product (PBP)] still pose a challenge in both types of active regions. In the MQW domain, various research paths have been explored and demonstrated to optimize PBP and spectral profile in particular. For instance, by employing: (a) identical MQWs active region and relying on simultaneous emission from

QWs (GS) and first (ES) [91, 98], (b) asymmetric MQWs based on simultaneous GS emissions [89, 96]; and (c) combination of both the above approaches [99]. In general, the method in (a) usually results in spectral dip in the amplified spontaneous emission (ASE) spectrum which affects the OCT resolution and usable power [61], while both approaches in (b) and (c) require comparatively complex and optimized epitaxial structure design. SLD with ultra-wide emission bandwidth of >250 nm, centered at ~1450 nm, have been reported based on approach (c); however, with a very lower output power of ~0.2 mW [99].

In this work, a simpler identical MQW epitaxial structure is utilized. By properly engineering the GS and ES e-hh and e-lh emission overlaps of each QW states with comparable emission intensities across the inhomogeneous optical transitions, in a compressively strained four QW active region; we demonstrate a SLD with simultaneous achievement of wide and flat-topped 125 nm optical bandwidth and output power of 70 mW, which corresponds to a PBP of 8750 mW.nm. This value is better than the commercially available pigtailed SLDs encompassing ~1300 nm wavelength, with exhibited PBP value in the range of 300 – 1650 mW.nm [99-102]. Moreover, wall-plug efficiency (WPE) in excess of 14% is demonstrated from this batch of devices while preserving the device performance. This is attributed to the variation in anti-reflection (AR) coating properties, which can be applied as a facet engineering technique to enhance PBP of SLDs. The WPE and optical bandwidth values, to our knowledge, are the best values reported at ~1300 nm wavelength window. Besides addressing the field of biomedical imaging, optical short reach communications, such high-power and broadband near infra-red SLD devices could serve as key sources in optical time domain reflectometry, fiber gyroscopes, etc., thus improving the respective system's performance characteristics [53, 95].

5.2 Photoluminescence (PL) Study

Room temperature PL results of the SLD device structure under different excitation power density values is presented in Figure 5-1Two emission peaks at ~1310 nm and ~1276 nm are visible at high excitation density of >975 W/cm^2 which persists even at low excitation power of 97 W/cm^2. However, the two peaks are found to merge and later separate out with increasing excitation power density, thus indicating a comparable radiative recombination from the same QW transition state. We attribute these emission peaks to the recombination at GS e-hh (1e-1hh) state within the QWs and the bimodal behavior to the 1e-1hh state inhomogeneity across the MQWs. This is due in part to the composition and thickness fluctuation during growth and primarily to the variation in the built-in compressive strain that each succeeding QW experiences, leading to broadening of the 1e-1hh optical transitions [90, 103]. The emission hump at ~1235 nm at high excitation power density of 1950 W/cm^2 again suggests bimodal peaks. In fact the evolution of the PL around this wavelength with increasing excitation power density show the hump composed of superposition of two emission peaks. Furthermore, a weak emission also appear at ~1185 nm under excitation power density of >325 W/cm^2. These short wavelength emission humps and shoulders indicate the existence of ES emission in the MQW system. Therefore, we ascribe the emission at ~1235 nm primarily to the ES e-hh (2e-2hh) transition states and partly to the 1e-1lh recombination [103]. The latter transition state is possible in our compressively-strained MQW system which separates the 1e-1hh and 1e-1lh recombination, thus contributing to the inhomogeneity of the active region [90]. We attribute the shortest emission shoulder at ~1185 nm to the emission from 2e-2lh radiative transition which is found to be weak. In general, the collective emission from the dispersive GS and ES states, with each representing e-hh and e-lh recombination, respectively, contributed to the inhomogeneous broadening of our MQW active region system. Comparable emission intensities among the GS and ES emissions (~0.7 dB difference between 1e-1hh and 2e-2hh) lead to an ultra-broad PL linewidth (full-width-at-half-maximum) of ~185 nm (144 meV) at 1950 W/cm^2. Such a broad and fairly flat-topped PL profile shows the effectiveness of our device design for realization of broadband devices such as broadband lasers, semiconductor optical amplifiers, and SLDs.

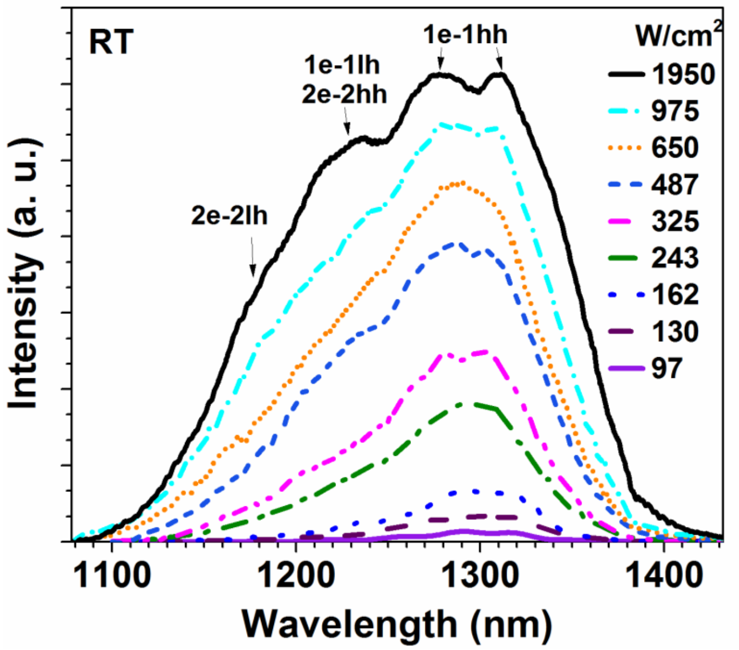

Figure 5-1: Room temperature PL measurement from the full SLD device structure as a function of excitation power density. A PL linewidth of ~185 nm is measured at 1950 W/cm^2 excitation power density.

5.3 Device Characterization

The SLD devices are fabricated utilizing the standard fabrication process with 7º tilted ridge-waveguides with respect to the normal of the device facets. The 2 µm ridge-width SLDs are later cleaved to 1.0 mm length with both facets coated with AR coating before electrical characterization. Several fabricated SLD devices were tested using both, pulsed mode (0.5 µs current pulse width and 0.01% duty cycle) and continuous wave (CW) operation, and under thermo-electric cooling. For emission spectra measurement, the optical power of the SLDs is butt-coupled into either a lensed multi-mode fiber which is connected to an optical spectrum analyzer pre-set at 1.0 nm resolution, or a wedge single-mode fiber with fine 0.1 nm resolutions.

Figure 5-2 (a) depicts the room temperature output power–current-voltage (*L*-*I*-*V*) characteristic of our SLD (SLD1). The device exhibited a series resistance and a turn-on voltage of ~1.1 V and 2 – 3 Ω, respectively. A super linear characteristic is evident with total measured output power (2 facets, assuming identical facets reflectivity) of >70 mW. The corresponding ASE spectra at different pulsed current injection are shown in Figure 5-2 (b). An ultra-broad and flat-top emission profile is apparent with -3dB bandwidth >100 nm for injection current ≥0.1 A and reaching a maximum of 125 nm at 1.0 A.

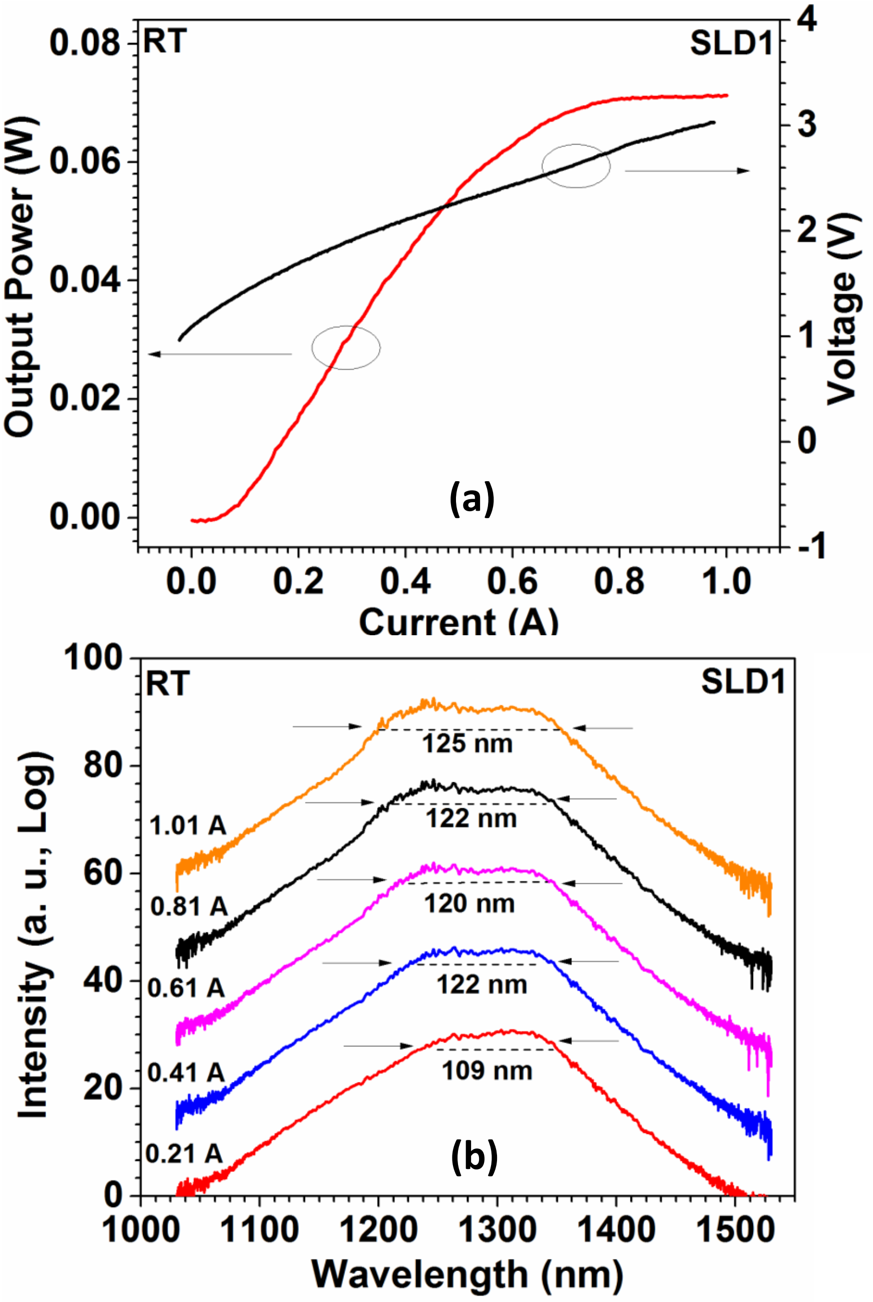

Figure 5-2: (a) Room temperature L-I-V characteristics of 7^o tilted, AR coated, ridge waveguide 2×1000 μm^2 SLD1 device under pulsed current operation. The corresponding measured (b) emission spectra as a function of pulsed current injection. The -3dB bandwidth at each injection current is shown in (b). The emission spectra in (b) are vertically offset for clarity.

The summary of SLD characteristics as a function of pulsed current injection, at room temperature, is shown in Figure 5-3 (a). The central emission wavelength (calculated by identifying the central wavelength at -3dB bandwidth) varied from ~1300 nm to ~1275 nm with increasing injection while the calculated PBP and average power spectral density (APSD) at 1.0 A are 8750 mW.nm and 0.56 mW/nm, respectively. The device displayed a coherence length in air of 11.5 µm (0.88 times ratio of central wavelength square and -3dB bandwidth) and maximum external quantum efficiency (EQE) and WPE of 11.7% and 5.2%, respectively, which are reasonable values in SLD domain [53]. The spectral ripple, measured within 10 nm span from the central emission wavelength, is also plotted in Figure 5-3 (a). The ripple stayed below 1.0 ± 0.5 dB up to a pulsed current injection of 0.5 A, and later increased to 1.2 ± 0.5 dB. In general, the spectral ripples using tilted configuration SLDs based on QW active region are expected to show high values owing to the possibility of device operation reaching the onset of lasing because of the high modal gain of QW nanostructures [104].

This achievement of SLD performance is a result of active region engineering to obtain simultaneous and comparable emission from different QW transition states of the MQW system. Notice in Figure 5-2 (b) that during the low current injection, the longer wavelength emission near ~1315 nm dominates compared to the shorter wavelength emission near ~1240 nm. This is ascribed to the state filling and recombination of lower energy 1e-1hh transitions by the carriers first resulting in domination of ASE at ~1315 nm [99]. However, the difference in the ASE level when compared to the emission from higher energy 1e-1lh and 2e-2hh states, corresponding to emission near ~1240 nm, is mere ~4.0 dB at 0.11 A (not shown). This value reduced considerably to ~2.0 dB at 0.31 A, and eventually becomes negligible at 0.41 A (*i.e.* <0.5 dB), thus providing a flat-topped emission beyond this current value with comparable emission from both the dominating QW states. This observation is a direct effect of 1e-1hh energy level saturation because of completely filled density of states and therefore carriers occupying the next available higher energy level (1e-1lh and 2e-2hh) with increasing current injection, thus contributing to the increase in ASE at shorter wavelengths [93]. This phenomenon increases the emission bandwidth and inherently blue shifts the central emission wavelength, as summarized in Figure 5-3 (a). Moreover, it is worth mentioning that the device demonstrated an emission bandwidth of >100 nm for entire current range of >0.11A, thus showing the effectiveness of the device design. Figure 5-3 (b) shows the SLD performance under CW operation, measured from another device SLD2 which underwent identical fabrication and AR coating process (same batch) besides exhibiting similar pulsed *L-I-V* and spectral characteristics, as that of SLD1. A total output power of >1.6 mW is measured at ~0.12 A current injection with corresponding measured bandwidth of ~60 nm. This is the maximum emission bandwidth measured from our device before power roll-off. The central emission wavelength is observed to be at ~1310 nm under low injection of 25 mA which blue shift to ~1296 nm at 0.12 A along with ~13 nm increase in the -3dB bandwidth. This again dictates the dominance of GS 1e-1hh transition state under this mode of current operation. On comparing the CW characteristics with pulsed operation Figure 5-3 (b), a different behavior in carrier emission process within the MQW active region is observed. An additional junction heating phenomenon under CW operation might have altered the carrier distribution among the QWs due to shallow conduction band offset and hence the way radiative recombination occurs in the inherent MQW inhomogeneous system [63, 91]. The device showed a red-shift in the emission wavelength and increase in the bandwidth by ~10 nm (i.e. ~72 nm) beyond 0.12 A with reduction in optical power because of excessive device heating. It is to be noted that our device structure and material quality is un-optimized and hence a substantial difference between the CW and pulsed operation is obvious.

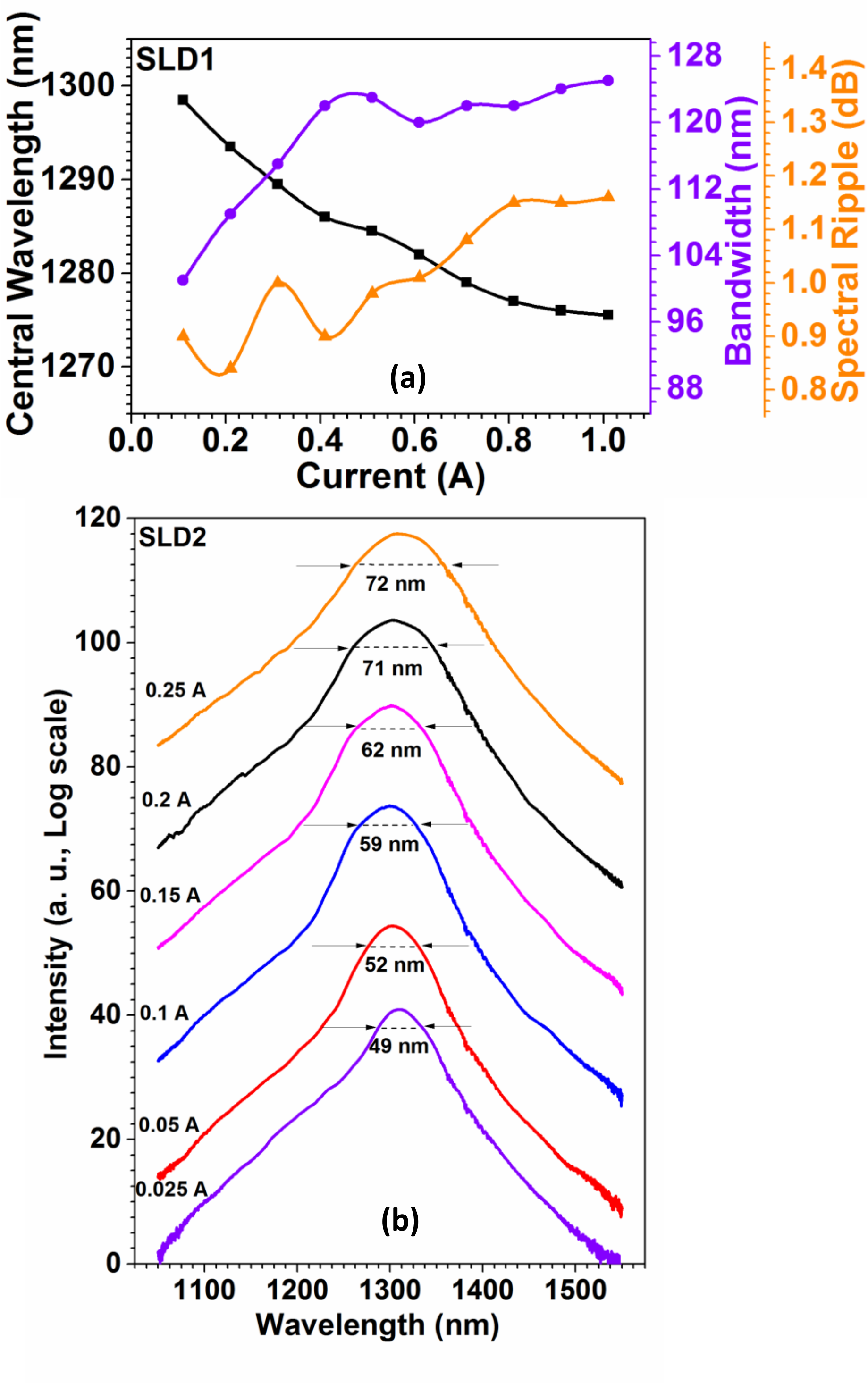

Figure 5-3: The effect of pulsed current injection on SLD1 device's central emission wavelength, emission bandwidth, and spectral ripple, at room temperature. (b) Room temperature L-I characteristics under CW current operation (inset), and emission spectra as a function of current injection, measured on SLD2 device. The solid lines in (a) are guide to eyes and the emission spectra in (b) are vertically offset for clarity.

5.3.1 Temperature Dependent Study

In order to investigate the SLD performance at elevated temperatures, SLD2 is tested at various temperatures under pulsed operation. The results are shown in Figure 5-4 . The device performance degraded substantially on varying the temperature from 15^{o}C to 45^{o}C with the APSD reducing from 0.8 mW/nm at 15^{o}C to 0.2 mW/nm at 45^{o}C, and eventually to 0.08 mW/nm at 75^{o}C. This is accompanied by an appreciable redshift in the central emission wavelength from ~1300 nm at 15^{o}C to ~1313 nm at 45^{o}C and eventually to ~1355 mW/nm at 75ºC. The drastic decrease in the optical power with increasing temperature is attributed to the shallow conduction band offsets of InGaAsP material system, thus favoring carrier spill over with increasing temperature rather than radiatively recombining within the QW (weak carrier confinement) [105]. Note that the emission bandwidth shows a sigmoidal behavior accompanied by reduction in the signal-to-noise ratio with increasing temperature, indicating competition between the QW energy states for eventual domination. In fact we observed multiple emission peaks in the ASE spectra at elevated temperatures (> 35^{o}C) with one of them dominating (and also found it to be a function of injection current), indicating non-uniform distribution of carriers among the QWs at high temperature [103, 106]. We attribute this complex temperature dependent ASE emission and red shift in the central emission wavelength to the collective phenomena such as junction heating, phonon-assisted tunneling, optical activation, etc., occurring simultaneously in the MQW system [107].

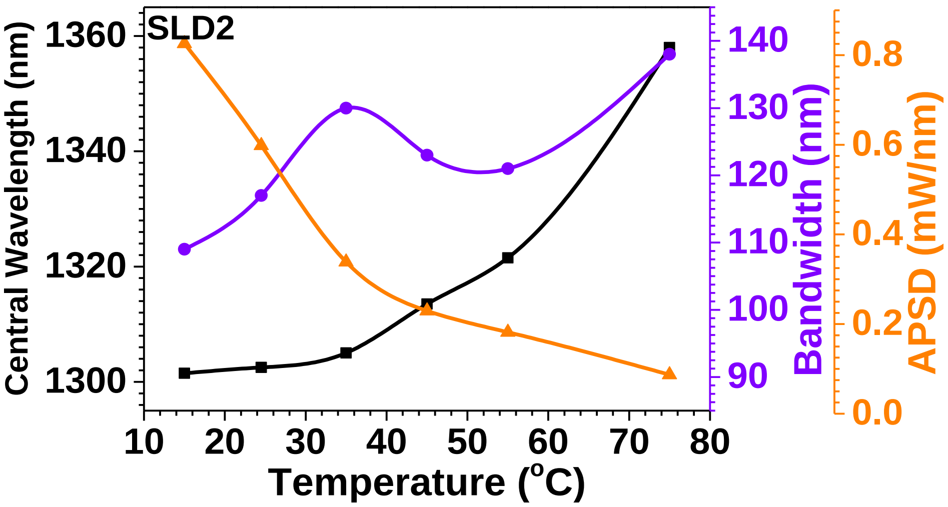

Figure 5-4: Summarized changes in central emission wavelength, emission bandwidth, and APSD, with sub-mount temperature, of SLD2 device. The solid lines are guide to eyes.

5.4 Summary

We demonstrated a high-power and ultra-wide bandwidth InGaAsP/InP MQW SLD. The room temperature PL linewidth of more than 180 nm from the device structure affirms the inhomogeneous nature of the MQW active region. The device exhibited a flat-top emission bandwidth of 125 nm and APSD ~0.56 mW/nm with a low spectral ripple of ≤1.2 ± 0.5 dB, asserting our achievement in designing an inhomogeneous active region with a comparable emission from different QW transition states. Our current demonstration of high efficiency, high power, flat-top, and broadband SLD may shift the paradigm, which is dominated by InAs/GaAs self-assembled QDs, back to MQW system.

6 CONCLUSIONS AND FUTURE WORK

6.1 Thesis Conclusions

The most significant conclusion in this work involves three main subjects:

- Highlight the best condition in IFVD post-growth engineering to achieve a highly optimized laser performance suitable for use in PICs applications, including a simple way to compare the rate of modifying the degree of intermixing-.
- Growth engineering in QW/SLD to gain a high-power and ultra-wide bandwidth.
- The important results extracted from the materials/device characterization.

Firstly, we demonstrated the viability of the IFVD process for use on InAs/GaAs SAQDs by various dielectric capping materials with an emission wavelength trimming to ~1100–1200 nm for a potential realization in photonic integrated circuits and a post-growth wavelength tuned optoelectronic devices. Compared with the traditional dielectric capping layers, we presented HfO_2 and $SrTiO_3$ as potential candidates for tailoring the bandgap properties of QDs with superior optical properties. The corresponding extracted interdiffusion rates in these materials of HfO_2 and $SrTiO_3$ were found to be 3.73 and 0.31 meV⁄°C, respectively. These values are significantly higher than those of common SiO_2 and Si_3N_4 dielectric films. Moreover, an assessment of other uncommon dielectric capping layers, such as TiO_2, Al_2O_3, and ZnO, was also performed, showing attractive features and thus increasing the flexibility in a capping layer selection for selective bandgap engineering for plethora of multidisciplinary applications. In general, all of the films exhibited a linewidth narrowing and peak/integrated PL intensity improvement after annealing, suggesting an enhanced material quality after intermixing.

Secondly, an extensive amount of laser characterization was performed; these results corroborate the significant results extracted from the material characterization. Both DC characterization and spectral analysis show that this simple, cost-effective, post-growth, bandgap engineering method can provide superior changes in the devices. For example, an InAs/GaAs quantum-dot laser with QDs transition states blue shifted by ~185 nm and lasing at ~1070 – 1190 nm was achieved. These devices are shown to maintain their performance characteristics. Such high-power devices pave the way for a potential achievement of visible light via a frequency doubling technique for use in various cross-disciplinary field applications. The current demonstration also paves the way for a possible realization of a multiple wavelength application from a single dedicated wavelength (1300 nm) InAs/GaAs QDs epitaxial wafer. From spectral analysis, simultaneous five-state lasing in the InAs/InGaAs intermixed quantum dot laser is experimentally demonstrated for the first time in a very important wavelength range of 1030 to 1125 nm. In addition, the blue shifting proved the ability to use this method to tune lasing wavelength for those materials.

Thirdly, we demonstrated a high-power and ultra-wide bandwidth InGaAsP/InP MQW SLD. The room temperature PL linewidth of more than 180 nm from the device structure confirms the inhomogeneous nature of the MQW active region. The device exhibited a flat-top emission bandwidth of 125 nm and APSD ~0.56 mW/nm with low spectral ripple of ≤ 1.2 ± 0.5 dB, thus asserting our achievement in designing an inhomogeneous active region with a comparable emission from different QW transition states. We believe our current demonstration of high efficiency, high power, flat-top, and broadband SLD to shift the current paradigm, which is dominated by InAs/GaAs self-assembled QDs, back to MQW systems.

Finally, our method, knowhow, and the great amount of resutls provide the required stepping-stones for further investigations to be carried out both at the research and application levels.

6.2 Future Work

The results obtained from this work are very promising and encouraging, especially the use of the new, simple approach to characterize the degree of intermixing. From the material level to the device level and through growth and post-growth engineering, the results achieved represent an extremely large amount of work. Applications based on this work can be performed.

- Combining one or more of intermixing techniques to achieve larger bandgap shift, such as LID with IFVD. Start by exposing the Semiconductor with photons of a higher energy than the absorption edge, followed by the use of HfO_2 as the capping material to promote intermixing. We expect to have a very large shift by combing these two effective methods.
- We can modify the study by using a QD material with different growth conditions, such as a number of monolayers and growth temperatures. From this study, we can obtain the best conditions to use to either promote or enhance intermixing.
- Examine different IFVD parameters, such as annealing temperature and duration. By this investigation, we can determine better conditions for the IFVD process and help to recrystallize the structure gradually.
- A theoretical model for the interdiffused QW/QDs can be applied. This model is used to compare the experimental results with the theoretical results to obtain and predict the essential parameters of the IFVD process.
- From the power-dependent PL, temperature and time-resolved density, we can extract the best quality capping material in terms of recombination emission.
- A promising result extracted from the material characterization work encouraged us to fabricate extra devices. For example, by using an HfO_2 cap, we expect to have a very narrow devise emission that is highly desirable for a high quality laser. In the same way, by using Al_2O_3, we expect to have a very broadband emission; such a source is very useful for OCT applications using SLDs.

REFERENCES

[1] E. Pavelescu, C. Gilfert, P. Weinmann, M. Dănilă, A. Dinescu, M. Jacob*, et al.*, "1100 nm InGaAs/(Al) GaAs quantum dot lasers for high-power applications," *Journal of Physics D: Applied Physics,* vol. 44, p. 145104, 2011.

[2] K. Watanabe, T. Akiyama, Y. Yokoyama, K. Takemasa, K. Nishi, Y. Tanaka*, et al.*, "Growth of high-density 1.06-µm InGaAs/GaAs quantum dots for high gain lasers by molecular beamepitaxy," *Journal of Crystal Growth,* vol. 378, pp. 627-630, 2013.

[3] C. Report. (May,2015). *The Zettabyte Era—Trends and Analysis*. Available: http://www.cisco.com/c/en/us/solutions/collateral/service-provider/visual-networking-index-vni/VNI_Hyperconnectivity_WP.html

[4] E. Report. (June,2015). *Ericsson Mobility Report*. Available: http://www.ericsson.com/res/docs/2015/ericsson-mobility-report-june-2015.pdf

[5] "Advanced 5G Network Infrastructure for the Future Internet Public Private Partnership in Horizon 2020," ed.

[6] D. Hofstetter, B. Maisenholder, and H. P. Zappe, "Quantum-well intermixing for fabrication of lasers and photonic integrated circuits," *Ieee Journal of Selected Topics in Quantum Electronics,* vol. 4, pp. 794-802, Jul-Aug 1998.

[7] W. D. Laidig, N. Holonyak, M. D. Camras, K. Hess, J. J. Coleman, P. D. Dapkus*, et al.*, "Disorder of an AlAs-GaAs superlattice by impurity diffusion," *Applied Physics Letters,* vol. 38, pp. 776-778, 1981.

[8] C. Jagadish, H. H. Tan, S. Yuan, and M. Gal, "Quantum Well Intermixing for Optoelectronic Applications," *MRS Online Proceedings Library Archive,* vol. 484, p. 397 (15 pages), 1997.

[9] C. K. Chia, S. J. Chua, J. R. Dong, and S. L. Teo, "Ultrawide band quantum dot light emitting device by postfabrication laser annealing," *Applied Physics Letters,* vol. 90, pp. -, 2007.

[10] V. Yakovlev, V. Lazarov, J. Reynolds, and M. Gajdardziska-Josifovska, "Laser-induced phase transformations in semiconductor quantum dots," *Applied Physics Letters,* vol. 76, pp. 2050-2052, 2000.

[11] H. S. Djie, B. S. Ooi, and V. Aimez, "Neutral ion-implantation-induced selective quantum-dot intermixing," *Applied Physics Letters,* vol. 87, Dec 26 2005.

[12] Y. Wang, H. Djie, and B. Ooi, "Group-III intermixing in InAs/InGaAlAs quantum dots-in-well," *Applied physics letters,* vol. 88, pp. 111110-111110-3, 2006.

[13] C. Chia, S. Chua, Y. Wang, A. Yong, and S. Chow, "Impurity free vacancy disordering of InAs/GaAs quantum dot and InAs/InGaAs dot-in-a-well structures," *Thin solid films,* vol. 515, pp. 3927-3931, 2007.

[14] R. Dingle, W. Wiegmann, and C. H. Henry, "Quantum States of Confined Carriers in Very Thin Alxga1-Xas-Gaas-Alxga1-Xas Heterostructures," *Physical Review Letters,* vol. 33, pp. 827-830, 1974.

[15] Z. M. Wang. . Springer, "Self Assembled Quantum Dots," A. W. Zhiming M. Wang, Gregory Salamo, Naoki Kishimoto, Ed., ed, 2007.

[16] Z. M. Wang, K. Holmes, Y. I. Mazur, and G. J. Salamo, "Fabrication of (In,Ga)As quantum-dot chains on GaAs(100)," *Applied Physics Letters,* vol. 84, pp. 1931-1933, Mar 15 2004.

[17] D. J. Kim and H. Y. Yang, "Shape control of InGaAs nanostructures on nominal GaAs(001): dashes and dots," *Nanotechnology,* vol. 19, Nov 26 2008.

[18] A. R. Kovsh, N. A. Maleev, A. E. Zhukov, S. S. Mikhrin, A. P. Vasil'ev, Y. M. Shernyakov*, et al.*, "InAs/InGaAs/GaAs quantum dot lasers of 1.3 mu m range with high (88%) differential efficiency," *Electronics Letters,* vol. 38, pp. 1104-1106, Sep 12 2002.

[19] A. R. Kovsh, N. A. Maleev, A. E. Zhukov, S. S. Mikhrin, A. P. Vasil'ev, E. A. Semenova*, et al.*, "InAs/InGaAs/GaAs quantum dot lasers of 1.3 µm range with enhanced optical gain," *Journal of Crystal Growth,* vol. 251, pp. 729-736, 4// 2003.

[20] S. Ryu, S. Yamamoto, H. Taga, N. Edagawa, Y. Yoshida, and H. Wakabayashi, "Long-haul coherent optical fiber communication systems using optical amplifiers," *Lightwave Technology, Journal of,* vol. 9, pp. 251-260, 1991.

[21] E.Herbert, *Semiconductor Quantum Well Intermixing: Material Properties and Optoelectronic Applications*, 2000.

[22] S. Charbonneau, E. S. Koteles, P. J. Poole, J. J. He, G. C. Aers, J. Haysom*, et al.*, "Photonic integrated circuits fabricated using ion implantation," *Selected Topics in Quantum Electronics, IEEE Journal of,* vol. 4, pp. 772-793, 1998.

[23] B. S. Ooi, C. J. Hamilton, K. McIlvaney, A. C. Bryce, R. M. DelaRue, J. H. Marsh*, et al.*, "Quantum-well intermixing in GaAs-AlGaAs structures using pulsed laser irradiation," *Ieee Photonics Technology Letters,* vol. 9, pp. 587-589, May 1997.

[24] E. Koteles, B. Elman, P. Melman, J. Y. Chi, and C. A. Armiento, "Quantum well shape modification using vacancy generation and rapid thermal annealing," *Optical and Quantum Electronics,* vol. 23, pp. S779-S787, 1991/01/01 1991.

[25] B. S. Ooi, A. C. Bryce, J. H. Marsh, and J. S. Roberts, "Effect of p and n doping on neutral impurity and SiO2 dielectric cap induced quantum well intermixing in GaAs/AlGaAs structures," *Semiconductor Science and Technology,* vol. 12, pp. 121-127, Jan 1997.

[26] S. R. Andrew, J. H. Marsh, M. C. Holland, and A. H. Kean, "Quantum-well laser with integrated passive waveguide fabricated by neutral impurity disordering," *Photonics Technology Letters, IEEE,* vol. 4, pp. 426-428, 1992.

[27] S. Mokkapati, S. Du, M. Buda, L. Fu, H. H. Tan, and C. Jagadish, "Multiple wavelength InGaAs quantum dot lasers using ion implantation induced intermixing," *Nanoscale Research Letters,* vol. 2, pp. 550-553, Nov 2007.

[28] N. Liu and J. J. Dubowski, "Chemical evolution of InP/InGaAs/InGaAsP microstructures irradiated in air and deionized water with ArF and KrF lasers," *Applied Surface Science,* vol. 270, pp. 16-24, 4/1/ 2013.

[29] J. H. Marsh, R. M. De La Rue, A. C. Bryce, B. Garrett, and R. W. Glew, "Layer selective disordering by photoabsorption-induced thermal diffusion in InGaAs/InP based multiquantum well structures," *Electronics Letters,* vol. 28, pp. 1117-1119, 1992.

[30] C. E. Dimas, C. L. Tan, H. S. Djie, and B. S. Ooi, "Coherence length characteristics from broadband semiconductor emitters: superluminescent diodes versus broadband laser diodes," in *SPIE*, 2009, pp. 72300B-72300B-8.

[31] J. H. Marsh, P. Cusumano, A. C. Bryce, B. S. Ooi, and S. G. Ayling, "GaAs/AlGaAs photonic integrated circuits fabricated using impurity-free vacancy disordering," in *SPIE*, 1995, pp. 74-85.

[32] J. H. Marsh, P. Cusumano, A. C. Bryce, B. S. Ooi, and S. G. Ayling, "GaAs/AlGaAs photonic integrated circuits fabricated using impurity-free vacancy disordering," 1995, pp. 74-85.

[33] P. Lever, H. H. Tan, and C. Jagadish, "Impurity free vacancy disordering of InGaAs quantum dots," *Journal of Applied Physics,* vol. 96, pp. 7544-7548, Dec 15 2004.

[34] D. Bhattacharyya, A. Helmy, A. Bryce, E. Avrutin, and J. Marsh, "Selective control of self-organized In 0.5 Ga 0.5 As/GaAs quantum dot properties: Quantum dot intermixing," *Journal of Applied Physics,* vol. 88, pp. 4619-4622, 2000.

[35] L. Fu, P. Lever, H. H. Tan, C. Jagadish, P. Reece, and M. Gal, "Study of intermixing in InGaAs/(Al)GaAs quantum well and quantum dot structures for optoelectronic/photonic integration," *Iee Proceedings-Circuits Devices and Systems,* vol. 152, pp. 491-496, Oct 2005.

[36] T. Ng, H. Djie, S. Yoon, and T. Mei, "Thermally induced diffusion in GaInNAs/GaAs and GaInAs/GaAs quantum wells grown by solid source molecular beam epitaxy," *Journal of applied physics,* vol. 97, pp. 013506-013506-8, 2005.

[37] L. J. Guido, N. Holonyak, K. C. Hsieh, R. W. Kaliski, W. E. Plano, R. D. Burnham*, et al.*, "Effects of dielectric encapsulation and As overpressure on Al-Ga interdiffusion in AlxGa1−x As-GaAs quantum-well heterostructures," *Journal of Applied Physics,* vol. 61, pp. 1372-1379, 1987.

[38] J. D. Ralston, S. O'Brien, G. W. Wicks, and L. F. Eastman, "Room-temperature exciton transitions in partially intermixed GaAs/AlGaAs superlattices," *Applied Physics Letters,* vol. 52, pp. 1511-1513, 1988.

[39] J. Beauvais, J. H. Marsh, A. H. Kean, A. C. Bryce, and C. Button, "Suppression of bandgap shifts in GaAs/AlGaAs quantum wells using strontium fluoride caps," *Electronics Letters,* vol. 28, pp. 1670-1672, 1992.

[40] B. S. Ooi, K. McIlvaney, M. W. Street, A. S. Helmy, S. G. Ayling, A. C. Bryce*, et al.*, "Selective quantum-well intermixing in GaAs-AlGaAs structures using impurity-free vacancy diffusion," *Ieee Journal of Quantum Electronics,* vol. 33, pp. 1784-1793, Oct 1997.

[41] X. C. Wang, S. J. Xu, S. J. Chua, Z. H. Zhang, W. J. Fan, C. H. Wang*, et al.*, "Widely tunable intersubband energy spacing of self-assembled InAs/GaAs quantum dots due to interface intermixing," *Journal of Applied Physics,* vol. 86, pp. 2687-2690, 1999.

[42] D. Bhattacharyya, A. S. Helmy, A. C. Bryce, E. A. Avrutin, and J. H. Marsh, "Selective control of self-organized In0.5Ga0.5As/GaAs quantum dot properties: Quantum dot intermixing," *Journal of Applied Physics,* vol. 88, pp. 4619-4622, Oct 15 2000.

[43] K. Zhou, Q. Jiang, Z. Zhang, S. Chen, H. Liu, Z. Lu*, et al.*, "Quantum dot selective area intermixing for broadband light sources," *Optics Express,* vol. 20, pp. 26950-26957, 2012.

[44] H. H. Alhashim, M. Z. M. Khan, M. A. Majid, T. K. Ng, and B. S. Ooi, "InAs/GaAs quantum-dot intermixing: comparison of various dielectric encapsulants," *Optical Engineering,* vol. 54, pp. 107107-107107, 2015.

[45] A. Zhukov, M. Maksimov, and A. Kovsh, "Device characteristics of long-wavelength lasers based on self-organized quantum dots," *Semiconductors,* vol. 46, pp. 1225-1250, 2012.

[46] J. Singh, *Physics of Semiconductors and Their Heterostructures*: McGraw-Hill, 1993.

[47] J. H. Marsh, "Quantum well intermixing," *Semiconductor Science and Technology,* vol. 8, p. 1136, 1993.

[48] V. Aimez, J. Beauvais, J. Beerens, D. Morris, H. Lim, and B.-S. Ooi, "Low-energy ion-implantation-induced quantum-well intermixing," *Selected Topics in Quantum Electronics, IEEE Journal of,* vol. 8, pp. 870-879, 2002.

[49] B. S. Ooi, T. K. Ong, and O. Gunawan, "Multiple-wavelength integration in InGaAs-InGaAsP structures using pulsed laser irradiation-induced quantum-well intermixing," *Ieee Journal of Quantum Electronics,* vol. 40, pp. 481-490, May 2004.

[50] P. Lever, H. H. Tan, N. Gal, and C. Jagadish, "Impurity free vacancy disordering of InGaAs quantum dots," *Quantum Dot Devices and Computing,* vol. 4656, pp. 43-48, 2002.

[51] H. Susanto Djie, Y. Wang, Y.-H. Ding, D.-N. Wang, J. Hwang, X.-M. Fang*, et al.*, "Quantum dash intermixing," *Selected Topics in Quantum Electronics, IEEE Journal of,* vol. 14, pp. 1239-1249, 2008.

[52] P. Judson, K. Groom, D. Childs, M. Hopkinson, N. Krstajic, and R. Hogg, "Maximising performance of optical coherence tomography systems using a multi-section chirped quantum dot superluminescent diode," *Microelectronics Journal,* vol. 40, pp. 588-591, 2009.

[53] Z. Zhang, R. Hogg, X. Lv, and Z. Wang, "Self-assembled quantum-dot superluminescent light-emitting diodes," *Advances in Optics and Photonics,* vol. 2, pp. 201-228, 2010.

[54] W. Zeller, M. Kamp, J. Koeth, and L. Worschech, "High-power pulsed 976-nm DFB laser diodes," in *SPIE Defense, Security, and Sensing*, 2010, pp. 76820T-76820T-9.

[55] F. Heinrichsdorff, C. Ribbat, M. Grundmann, and D. Bimberg, "High-power quantum-dot lasers at 1100 nm," *Applied Physics Letters,* vol. 76, pp. 556-558, Jan 31 2000.

[56] E. M. Pavelescu, C. Gilfert, P. Weinmann, M. Danila, A. Dinescu, M. Jacob*, et al.*, "1100 nm InGaAs/(Al) GaAs quantum dot lasers for high-power applications," *Journal of Physics D-Applied Physics,* vol. 44, Apr 13 2011.

[57] W. Zeller, L. Naehle, P. Fuchs, F. Gerschuetz, L. Hildebrandt, and J. Koeth, "DFB Lasers Between 760 nm and 16 µm for Sensing Applications," *Sensors,* vol. 10, p. 2492, 2010.

[58] L. Fan, C. Hessenius, M. Fallahi, J. Hader, H. Li, J. V. Moloney*, et al.*, "Highly strained InGaAs/GaAs multiwatt vertical-external-cavity surface-emitting laser emitting around 1170 nm," *Applied Physics Letters,* vol. 91, p. 1114, 2007.

[59] Q. Cao, S. Yoon, C. Liu, and C. Tong, "Effects of rapid thermal annealing on optical properties of p-doped and undoped InAs/InGaAs dots-in-a-well structures," *Journal of Applied Physics,* vol. 104, pp. 033522-033522-6, 2008.

[60] L. Fu, P. Lever, H. H. Tan, C. Jagadish, P. Reece, and M. Gal, "Suppression of interdiffusion in InGaAs/GaAs quantum dots using dielectric layer of titanium dioxide," *Applied Physics Letters,* vol. 82, pp. 2613-2615, 2003.

[61] K. J. Zhou, Q. Jiang, Z. Y. Zhang, S. M. Chen, H. Y. Liu, Z. H. Lu*, et al.*, "Quantum dot selective area intermixing for broadband light sources," *Optics Express,* vol. 20, pp. 26950-26957, Nov 19 2012.

[62] L. Fu, J. Wong-Leung, P. Deenapanray, H. Tan, C. Jagadish, B. Gong*, et al.*, "Suppression of interdiffusion in GaAs/AlGaAs quantum-well structure capped with dielectric films by deposition of gallium oxide," *Journal of applied physics,* vol. 92, pp. 3579-3583, 2002.

[63] Y. Wang, H. S. Djie, and B. S. Ooi, "Group-III intermixing in InAs/InGaAlAs quantum dots-in-well," *Applied Physics Letters,* vol. 88, Mar 13 2006.

[64] Z. Y. Zhang, R. A. Hogg, B. Xu, P. Jin, and Z. G. Wang, "Realization of extremely broadband quantum-dot superluminescent light-emitting diodes by rapid thermal-annealing process," *Optics Letters,* vol. 33, pp. 1210-1212, 2008/06/01 2008.

[65] Q. Cao, S. F. Yoon, C. Y. Liu, and C. Z. Tong, "Effects of rapid thermal annealing on optical properties of p-doped and undoped InAs/InGaAs dots-in-a-well structures," *Journal of Applied Physics,* vol. 104, p. 033522, 2008.

[66] T. Lin, H. Zhang, H. Sun, C. Yang, and N. Lin, "Impurity free vacancy diffusion induced quantum well intermixing based on hafnium dioxide films," *Materials Science in Semiconductor Processing,* 2014 2014.

[67] A. Babiński, J. Jasiński, R. Bożek, A. Szepielow, and J. Baranowski, "Rapid thermal annealing of InAs/GaAs quantum dots under a GaAs proximity cap," *Applied Physics Letters,* vol. 79, pp. 2576-2578, 2001.

[68] Z. Y. Zhang, Q. Jiang, M. Hopkinson, and R. A. Hogg, "Effects of intermixing on modulation p-doped quantum dot superluminescent light emitting diodes," *Optics Express,* vol. 18, pp. 7055-7063, Mar 29 2010.

[69] H. Djie, B. Ooi, X.-M. Fang, Y. Wu, J. Fastenau, W. Liu*, et al.*, "Room-temperature broadband emission of an InGaAs/GaAs quantum dots laser," *Optics letters,* vol. 32, pp. 44-46, 2007.

[70] W. Zeller, M. Kamp, J. Koeth, and L. Worschech, "High power pulsed 976 nm DFB laser diodes," *Photonic Microdevices/Microstructures for Sensing Ii,* vol. 7682, 2010.

[71] S. H. Hwang, J. C. Shin, J. D. Song, W. J. Choi, J. I. Lee, and H. Han, "Detection wavelength tuning of InGaAs/GaAs quantum dot infrared photodetector with thermal treatment," *Microelectronics Journal,* vol. 36, pp. 203-206, 3// 2005.

[72] Y. Hu, K. Stamnes, M. Vaughan, J. Pelon, C. Weimer, D. Wu*, et al.*, "Sea surface wind speed estimation from space-based lidar measurements," *Atmos. Chem. Phys.,* vol. 8, pp. 3593-3601, 2008.

[73] V. V. Yakovlev, V. Lazarov, J. Reynolds, and M. Gajdardziska-Josifovska, "Laser-induced phase transformations in semiconductor quantum dots," *Applied Physics Letters,* vol. 76, pp. 2050-2052, Apr 10 2000.

[74] F. Karouta, E. Smalbrugge, W. C. van der Vleuten, S. Gaillard, and G. A. Acket, "Fabrication of short GaAs wet-etched mirror lasers and their complex spectral behavior," *Ieee Journal of Quantum Electronics,* vol. 34, pp. 1474-1479, Aug 1998.

[75] Z. Zaaboub, B. Ilahi, L. Sfaxi, and H. Maaref, "Thermal-induced intermixing effects on the optical properties of long wavelength low density InAs/GaAs quantum dots," *Materials Science & Engineering C-Biomimetic and Supramolecular Systems,* vol. 28, pp. 1002-1005, Jul 1 2008.

[76] T. M. Hsu, Y. S. Lan, W.-H. Chang, N. T. Yeh, and J.-I. Chyi, "Tuning the energy levels of self-assembled InAs quantum dots by rapid thermal annealing," *Applied Physics Letters,* vol. 76, pp. 691-693, 2000.

[77] S. Martini, A. E. B. Marques, M. Marques, A. A. Quivy, and L. K. h. Teles, "Radiative Recombination Mechanisms of Large InAs/GaAs Quantum Dots," *World Journal of Condensed Matter Physics,* vol. Vol.01No.04, p. 6, 2011.

[78] R. Leon, Y. Kim, C. Jagadish, M. Gal, J. Zou, and D. J. H. Cockayne, "Effects of interdiffusion on the luminescence of InGaAs/GaAs quantum dots," *Applied Physics Letters,* vol. 69, pp. 1888-1890, 1996.

[79] S. Malik, C. Roberts, R. Murray, and M. Pate, "Tuning self-assembled InAs quantum dots by rapid thermal annealing," *Applied Physics Letters,* vol. 71, pp. 1987-1989, 1997.

[80] S. J. Xu, X. C. Wang, S. J. Chua, C. H. Wang, W. J. Fan, J. Jiang*, et al.*, "Effects of rapid thermal annealing on structure and luminescence of self-assembled InAs/GaAs quantum dots," *Applied Physics Letters,* vol. 72, pp. 3335-3337, 1998.

[81] P. S. Zory, A. R. Reisinger, R. G. Waters, L. J. Mawst, C. A. Zmudzinski, M. A. Emanuel*, et al.*, "Anomalous Temperature-Dependence of Threshold for Thin Quantum-Well Algaas Diode-Lasers," *Applied Physics Letters,* vol. 49, pp. 16-18, Jul 7 1986.

[82] M. Mittelstein, Y. Arakawa, A. Larsson, and A. Yariv, "Second quantized state lasing of a current pumped single quantum well laser," *Applied Physics Letters,* vol. 49, pp. 1689-1691, 1986.

[83] H. H. Alhashim, M. Z. M. Khan, M. A. Majid, T. K. Ng, and B. S. Ooi, "Sub-1100 nm lasing from post-growth intermixed InAs/GaAs quantum-dot lasers," *Electronics Letters,* vol. 51, pp. 1444-1445, Sep 3 2015.

[84] T. Ko, D. Adler, J. Fujimoto, D. Mamedov, V. Prokhorov, V. Shidlovski*, et al.*, "Ultrahigh resolution optical coherence tomography imaging with a broadband superluminescent diode light source," *Optics Express,* vol. 12, pp. 2112-2119, 2004.

[85] L. Burrow, F. Causa, and J. Sarma, "1.3-W ripple-free superluminescent diode," *IEEE Photonics Technology Letters,* vol. 17, pp. 2035-2037, 2005.

[86] S. Haffouz, P. Barrios, R. Normandin, D. Poitras, and Z. Lu, "Ultrawide-bandwidth, superluminescent light-emitting diodes using InAs quantum dots of tuned height," *Optics Letters,* vol. 37, pp. 1103-1105, 2012.

[87] H. S. Djie, C. E. Dimas, D.-N. Wang, B.-S. Ooi, J. C. Hwang, G. T. Dang*, et al.*, "InGaAs/GaAs quantum-dot superluminescent diode for optical sensor and imaging," *IEEE Sensors Journal,* vol. 7, pp. 251-257, 2007.

[88] J. Wang, M. J. Hamp, and D. T. Cassidy, "Design considerations for asymmetric multiple quantum well broad spectral width superluminescent diodes," *IEEE Journal of Quantum Electronics,* vol. 44, pp. 1256-1262, 2008.

[89] O. Mikami, H. Yasaka, and Y. Noguchi, "Broader spectral width InGaAsP stacked active layer superluminescent diodes," *Applied Physics Letters,* vol. 56, pp. 987-989, 1990.

[90] H. Ma, S. Chen, X. Yi, G. Zhu, and J. Jin, "High power polarization-insensitive 1.3 µm InGaAsP–InP quantum-well superluminescent emission diodes grown by MOVPE," *Semiconductor Science and Technology,* vol. 19, p. 823, 2004.

[91] L. Fu, H. Schweizer, Y. Zhang, L. Li, A. M. Baechle, S. Jochum*, et al.*, "Design and realization of high-power ripple-free superluminescent diodes at 1300 nm," *IEEE Journal of Quantum Electronics,* vol. 40, pp. 1270-1274, 2004.

[92] M. Sugo, Y. Shibata, H. Kamioka, M. Yamamoto, and Y. Tohmori, "High-power (> 50 mW) and wideband (> 50 nm) 1.3 µm super-luminescent diodes," *Electronics Letters,* vol. 41, pp. 500-501, 2005.

[93] M. Faugeron, C. Fortin, Y. Robert, E. Vinet, F. Lelarge, R. Brenot*, et al.*, "Wide Optical Bandwidth and High Output Power Superluminescent Diode covering C and L Band," *IEEE Photonics Technology Letters,* vol. 26, pp. 841-844, 2014 2014.

[94] M. Khan, T. Ng, and B. Ooi, "High Performance 1.55 µm Superluminescent Diode Based on Broad Gain InAs/InGaAlAs/InP Quantum Dash Active Region," *IEEE Photonics Journal,* vol. 6, p. 1600108, August 2014 2014.

[95] B. S. Ooi, H. S. Djie, Y. Wang, C. L. Tan, J. C. M. Hwang, X. M. Fang*, et al.*, "Quantum dashes on InP substrate for broadband emitter applications," *IEEE Journal of Selected Topics in Quantum Electronics,* vol. 14, pp. 1230-1238, 2008.

[96] Y. Wang, H. S. Djie, B. S. Ooi, J. C. M. Hwang, X. M. Fang, Y. Wu*, et al.*, "Monolithic InAs/InAlGaAs/InP quantum-dash-in-well extended-cavity laser fabricated by postgrowth intermixing," *Laser Physics,* vol. 18, pp. 400-402, Apr 2008.

[97] S. Chen, N. Peyvast, K. Zhou, N. Babazadeh, Z. Zhang, D. Childs*, et al.*, "Broad Bandwidth Emission From Hybrid QW/QD Structures," in *Conference on Lasers and Electro-Optics/Pacific Rim*, 2013, p. WK1_3.

[98] T. R. Chen, L. Eng, Y. H. Zhuang, A. Yariv, N. S. Kwong, and P. C. Chen, "Quantum well superluminescent diode with very wide emission spectrum," *Applied Physics Letters,* vol. 56, pp. 1345-1346, 1990.

[99] C. F. Lin, B. R. Wu, L. W. Laih, and T. T. Shih, "Sequence influence of nonidentical InGaAsP quantum wells on broadband characteristics of semiconductor optical amplifiers-superluminescent diodes," *Optics Letters,* vol. 26, pp. 1099-1101, Jul 15 2001.

[100] THORLABS, "Superluminescent Diode 1310 nm, Butterfly Package," *https://www.thorlabs.com/newgrouppage9.cfm?objectgroup_id=3902,* 2016.

[101] M. Z. M. Khan, H. H. Alhashim, T. K. Ng, and B. S. Ooi, "High-Power and High-Efficiency 1.3-mu m Superluminescent Diode With Flat-Top and Ultrawide Emission Bandwidth," *Ieee Photonics Journal,* vol. 7, Feb 2015.

[102] D. SEMICONDUCTOR, "Broadband Light Sources," *http://www.denselight.com/product4.htm,* 2016.

[103] H. Carrère, V. Truong, X. Marie, R. Brenot, G. De Valicourt, F. Lelarge*, et al.*, "Large optical bandwidth and polarization insensitive semiconductor optical amplifiers using strained InGaAsP quantum wells," *Applied Physics Letters,* vol. 97, p. 121101, 2010.

[104] C. L. Tan, Y. Wang, H. S. Djie, and B. S. Ooi, "The role of optical gain broadening in the ultrabroadband InGaAs/GaAs interband quantum-dot laser," *Computational Materials Science,* vol. 44, pp. 167-173, Nov 2008.

[105] S. Seki, H. Oohasi, H. Sugiura, T. Hirono, and K. Yokoyama, "Dominant mechanisms for the temperature sensitivity of 1.3 μm InP-based strained-layer multiple-quantum-well lasers," *Applied Physics Letters,* vol. 67, pp. 1054-1056, 1995.

[106] H. Wang, A. D. Vandermeer, and D. T. Cassidy, "Carrier distribution and its dependence on barrier thickness in InGaAsP⁄InP asymmetric multiple quantum well lasers," *Journal of Applied Physics,* vol. 100, pp. -, 2006.

[107] C. Rejeb, R. Maciejko, D. Morris, and T. Makino, "Carrier dynamics in InGaAsP MQW laser structures," in *1998 International Conference on Applications of Photonic Technology*, 1998, pp. 1065-1070.

APPENDIX A: BASIC LASER PRINCIPLE

In the 1960s the first laser was invented by Theodore H. Maiman at Hughes Laboratories. LASER definition -based on operation- is “light Amplification by Stimulated emission of Radiation “. On other words -based on properties- it’s a device that produce coherent, monochromatic and a highly collimated beam of light. Spatial coherence allows a laser to be focused to a tight spot, enabling applications such as laser cutting and lithography. Lasers can also have high temporal coherence, which allows them to emit light with a very narrow spectrum, i.e., they can emit a single color of light. Temporal coherence can be used to produce pulses of light as short as a femtosecond.

The amplification of light by stimulated emission is a fundamental concept in the basic understanding of laser action. Stimulated emission is one of the three types of transition that can occur in the semiconductor laser cavity (absorption, spontaneous, stimulated emission). As shown in in *Figure 0-1*(a) the absorption is a process in which an incoming photon is absorbed by the transition of an electron in the conduction band and creation of hole in the V.B. The energy of the absorbed photon must be equal to or greater than the band gap. *Figure 0-1* (b), spontaneous emission is radiative process in which the electron recombines with hole at random and generates a photon (of random direction and phase). In contrast, stimulated emission *Figure 0-1* (c) occurs when an electron-hole pair is perturbed by an incoming photon, which stimulates the electron-hole recombination and produces a new photon. The emitted light (Photon) has the same wavelength, phase and direction as the incident light (photon). In the stimulated emission one incident photon generates two photons; as a result the incident light is amplified.

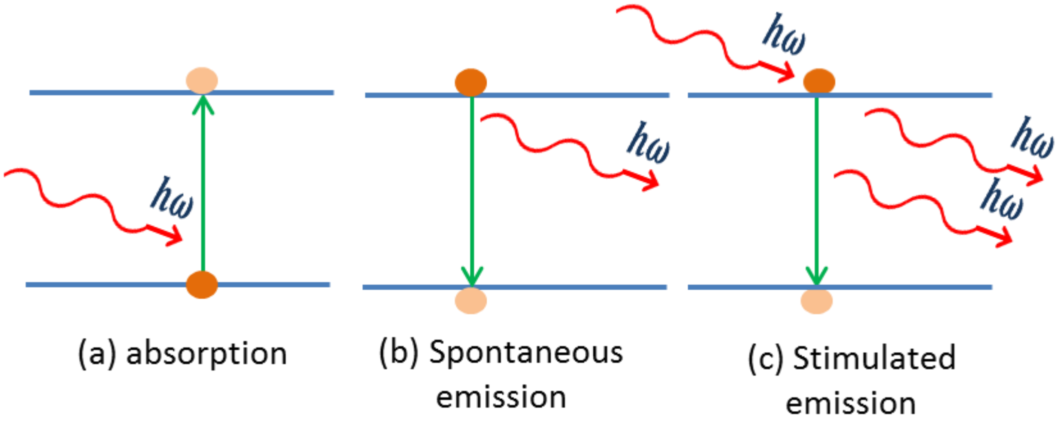

Figure 0-1: Radiation and absorption: (a) absorption, (b) spontaneous emission, and (c) stimulated emission.

Stimulated recombination of electron-hole pairs takes place within the undoped GaAs active region. Figure 0-2 illustrates schematically some of the key concept in the laser operation. Here heterostructure provides the confinement of carriers, and at the same time, steps in the refractive index on both sides of the active region provide an optical waveguide to confine optical modes. Optical confinement and feedback are required to produce regenerative feedback (reduce the loss of stimulated photons). The stimulated photons can either stimulate other photons or get absorbed.

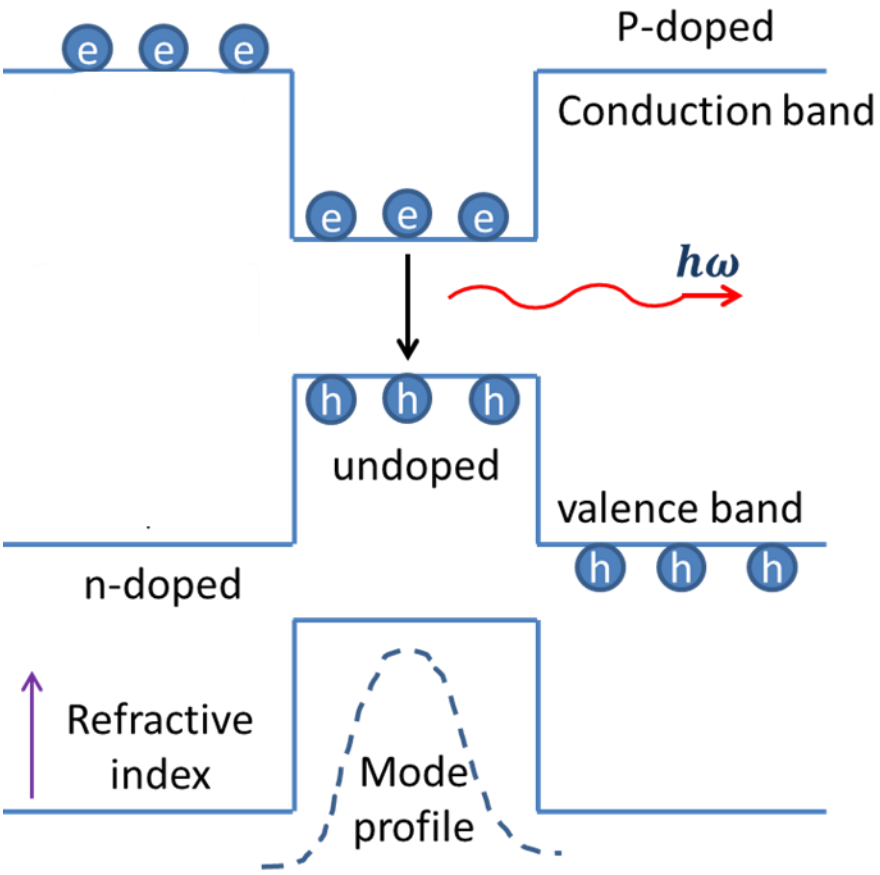

Figure 0-2: Schematic illustration of the confinement for both the carriers and optical light in a double-heterostructure semiconductor laser.

The normal optical feedback design simply called the Fabry-Perot laser (FPL) cavity. This laser cavity is formed by producing two parallel mirrors with reflectivity, R_1 and R_2. Figure 0-3 shows the sketch of (FPL) cavity of semiconductor laser. Mirrors are usually formed by cleaving along the crystallographic axes. To confine the light laterally, dielectric wave guiding is used in which the optical mode is confined by total internal reflection, in which the high refractive index gain material is surrounded by slightly lower refractive index cladding layers.

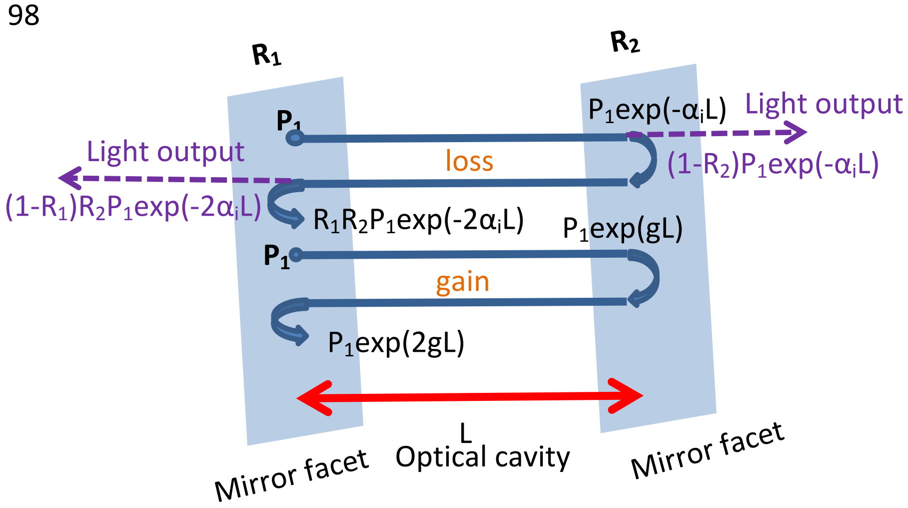

Figure 0-3: The propagation of light in the (FPL) cavity of semiconductor laser.

For laser operation the round trip gain must be equal to the sum of the internal loss (α_i) and the mirror loss (α_m). The internal loss is the losses due to parasitic effects (absorption, scattering etc.) in the cavity and the mirror loss is the emitted light from the facets due to the non-100% reflectivity of the mirrors.

On each round trip the beam passes through the medium twice. Hence the fractional loss incurred by a light beam is

$$loss = R_1 R_2 e^{-2L\alpha_i} \qquad \textit{Equation 0-1}$$

If the gain coefficient per unit length produced by stimulated emission is g_{th} cm^{-1}, the fractional round trip gain is given by

$$gain = e^{2Lg_{th}} \qquad \textit{Equation 0-2}$$

Hence:

$$R_1 R_2 e^{-2L\alpha_i} e^{2Lg_{th}} = 1 \qquad \textit{Equation 0-3}$$

Hence, the threshold gain per unit length is given by:

$$g_{th} = \alpha_i + \frac{1}{2L}\ln[\frac{1}{R_1R_2}]$$

Equation 0-4

Where:

$$\alpha_m = \frac{1}{2L}\ln[\frac{1}{R_1R_2}]$$

Equation 0-5

APPENDIX B: LASER PERFORMANCE PARAMETERS

- **Power vs. Current (L-I) Characteristics.**

The most important and the most fundamental laser characterization is the measurement of the amount of light it emits as a current is injected into the device. This generates the output light vs. input current curve, more commonly referred as the L.I. curve. As the injected current is increased, the laser first demonstrates a spontaneous emission, increasing very gradually until it begins to emit a stimulated radiation, which is the onset of laser action.

- **Threshold current (I_{th})**.

The first parameter of interest is the exact current value where the stimulated emission takes place. This is typically referred as the (I_{th}) and is denoted by the symbol I_{th}. It is generally desirable that the (I_{th}) be as low as possible, resulting in a more efficient device.

- **Threshold current density (J_{th}):**

(J_{th}) is determined by dividing the experimentally obtained threshold current value I_{th} by the area of the laser.

- **Transparency Current Density J_o:**

Another parameter that can be used to compare one set of lasers to another is the transparency current density (J_o). The J_o is a measurement of the **(J_{th})** of an infinitely long device, for which it is considered that the mirror loss is zero. It can be extracted from the intercept of the linear fit curve to the J_{th} versus the inverse cavity length.

- **External Differential Quantum Efficiency (ηd)**

The efficiency of a laser device in converting the injected electron-hole pairs (input electric charges) to photons emitted (output light) is simply the external quantum efficiency ηd. This parameter results directly from the experimental measurement of the slope of the L-I curve. In an ideal laser ‘q’ Coulombs per second of electrical current results in an output power of hc/λ per second. Therefore, the theoretical slope of a typical perfect laser is (hc/λq), where h is the Planck’s constant, λ is photon wavelength, and c is velocity of light.

To determine η_d, we need to compare the slope of the L-I curve (ΔP/ΔI) to that (hc/λq) of a 100% efficient device. Therefore, the external differential quantum efficiency of the laser is displayed as:

$$\eta_d = \frac{2\Delta p}{\Delta I}[\frac{q\lambda}{hc}] \qquad \textit{Equation 0-1}$$

Where ΔP/ΔI is multiplied by a factor of 2 to account for the output light from the back facet that was not measured. Equivalent, perfect facets are assumed in the above.

- **Internal Quantum Efficiency (η_i) and Internal Loss (α_i)**

Unlike the external differential quantum efficiency, the internal quantum efficiency is independent of the geometrical properties of the laser device, such as the cavity length or the strip width. Therefore, it is one of the main parameters used in assessing the quality of the laser, from which it was manufactured.

$$\eta\mathbf{d} = \eta\mathbf{i}\,(\frac{\boldsymbol{\alpha}\mathbf{i}}{\boldsymbol{\alpha}\mathbf{i}+\boldsymbol{\alpha}\mathbf{m}}) \qquad \textit{Equation 0-2}$$

where *α_m=1/L (ln(1/R))* is mirror loss (R- reflectivity of the mirror, L is the cavity lengths) after re-arranging:

$$1/\eta_d = \frac{1}{\eta_i}[1 + \alpha_i L/\ln(\frac{1}{R})] \qquad \textit{Equation } 0\text{-}3$$

The internal quantum efficiency is then determined by plotting the curve of inverse external differential quantum efficiency versus the cavity length. The inverse of the intercept point of the linear fit line of the set of data points with the vertical axis is the internal quantum efficiency parameter, indicating in a percentage form. Measuring the L-I curves for different cavity lengths is followed by calculating the slope, and the simple calculation is required for calculating the internal efficiency.

As a result of the material nature, not all of the photons generated find their way out of the device, and some photons are reabsorbed due to various internal loss mechanisms. Internal loss αi is equal to the slope of the line multiplied by (η_i)ln(1/R), where R = 0.32 for a typical GaAs/AlGaAs laser with as-cleaved facets.

- **Characteristic Temperature (*To*).**

The characteristics temperature (T_0) is a measure of how sensitive the **(I_{th})**is to a changing temperature. T_0 can be extracted by plotting the natural log of the **(J_{th})** at each temperature; it is the inverse of the slope of the linear fit line to the data points. This is found by:

$$T_0 = \Delta T/\Delta \ln(Jth) \qquad \text{Equation 0-4}$$

APPENDIX C: LASER DEVICE FABRICATION

- **Cleaving:** by using special tools cleave the wafer in the [110] direction to have the desired sample size.
- **Cleaning:** rinse the sample in acetone/IPA Dry by N_2, by using Solvent Bench (LIT 016),
- **Insulator deposition**: deposited 200 nm of SiO_2, by using PECVD - Oxide and Nitride (DEP-009). The Recipe used: SiH_4 60 sccm (standard cubic centimeter per minute), N_2O 850 sccm, N2 162.5 sccm, RF power 20W, Pressure 1000 mT, table temperature 300 ^oC , deposition rate 63 nm/minute.
- **Spin coating carrier wafer:** carrier wafer is coated by a thick photoresist (AZ9260) to fix the sample, by using JST Resist Spin/Bake (LIT-001), the recipe used have 3 steps; Step1: speed 300 rpm (rotation per minute), ramp 150 rmp/s, time 3 s. Step 2: speed 1500 rpm, ramp 1000 rmp/s, time 3. Step 3: speed 2400 rpm, ramp 1500 rpm/s, time 60 s. Thickness 10 um.
- **Align sample on carrier wafer:** the sample is align on the carrier wafer parallel to the wafer line, by using JST Resist Spin/Bake.
- **Carrier wafer baking:** baking to stick the sample, using JST Resist Spin/Bake -110 C, 180 s.
- **Spin coating:** spin coat the sample for negative lithography, by using JST Resist (Az5142) Spin/Bake in recipe : recipe 3; step 1: speed 800 rpm, ramp rate 1000 rpm/s, time 3 s; step 2: speed 1500 rpm, ramp rate 1500 rpm/s, time 3 sec; step 3: speed 3000 rpm, ramp rate 3000 rpm/s, time 30 s. Thickness 1.6 um.
- **Pre-baking:** this step is critical for negative lithography, using JST Resist Spin/Bake, with recipe 120 s, 105 ^oC.
- **UV exposure:** unwanted areas are covered using Mask-1 DEV6 broad-area laser, using EVG 6200 UV contact aligner.
- **Baking:** put sample onto the hot plate, using JST Resist Spin/Bake (120" 110 C).
- **Flood UV exposure:** use clear glass mask to expose all areas of the photoresist to UV light using EVG 6200 UV contact aligner.

- **Development:** remove unwanted photoresist, by using Dev 7261 MIF under Base Develop Hood, for 30 s only.
- **Dry etching:** remove exposed SiO_2 by ICP plasma etcher.
- **Removing PR residual:** remove residuals of PR by plasma striping, using NanoPlas DBS-6000 Plasma Strip, recipe is Module 3, Oxygen only 1 Minute.
- **Cleaning:** clean by acetone and IPA and dry by N_2 in Solvent Bench.
- **Spin coating:** spin coat the sample with Az5142 photoresist, using JST Resist Spin/Bake, thickness 1.6 um the recipe is:
- **Mask alignment:** align samples to mask-2, using EVG 6200 UV contact aligner.
- **UV exposure:** using EVG 6200 UV contact aligner.
- **Development:** removing unwanted photoresist, using Dev 7261 MIF in Base Develop Hood.
- **Sputtering top contact:** deposited top contact, using Reactive sputter (Ti 10, Pt 20, Au 250).
- **Lift-off:** immerse the sample in acetone until lift-off starts in Solvent Parts Clean hood. It may take up to 1 day.
- **Annealing:** anneal to have better contact, using Rapid Thermal Process. (60 s at 340 ^{o}C).
- **Fix to thinner plate:** using hot plate at 150^{o}C put wax on the thinner plate then put the sample. Heat until wax becomes liquid.
- **Thinning:** thin the back side of the sample in Multiprep polisher using 9 um thinning paper to remove 150-200 um.
- **Back contact evaporation:** deposit back contact using evaporation, using electron beam evaporator (In 10nm, Ge 10nm, Au 200nm).
- **Annealing:** anneal to have better contact, using rapid thermal annealing equipment (60 s at 380 ^{o}C in vacuum).
- **Laser bar cleaving:** Cut laser bars into desired length, using Loomis scriber.